Ricerca di Sistema elettrico

Modelli di rilascio dei gas di fissione per combustibili MOX ad elevato burnup

Lello Luzzi, Giovanni Pastore, Pietro Botazzoli

MODELLI DI RILASCIO DEI GAS DI FISSIONE PER COMBUSTIBILI MOX AD ELEVATO BURNUP

Lelio Luzzi, Giovanni Pastore, Pietro Botazzoli (POLIMI)

Settembre 2013

Titolo

Modelli di rilascio dei gas di fissione per combustibili MOX ad elevato burnup

Ente emittente.

PAGINA DI GUARDIA

Descrittori

    Tipologia del documento: **Rapporto Tecnico**
    Collocazione contrattuale: Accordo di programma ENEA-MSE su sicurezza nucleare e reattori di IV generazione

    Argomenti trattati: Sicurezza nucleare
                               Generation IV reactors
                               Combustibile nucleare
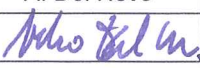
Sommario

Il lavoro svolto ha inteso offrire un contributo alla modellazione dei fenomeni accoppiati di rigonfiamento gassoso e rilascio di gas di fissione. Il lavoro ha visto lo sviluppo di un nuovo modello integrato, fondato su un approccio ingegneristico orientato al compromesso pratico tra una descrizione fisica e i requisiti computazionali. Il modello è stato implementato con successo nel codice di performance TRANSURANUS e validato. Sviluppato su base fisica, può essere applicato in generale ai combustibili ossidi (UO2), sia a ossidi misti di uranio e plutonio (MOX). I principali aspetti innovativi del presente lavoro risiedono: (i) nella base fisica del nuovo modello, (ii) nell'accoppiamento tra il rigonfiamento gassoso e il rilascio di gas di fissione e (iii) nella descrizione della dipendenza dei fenomeni dallo stato di sforzo del combustibile. Inoltre, è stata condotta una revisione critica degli approcci attualmente adottati in letteratura e nei codici di performance per la modellazione del rilascio dei gas di fissione e dell'elio in combustibili MOX. Con riferimento a tali problematiche, nel presente lavoro sono stati sviluppati, accoppiati e implementati nel codice TRANSURANUS modelli di rilascio dei gas di fissione e di elio rilevanti per la performance di combustibile del tipo UO2 e MOX ad elevato burn-up.

Note

CERSE-POLIMI RL 1487/2013
Autori: Lelio Luzzi, Giovanni Pastore, Pietro Botazzoli (POLIMI)

Copia n.			In carico a:			
1			NOME			
			FIRMA			
0	**EMISSIONE**	**18/09/13**	NOME	A. Del Nevo	NA	M. Tarantino
			FIRMA			
REV.	**DESCRIZIONE**	**DATA**		**CONVALIDA**	**VISTO**	**APPROVAZIONE**

Modelli di rilascio dei gas di fissione per combustibili MOX ad elevato burnup

Lelio Luzzi, Giovanni Pastore, Pietro Botazzoli

Index

Sommario

Il presente rapporto offre un contributo alla modellazione dei fenomeni accoppiati di rigonfiamento gassoso e rilascio di gas di fissione in combustibili nucleari a base di ossidi, con applicazione all'analisi termo-meccanica integrale (e, in definitiva, alla progettazione e al *licensing*) delle barrette di combustibile. Il lavoro ha visto lo sviluppo di un nuovo modello integrato per i suddetti fenomeni, fondato su un approccio ingegneristico orientato al compromesso pratico tra una descrizione fisica e i requisiti computazionali inerenti all'analisi integrale di barretta. Il modello è stato implementato con successo nel codice di *performance* TRANSURANUS e validato tramite confronto dei risultati con un ampio *database* sperimentale. Il modello qui descritto è stato sviluppato su base fisica, al fine di garantirne l'applicabilità generale ai combustibili ossidi – sia biossido di uranio (UO$_2$), impiegato nei reattori nucleari ad acqua leggera, sia ossidi misti di uranio e plutonio (MOX). In considerazione della vasta disponibilità di dati sperimentali, questa prima fase di validazione ha previsto la simulazione di prove di irraggiamento in reattore di barrette di combustibile UO$_2$, appartenenti all'*International Fuel Performance Experiments* (IFPE) *Database* dell'OECD/NEA. I risultati indicano una riproduzione conforme dei meccanismi fisici, un buon accordo con i dati sperimentali e significativi miglioramenti del codice TRANSURANUS. Rispetto ai trattamenti empirici comunemente adottati nei codici di *performance*, i principali aspetti innovativi del presente lavoro risiedono: (i) nella base fisica del nuovo modello, (ii) nell'accoppiamento tra il rigonfiamento gassoso e il rilascio di gas di fissione e (iii) nella descrizione della dipendenza dei fenomeni dallo stato di sforzo del combustibile. Quest'ultimo aspetto, essenziale in condizioni di interazione meccanica guaina-combustibile, è di rilevanza nell'ottica dell'estensione dei margini operativi e del bruciamento (*burnup*) del combustibile nucleare, tendenza attuale a livello industriale.

Inoltre, è stata condotta una revisione critica degli approcci attualmente adottati in letteratura e nei codici di *performance* per la modellazione del rilascio dei gas di fissione e dell'elio in combustibili MOX, focalizzandosi in particolare sulle problematiche dovute al rilascio di elio. Quest'ultimo, infatti, può influenzare in maniera significativa la *performance* del combustibile in reattore, così come il suo comportamento in condizioni di stoccaggio a lungo termine. Durante l'irraggiamento, l'elio intrappolato nelle pastiglie di combustibile può contribuire a degradarne le proprietà; d'altro

canto, la frazione di elio rilasciata nel volume libero della barretta influenza la pressione interna con conseguenze sulla sicurezza. Tali aspetti sono particolarmente importanti per i combustibili MOX, il cui impiego è previsto per una migliore sostenibilità dell'energia nucleare (chiusura del ciclo del combustibile) e per la gestione del plutonio di origine militare. La produzione di elio aumenta esponenzialmente con il *burnup* ed è particolarmente significativa per i MOX, in quanto il plutonio inizialmente presente comporta una maggiore produzione di emettitori α. Con riferimento a tali problematiche, nel presente lavoro sono stati sviluppati, accoppiati e implementati nel codice TRANSURANUS modelli di rilascio dei gas di fissione e di elio rilevanti per la *performance* di combustibile del tipo UO_2 e MOX ad elevato *burnup*.

Summary

The present report provides a contribution to the modelling of the coupled phenomena of fission gas swelling and release in oxide nuclear fuels, with application to the integral thermo-mechanical analysis of the fuel rods (hence, to the fuel design and licensing). Through an engineering approach, which practically combines a physics-based treatment and the computational efficiency required for application to fuel rod analysis, a new integrated model of fission gas swelling and release was developed. The model was effectively implemented in the TRANSURANUS fuel rod analysis code and verified through an extensive comparison with experimental irradiation data. The model described here was developed on a physical basis, in order to obtain a general applicability to oxide nuclear fuels – both LWR-UO_2 and (U,Pu) Mixed Oxide (MOX). In view of the large availability of experimental data, irradiation experiments of UO_2 fuel rods from the OECD/NEA International Fuel Performance Experiments (IFPE) Database were analysed during this first step of validation. The results showed a physically sound representation of the phenomena, a satisfactory agreement with the experimental irradiation data, and improvements of the TRANSURANUS code. Compared with the empirical treatments commonly adopted in the fuel rod analysis codes, the innovative aspects of the present work mainly lie in: (i) the physical foundation of the developed model, allowing higher flexibility of application, (ii) the consistent coupling between the fission gas swelling and release, and (iii) the appropriate evaluation of the role of the stress field in the fuel. The latter aspect is of high importance for properly analysing the conditions of fuel-cladding mechanical interaction, and is topical in view of the tendency to extend the operating margins and the discharge burn-up of the nuclear fuel.

A critical review of the approaches currently adopted in the literature as well as in the fuel rod performance codes for modelling the fission gas and helium release in MOX fuels was also performed, focusing on the issues related to the helium release. Actually, helium (He) behaviour can influence in a significant way the in-reactor performance and the long term storage of nuclear fuel. During the irradiation, He trapped in the pellet can contribute to the degradation of the properties of the fuel. On the other hand, the fraction released in fuel rod free volume influences the inner pressure with consequences for the safety. This is especially relevant for MOX fuels, which are envisaged to be employed for a better sustainability of the nuclear energy resources (closed fuel cycle) and for the

management of military grade plutonium (e.g., Fissile Material Disposition Program). In fact, He production increases exponentially with the burn-up and it is particularly important for MOX fuel, since the initial presence of Pu leads to a larger production of α emitters. With reference to these issues, in the present work, models relevant for the performance of LWR UO_2 and MOX fuels at high burn-ups have been developed, coupled and implemented in the TRANSURANUS code.

Introduction

Among the various issues involved in fuel rod modelling, the behaviour of the fission gases xenon and krypton represents a challenging task in view of the complexity of the relevant physical mechanisms and the strong implications on the thermo-mechanical behaviour of the fuel rods. On the one hand, the fission gases generated in the fuel tend to precipitate into bubbles resulting in fuel swelling (volumetric and permanent deformation), which may give rise to enhanced pellet-cladding mechanical interaction (PCMI). On the other hand, the inter-connection of the gas bubbles developing at the fuel grain boundaries leads to fission gas release (FGR) to the free volume of the fuel rod, which causes pressure build-up and thermal conductivity degradation of the rod filling gas. The inherently coupled kinetics of fission gas swelling and release calls for the development of physics-based, integrated models of these phenomena to be employed in the fuel rod analysis codes. As of today, however, empirical approaches are widely adopted, which are inexpensive to use but unfit for providing insight into the underlying mechanisms, and cannot be applied beyond their range of calibration. A further open issue concerns the dependence of both fission gas swelling and release on the hydrostatic stress in the fuel, which is often neglected or treated in a simplified way in view of the involved complexity of the numerical treatment.

The present report represents a contribution to the modelling of fission gas swelling and release in the fuel rod analysis codes. The work comprises (i) a development aspect, which entails the construction of a physics-based and integrated model of fission gas swelling and release in oxide fuel during irradiation, properly taking into account the intrinsic coupling as well as the dependence of both phenomena on the hydrostatic stress, and (ii) an application aspect, including the implementation in the TRANSURANUS code, the employment in fuel rod analyses and the verification of the model.

Through an engineering modelling approach, which practically combines a physics-based treatment and the simplicity that is a prerequisite for the effective application to the fuel rod analysis codes, a new model with the above characteristics was developed. The model describes the relevant processes of gas diffusion and precipitation, bubble growth and inter-connection, providing a consistent, integrated treatment of the fission gas swelling and release.

As a first step of verification, the model was coded as stand-alone version and applied to the analysis of either power ramped or power cycled fuel specimens. The model was proven to consistently reproduce the main peculiarities of the fission gas behaviour, in accordance with the observations reported in the literature. A first quantitative assessment was carried out of the predictive capability of the model against a dataset of swelling measurements from the OECD/NEA International Fuel Performance Experiments (IFPE) database[1], pointing out a reasonable predictive accuracy, without fitting of the model parameters.

The applicability of the new model to fuel rod modelling (hence, to the nuclear fuel design and licensing) was demonstrated by successful implementation in the TRANSURANUS fuel rod analysis code. During the implementation, consistent matching was provided between the non-linear, stress-dependent model calculations and the thermo-mechanical fuel rod analysis. Numerical stability and reasonable computational times were obtained. Adopting the new model, the TRANSURANUS code was employed for an extensive set of simulations of LWR fuel rod irradiation experiments involving power ramps. The coupling between the fission gas swelling and release, and the dependence of both phenomena on the hydrostatic stress, were confirmed to be reproduced consistently with the experimental observations. Moreover, the assessment of the results against experimental data of FGR pointed out a satisfactory agreement, without applying any tuning to the model parameters.

The implementation of the new model represents a significant progress in the development of the TRANSURANUS code. The innovative aspects are mainly related to (i) the advantages of a physics-based and integrated treatment in terms of flexibility of application and understanding of the underlying mechanisms, compared to the previously adopted empirical approaches, (ii) the observed improvement of the predictive accuracy in terms of FGR, and (iii) the consistent evaluation of the dependence of both fission gas swelling and release on the hydrostatic stress. The latter aspect is of high importance in view of the current tendency to extend the flexibility of use (load-following) and the discharge burn-up of the nuclear fuel, which can involve the occurrence of strong PCMI and the consequent development of high hydrostatic stress in the fuel due to cladding restraint.

---

[1] http://www.oecd-nea.org/science/fuel/ifpelst.html

The results achieved in the present work are promising in view of future applications of the model, implemented in the TRANSURANUS code, in both research and industrial frameworks. Also, the successful implementation in the TRANSURANUS code indicated that the model may be of interest for application to other fuel rod analysis codes.

To summarize, the general features of the model developed in the present work, in terms of physical foundation and computational efficiency, constitute a framework that allows the application to fuel rod modelling of the physics-based, integrated and stress-dependent treatment of the fission gas swelling and release. The underlying approach is generally applicable and can be reproduced in order to develop increasingly complex and advanced models with the above fundamental capabilities to be implemented in the fuel rod analysis codes.

Among the issues currently investigated, the production and the behaviour of helium in oxide fuels at high burn-up is one of the most important. This topic is especially relevant for the (U,Pu) Mixed Oxide fuels (MOX), which are envisaged to be employed both for a better sustainability of the nuclear energy resources (closed fuel cycle) and for the management of military grade plutonium (e.g., FMDP - Fissile Material Disposition Program, sponsored by the United States Department of Energy, and now included in the IFPE database[2]). In particular, helium production and behaviour is of relevance in view of increasing burn-ups and linear heat generation rates, since its production increases exponentially as a function of the burn-up. This can have two important consequences: (i) if trapped in the pellets, helium can contribute to the degradation of the fuel thermal conductivity and swelling; (ii) if helium diffuses to the gap between the fuel and the cladding, it enhances the rod pressure with important consequences for the safety.

In the light of the above items (i) and (ii), when describing the gas behaviour in MOX fuel at high burn-up, it is also important to properly model the behaviour of helium. To this specific issue, a critical review on the mechanisms for the release of helium during LWR operations has been also carried out in the present work, and is presented in Appendix to this report. On the basis of the evaluated information, a preliminary model for the helium release has been developed as well. It has been coupled with the helium production and grain growth models already available in the TRANSURANUS code, and tested against experimental data.

---

[2] http://www.oecd-nea.org/tools/abstract/detail/nea-1774

The report is organized as follows.

- Chapter 1 gives the premises of the work by briefly surveying the physical processes involved in fission gas swelling and release and the fundamental characteristics of the TRANSURANUS code.

- Chapter 2 describes the new integrated model for fission gas swelling and release in oxide fuel. The basic equations of the model are given, and the underlying concepts and innovative aspects of the constructed approach are discussed.

- Chapter 3 concerns the application of the new model as stand-alone version. Calculations are presented of fission gas swelling and release in either power ramped or power cycled fuel specimens from the IFPE database. The results are discussed, both in terms of model capabilities to represent the relevant physical processes and by assessment of the predictions against experimental data of fission gas swelling.

- Chapter 4 deals with the application of the new model to the TRANSURANUS code. The implementation issues and methods are summarized, and the employment in fuel rod analyses is discussed. Following a critical analysis of the relevant databases, an extensive set of simulations is carried out of LWR fuel rod irradiation experiments involving power ramps and for the most part selected as cases of priority interest in the FUMEX-III Project. The results of the calculations are presented, showing the capabilities of the model to reproduce the peculiarities of the fission gas swelling and release, as well as the obtained predictive accuracy in terms of integral fuel rod FGR by comparison with experimental data from the IFPE database.

- The Appendix presents a critical review of the approaches currently adopted in the literature as well as in the fuel rod performance codes for modelling the fission gas and helium release in MOX fuels. On the basis of the studied approaches, models have been developed and are proposed for the implementation in the TRANSURANUS fuel performance code. In particular, a specific model for the helium release has been implemented in TRANSURANUS, coupled with the helium production and grain growth models, and preliminarily validated on the basis of the ATR (Advanced Test Reactor) irradiation test.

List of acronyms

AGR	Advanced Gas-cooled Reactor
ANL	Argonne National Laboratory
ATR	Advanced Test Reactor
BNFL	British Nuclear Fuels Limited
BOL	Beginning-Of-Life
BWR	Boiling Water Reactor
CEA	Commissariat à l'Énergie Atomique
CEN	Centre d'Étude de l'énergie Nucléaire
CPL	Conditioning Power Level
CRP	Coordinated Research Project
EOL	End-Of-Life
EPRI	Electric Power Research Institute
FBR	Fast Breeder Reactor
FG	Fission Gas
FGR	Fission Gas Release
FMDP	Fissile Material Disposition Program
FP	Fission Product
FUMEX	FUel Modelling at EXtended burn-up
GB	Grain Boundary
HBS	High Burn-up Structure
IAEA	International Atomic Energy Agency
IFPE	International Fuel Performance Experiments
INEEL	Idaho National Engineering and Environmental Laboratory
ITU	Institute for Transuranium Elements
JRC	Joint Research Centre
KAERI	Korea Atomic Energy Research Institute
LOCA	Loss-Of-Coolant Accident
LWR	Light Water Reactor

MIMAS	MIcronized MASterblend
MOX	Mixed OXide
NEA	Nuclear Energy Agency
NFD	Nippon Nuclear Fuel Development
PCCI	Pellet-Cladding Chemical Interaction
PCI	Pellet-Cladding Interaction
PCMI	Pellet-Cladding Mechanical Interaction
PIE	Post-Irradiation Examinations
PNNL	Pacific Northwest National Laboratory
POLIMI	Politecnico di Milano
PWR	Pressurized Water Reactor
OD	Outer Diameter
OECD	Organisation for Economic Co-operation and Development
ORNL	Oak Ridge National Laboratory
PIE	Post Irradiation Examinations
PSI	Paul Scherrer Institut
R&D	Research & Development
RIA	Reactivity-Initiated Accident
RTL	Ramp Terminal Level
SBR	Short Binderless Route
SCC	Stress Corrosion Cracking
SCK	Studiecentrum voor Kernenergie
SEM	Scanning Electron Microscopy
STP	Standard Temperature and Pressure
TEM	Transmission Electron Microscopy

List of symbols

The following list includes the symbols that are of most extensive use in the present report. The other symbols are defined in the text.

A_c	Cross-sectional area of the coolant channel [m²]
A_{gb}	Projected area of grain-boundary bubbles [m³]
b	Irradiation-induced resolution parameter [s⁻¹]
B	Model parameter [m]
bu	Burn-up [at%]
c	Specific heat [J·kg⁻¹·K⁻¹]
C_b	Concentration of intra-granular gas residing in bubbles [(at.)·m⁻³]
C_{gb}	Concentration of gas at the grain boundaries [(at.)·m⁻²]
C_s	Concentration of intra-granular gas existing as single atoms [(at.)·m⁻³]
C_{SB}	Stefan-Boltzmann constant [W·m⁻²·K⁻⁴]
C_t	Concentration of intra-granular gas (single atoms + bubbles) [(at.)·m⁻³]
D_{eff}	Effective intra-granular gas diffusion coefficient [m²·s⁻¹]
d_{gap}	Radial gap width [m]
D_s	Single gas atom diffusion coefficient in grains [m²·s⁻¹]
D_v	Vacancy diffusion coefficient in grain boundaries [m²·s⁻¹]
e	Emissivity [-]
E	Young's modulus [Pa]
F	Fission rate density [(fiss.)·m⁻³·s⁻¹]
F_c	Fraction of grain boundary surface covered by bubbles (fractional coverage) [/]
$F_{c,sat}$	Fractional coverage at grain boundary saturation [/]
$f(r)$	Radial power density distribution function [-]
g	Trapping parameter [s⁻¹]
$h_{cl,c}$	Heat transfer coefficient between the cladding and the coolant [W·m⁻²·K⁻¹]
h_{film}	Heat transfer coefficient in the cladding-coolant convection film [W·m⁻²·K⁻¹]
h_{gap}	Gap conductance [W·m⁻²·K⁻¹]

h_{rad}	Radiative component of the gap conductance [W·m^{-2}·K^{-1}]
h_{con}	Contact pressure contribution to the gap conductance [W·m^{-2}·K^{-1}]
h_g	Conductive component of the gap conductance [W·m^{-2}·K^{-1}]
H	Meyer hardness [Pa]
k	Boltzmann constant [J·K^{-1}]
l_f	Length of a fission fragment track [m]
l_{gas}	Gas extrapolation length [m]
m	Number of fission gas atoms contained in each intra-granular bubble [(at.)]
n_{fgr}	Number of fission gas atoms released into the fuel rod free volume [(at.)]
n_g	Number of fission gas atoms per grain-boundary bubble [(at.)]
N_{gb}	Number density of grain-boundary bubbles [(bub.)·m^{-2}]
$N_{gb,0}$	Initial number density of grain-boundary bubbles [(bub.)·m^{-2}]
N_{ig}	Number density of intra-granular bubbles [(bub.)·m^{-3}]
n_v	Number of vacancies per grain-boundary bubble [(vac.)]
p	Gas pressure in grain-boundary bubbles [Pa]
p_{cool}	Coolant pressure [Pa]
p_{con}	Fuel-cladding contact pressure [Pa]
p_{eq}	Mechanical equilibrium pressure of the gas in grain-boundary bubbles [Pa]
q'	Linear heat rate [W·m^{-1}]
q''	Heat flux [W·m^{-2}]
$q''_{cl,c}$	Heat flux from the cladding to the coolant [W·m^{-2}]
q'''	Power density [W·m^{-3}]
q'''_c	Power density in the coolant [W·m^{-3}]
q'''_{cl}	Heat generation in the cladding [W·m^{-3}]
$\bar{q}'''_{cl}$	Average power density in the cladding [W·m^{-3}]
$\bar{q}'''_f$	Average power density in the fuel [W·m^{-3}]
q_s	Specific power [W·g^{-1}]
r	Radial co-ordinate [m]
R	Radial co-ordinate in the fuel rod deformed geometry [m]

$r_{cl,i}$	Inner cladding radius [m]
$r_{cl,o}$	Outer cladding radius [m]
$r_{f,i}$	Inner fuel radius [m]
$r_{f,o}$	Outer fuel radius [m]
R_{gb}	Radius of curvature of the grain-boundary bubbles [m]
r_{gr}	Grain radius [m]
R_{ig}	Radius of intra-granular bubbles [m]
S	Model parameter [-]
t	Time [s]
T	Temperature [K]
T_c	Bulk coolant temperature [K]
$T_{cl,i}$	Temperature at the inner surface of the cladding [K]
$T_{cl,o}$	Temperature at the outer surface of the cladding [K]
$T_{f,o}$	Temperature at the outer surface of the fuel [K]
V	Volume of fuel [m^3]
V_{gb}	Volume of grain-boundary bubbles [m^3]
w	Coolant velocity [m·s^{-1}]
Y_{fg}	Yield of fission gas atoms [/]
z	Axial co-ordinate [m]
Z_0	Radius of influence of a fission fragment track [m]
α	Coefficient of linear thermal expansion [K^{-1}]
β	Fission gas generation rate [(at.)·m^{-3}·s^{-1}]
γ	fuel/gas specific surface energy [J·m^{-2}]
δ_{gb}	Thickness of the diffusion layer in grain boundaries [m]
$\Delta\overline{R}$	Arithmetic mean roughness [m]
Δt	Time step length [s]
ΔT_{gap}	Temperature drop in the gap [K]
$\Delta V/V$	Fractional variation in fuel volume [/]
$(\Delta V/V)_{ig}$	Volumetric intra-granular fission gas swelling [/]
$(\Delta V/V)_{gas}$	Volumetric fission gas swelling [/]

$(\Delta V/V)_{gb}$	Volumetric grain-boundary fission gas swelling [/]
ε	Strain [/]
ε^{el}	Elastic strain [/]
ε^{ex}	Sum of the non-elastic strains [/]
ε^{gas}	Strain due to fission gas swelling [/]
ε_r	Radial strain [/]
ε_θ	Circumferential strain [/]
ε_z	Axial strain [/]
ε^c_{eff}	Effective creep strain [/]
ε^p	Plastic strain [/]
ε^p_{eff}	Effective plastic strain [/]
θ	Circumferential co-ordinate [m]
Θ	Semi-dihedral angle of the grain-boundary bubbles [°]
λ	Thermal conductivity [W·m^{-1}·K^{-1}]
$\overline{\lambda}$	Average thermal conductivity [W·m^{-1}·K^{-1}]
$\overline{\lambda}_{fc}$	Mean fuel-cladding thermal conductivity [W·m^{-1}·K^{-1}]
λ_{gas}	Thermal conductivity of the plenum gas mixture [W·m^{-1}·K^{-1}]
ν	Poisson's ratio [-]
ξ	Molar concentration [mol·m^{-3}]
ρ	Density [kg·m^{-3}]
ρ_f	Density of the fuel [kg·m^{-3}]
ρ_{ig}	Density of the gas residing in intra-granular bubbles [kg·m^{-3}]
σ_{eff}	Effective (Von Mises) stress [Pa]
σ_h	Hydrostatic stress [Pa]
σ_r	Radial stress [Pa]
σ_z	Axial stress [Pa]
σ_θ	Circumferential stress [Pa]
σ^{dev}	Deviatoric stress [Pa]
σ^{th}	Thermal stress [Pa]

ϕ	Weighting factor used in the thermal analysis [-]
$\varphi(\Theta)$	Geometric factor relating the volume of a lenticular bubble to that of a sphere [-]
ω	Van der Waals' volume of a fission gas atom [m^3·(at.)$^{-1}$]
Ω_{gb}	Vacancy volume in grain-boundary bubbles [m^3]
Ω_{ig}	Volume per gas atom in intra-granular bubbles [m^3]

Chapter 1

Background of the work

Abstract. *The subject of the present work comprises the development and the testing in the TRANSURANUS code of an integrated model of fission gas swelling and release in oxide fuels. Both the development and application aspects of the work are introduced in this chapter, by presenting the physical scope and computer framework. Then, the rationale and objectives of the work are discussed. In Section 1.1, the basic physical mechanisms involved in fission gas swelling and release are summarized. In Section 1.2, the main features of the TRANSURANUS fuel rod analysis code are overviewed. The work objectives are outlined in Section 1.3.*

1.1 Basic mechanisms of fission gas swelling and release

The processes of fission gas generation, diffusion, retention and release have a strong impact on the thermo-mechanical behaviour of the nuclear fuel rods. On the one hand, the fission gases generated in the fuel tend to precipitate into bubbles, resulting in (i) fuel swelling, which may give rise to enhanced pellet-cladding mechanical interaction (PCMI), and (ii) degradation of the fuel thermal conductivity, possibly leading to overheating of the fuel and local melting. On the other hand, fission gas release (FGR) to the free volume of the fuel rod causes pressure build-up and thermal conductivity degradation of the rod filling gas. Consequently, the fuel temperature increases, which in turn may lead to higher FGR (*thermal feedback*) until the rod fails due to cladding ballooning and cladding burst.

The effects of fission gas swelling and release as potential design-limiting factors for the nuclear fuel rods can be particularly marked at high burn-up and during power ramps (Kashibe et al., 1993; Mogensen et al., 1985). In fact, the FGR increases with increasing burn-up and following the power and temperature rise during a power ramp, possibly affecting the integrity of the cladding through increased internal pressure. Moreover, at high burn-up or during power ramps, when PCMI takes place and consequently the fuel deformation affects the deformation of the cladding, the fission gas swelling can give an important contribution to cladding strain and possibly to cladding

failure (OECD/NEA, 2004). In reference to the analyses of Arimescu (2004), fission gas swelling accounted for as much as half of the permanent cladding diametral strain in PWR fuel rods subjected to power ramps to peak power levels of 39.5, 42 and 44 kW·m^{-1}.

In view of the above implications on the thermo-mechanical behaviour of the fuel rods, the treatment of the fission gas swelling and release needs to be covered in fuel rod modelling. The basic mechanisms involved in fission gas swelling and release in oxide fuel during irradiation, which represent the physical scope of the present work, are summarized briefly in the following sub-sections.

1.1.1 Fission gas generation

The yield of the fission products from thermal fission of ^{235}U according to the mass number (A) is reported in Fig. 1.1. The stable xenon (A=131-136) and krypton (A=83-86) isotopes, generally referred to as fission gases, are close to the peaks in the distribution and consequently comprise a significant proportion of the fission products. On average, each fission event produces about 0.3 atoms of Xe and Kr. Due to their extremely low solubility, the fission gases tend either to precipitate into bubbles or to be released from the fuel.

1.1.2 Recoil and knockout

In general, a fission event entails (among others) two fission fragments that transfer their kinetic energy to the fuel lattice. A fission fragment, close enough to a free surface (< 6-7 μm), can escape from the fuel due to its high kinetic energy (60-100 MeV). This is called recoil release. When fission fragments make elastic collisions with the nuclei of lattice atoms, a collision cascade appears. The interaction of a fission fragment, a collision cascade, or a fission track with a stationary gas atom near the surface can also cause the latter to be ejected if it happens within a distance close enough to the surface. This process is called release by knockout. Recoil and knockout can only be observed at temperatures below 1000°C, when thermally activated processes (see the following sub-sections) do not dominate. They are almost temperature-independent and therefore called athermal release mechanisms. Recoil and knockout generally contribute less than 1% to the release of the generated gas (Wise, 1985; Lewis, 1987).
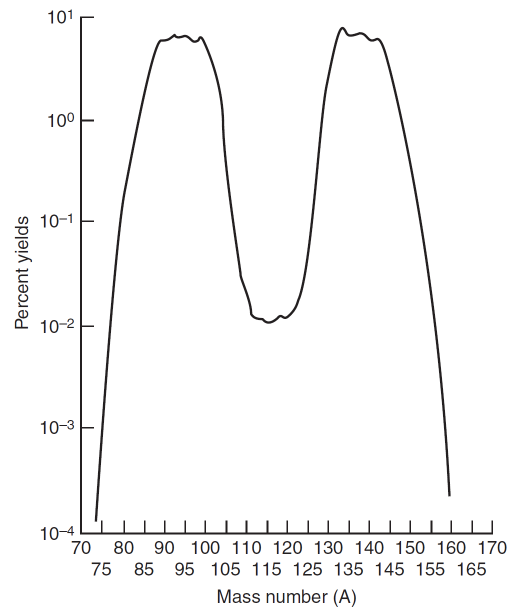
Fig. 1.1. Yield of fission products from thermal fission of 235U according to mass number.

1.1.3 Intra-granular diffusion

The first step for significant release from the fuel is fission gas transport from within the grains to the grain boundaries by intra-granular diffusion of gas atoms through the crystal lattice. Mechanisms for the transport of single Xe and Kr atoms through the fuel were studied by Grimes and Catlow (1991) by considering low-energy migration pathways between solution sites as well as the stability of gas atoms at the solution sites within a defective UO_2 lattice. They postulated a cation vacancy-controlled migration pathway for Xe atoms, for which the mechanism of diffusion involves the association of a cation vacancy to the trap sites. Uranium vacancies as the slower moving species are rate-controlling for most diffusion-related processes in oxide fuel.

Despite the considerable effort in determining the lattice diffusion coefficient of fission gases in oxide fuel (e.g., Matzke, 1980; Turnbull et al., 1982, 1988; Govers et al., 2008), strong variation still exists in the available data. The lattice diffusion coefficient is influenced by the temperature, deviations from stoichiometry and additives (e.g., Cr, Nb), phase changes and therefore also indirectly by the burn-up. Also the fission fragments are supposed to contribute to the diffusion process, which is referred to as irradiation-enhanced diffusion. This is due to the interaction of the fission fragments and the associated irradiation damage cascades with the fission gas atoms in the lattice, resulting in displacement of the gas atoms. Indeed, there is a constant process of slowing

down of fission fragments in the fuel causing fission spikes or tracks to be formed. The fission tracks have a length in the order of 6-7 microns, wherein about 15000 Frenkel pairs are produced instantaneously (Matzke, 1980). Only 5000 pairs remain after direct annihilation. The width of the permanently disturbed zone is of approximately 7 nm. Significant temperature increases along the axis occur causing large stress gradients leading, for instance, to a separation of vacancies from interstitials and hence a largely temperature-independent, irradiation-enhanced diffusion, as well as irradiation-induced resolution of inert gas atoms from intra-granular bubbles or even complete bubble destruction.

Irradiation-induced diffusion dominates at temperatures below 1000°C, indicatively, and is temperature-independent. For temperatures between 1000°C and 1400°C, vacancies controlling the gas atom diffusion are generally assumed to be created both thermally and by the damage cascades related to fission fragments. Above 1400°C, purely thermal (intrinsic) diffusion is considered, that is, diffusion by thermally created vacancies predominates. These three temperature regimes are reflected in the three components of the single gas atom diffusion coefficient proposed by Turnbull et al. (1982, 1988) and often applied in the fuel rod analysis codes (for details, see Section 2.2).

1.1.4   Trapping

In nuclear fuels, either natural (e.g., impurities, dislocation lines, and closed pores) or irradiation-induced imperfections in the solid (e.g., intra-granular fission gas bubbles, vacancy clusters in fission tracks, and solid fission product precipitates) depress the amount of fission gas available for diffusion by temporarily or permanently trapping the migrating atoms.
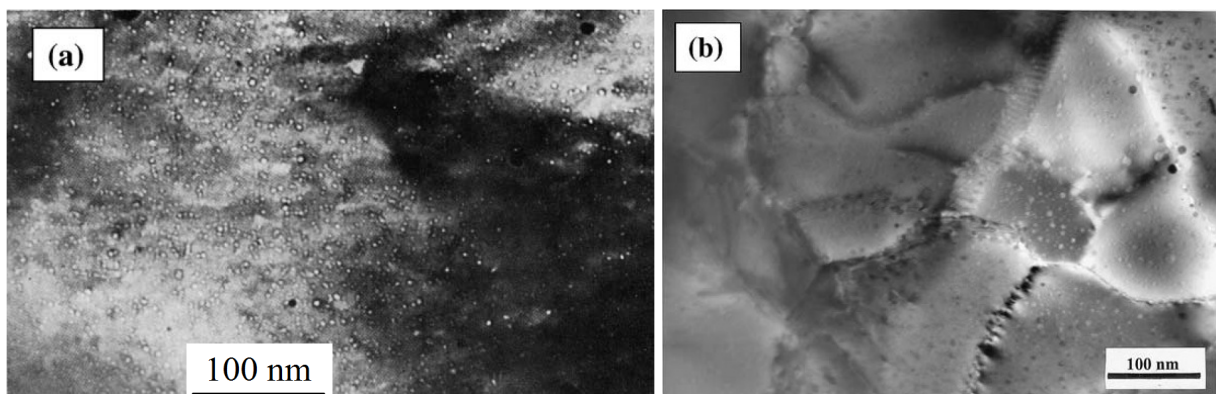

Fig. 1.2. TEM images of intra-granular gas bubbles – from (Olander and Wongsawaeng, 2006).

Experiments show that for burn-ups characteristic of power reactors, gas atom trapping due to intra-granular fission gas bubbles is predominant. Transmission electron microscopy (TEM) images of intra-granular bubbles in irradiated fuel are shown in Fig. 1.2. Experimental observations reveal a population of nanometre-size bubbles within the grains that stabilizes early during irradiation to a bubble size of a few nanometres and bubble densities of ~10^{23}-10^{24} (bub.)·m^{-3} (Cornell et al., 1969; Cornell, 1971; Baker, 1977a, 1977b).

The fission gas swelling induced by intra-granular bubbles is generally less important than the swelling due to grain-boundary bubbles, at least for burn-ups below about 45 GWd·(tM)$^{-1}$ (White and Tucker, 1983; Mogensen et al., 1985; Kashibe et al., 1993).

1.1.5   *Irradiation-induced resolution*

A fraction of the gas atoms trapped into the intra-granular bubbles can be re-dissolved in the lattice through the interaction of the fission fragments with the bubbles. Irradiation-induced resolution of fission gas atoms from bubbles takes place by one of two mechanisms (Olander and Wongsawaeng, 2006). The heterogeneous mechanism occurs by complete destruction of small bubbles by fission fragments passing through or nearby them. The homogeneous mechanism occurs by removal of single fission gas atoms by scattering collisions with fission fragments or uranium recoils whose paths intersect the bubbles. The irradiation-induced resolution process favours intra-granular diffusion of fission gas by countering the effect of trapping into intra-granular bubbles. For (larger) grain-boundary bubbles, irradiation-induced resolution is supposed to be less effective (Rest, 2003; Spino et al., 2005).

1.1.6   *Intra-granular bubble motion*

The motion of intra-granular bubbles provides an additional mechanism with respect to single gas atom diffusion in order to describe fission gas transport to the grain boundaries. Bubble motion was experimentally observed in oxide fuel during post-irradiation annealing experiments (Gulden, 1967; Baker, 1977b), and may significantly contribute to the gas transport to the grain boundaries during power transients and at high temperature (Matthews and Wood, 1979). It is known that diffusion models commonly adopted in the fuel rod analysis codes and based on single gas atom diffusion have a tendency to under-predict the rate of gas transport to the grain boundaries during irradiation at high temperature (Lassmann and Benk, 2000). This tendency may be ascribed to the neglected

contribution of bubble motion to gas diffusion. An approach to the modelling of intra-granular gas diffusion, including an estimation of the effect of bubble motion, is presented in (Van Uffelen et al., 2011).

1.1.7   Grain growth

Grain growth is observed in LWR fuel under irradiation, that is, large grains grow at the expense of smaller ones. Grain growth affects fission gas release in two ways. Firstly, due to the low solubility of the fission gas, the moving grain boundary does not redeposit any gas in the newly formed crystal behind, thus acting as a filter and contributing to the collection of gas at the grain boundaries (*grain boundary sweeping*). Secondly, the average diffusion distance for the fission gas increases as the grain grows, thus tending to reduce the rate of gas transport to the grain boundaries.

1.1.8   Grain-boundary diffusion

It is generally accepted that diffusion in crystalline solids proceeds more rapidly along grain boundaries than through the lattice. This is due to the atomic jump frequency in these planar defects, which is about a million times greater than the jump frequency of regular lattice atoms in stoichiometric materials at 0.6 times the absolute melting temperature (Van Uffelen et al., 2010). Nevertheless, release of fission gas from irradiated fuel is mainly assisted by growth and eventual inter-connection of grain-boundary bubbles (Sub-section 1.1.9). Hence, grain boundary diffusion is only considered to contribute to the inflow of fission gas atoms in the grain-boundary bubbles, rather than to the long-range transport along grain boundaries to the fuel exterior (Olander and Van Uffelen, 2001).

1.1.9   Grain-boundary bubble development

The kinetics of both the fission gas swelling and release is determined by the development of the grain-boundary bubbles. Observations of lightly irradiated fuel reveal large numbers of small, discrete, lenticular bubbles on the grain boundaries. As irradiation proceeds, the size of the bubbles increases due to the inflow of gas atoms and vacancies, and their number density decreases as a consequence of coalescence. The (μm-size) grain-boundary bubbles act to retain the fission gases on the grain boundaries, thereby contributing to swelling (grain-boundary swelling). At high exposures and temperatures, the growing bubbles inter-connect leading to the formation of continuous pathways
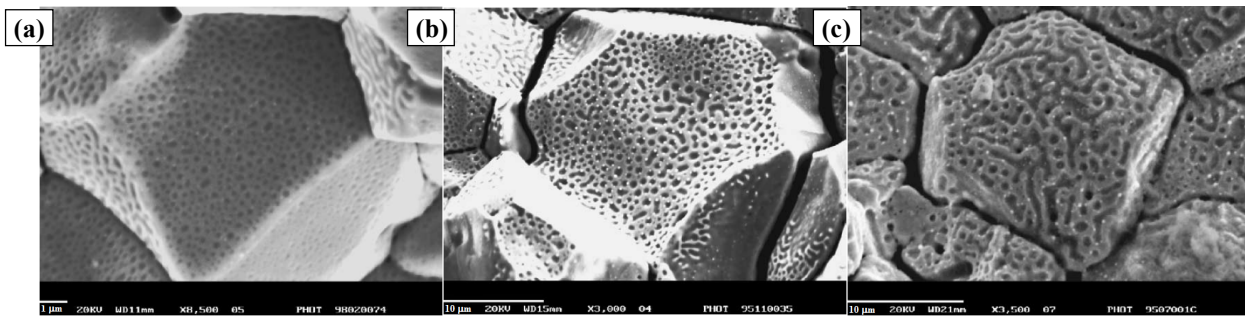
Fig. 1.3. SEM images of grain-boundary gas bubbles in oxide fuel at different irradiation times and conditions. (a) Early stage of bubble development, (b) intermediate stage of bubble development, (c) advanced bubble development – from (White, 2004).

(tunnel network), through which the gas can be released to the fuel rod free volume. The release of gas from the fuel assisted by inter-connection of grain-boundary bubbles is sometimes called thermal FGR (and referred to simply as FGR in this report).

The compressive hydrostatic stress in the fuel was proven to significantly affect both the fission gas swelling and release by inhibiting the growth of the grain-boundary bubbles. This effect may be particularly marked under PCMI conditions, when high compressive hydrostatic stress may develop in the fuel due to cladding restraint (Turnbull and Tucker, 1974; Zimmermann, 1978; Kogai et al., 1988; Walker et al., 1988, Mogensen et al., 1993; Kashibe and Une, 1997).

In Fig. 1.3, scanning electron microscopy (SEM) images of grain-boundary bubbles in oxide fuel at different irradiation times and conditions are presented. Figure 1.3-a shows an example of the very early stages of bubble development, with high bubble density and low bubble size. Figure 1.3-b shows the results of extensive bubble coalescence as an increased bubble size and a reduced bubble density. Figure 1.3-c shows an advanced stage of bubble development, involving the presence of large bubbles and a high degree of inter-connection.

As emerging from the above scenario, the grain-boundary swelling and the FGR are inherently coupled phenomena, since they both ensue from the development of the grain-boundary gas bubbles.

1.2 The TRANSURANUS code

The prerequisite for the application of a physical model to fuel design and licensing is the effective incorporation in a fuel rod analysis code, which provides the framework for the analysis of the

overall (integral) fuel rod behaviour. The TRANSURANUS fuel rod analysis code (Lassmann, 1992) constitutes the computer framework of application of the present work. In particular, reference is made to the v1m1j11 version of the code (Lassmann et al., 2011).

Developed at the Institute for Transuranium Elements (JRC/ITU, Karlsruhe, Germany), the TRANSURANUS code is designed to perform the analysis of a whole nuclear fuel rod based on quasi two-dimensional modelling – that is, the axisymmetric behaviour of the fuel rod is described by axially coupling a stack of one-dimensional radial calculations. The code is written in the FORTRAN 95 programming language (Metcalf et al., 2004), and is featured by a flexible mathematical-numerical structure into which physical models can be incorporated. The fuel rods found in the majority of power reactors can be analysed for a wide range of different situations, as given in experiments, under normal, off-normal and accident conditions. Also, the code incorporates a comprehensive data bank for various fuel, cladding, and coolant materials. The time scale of the problems to be treated may range from milliseconds to years, thanks to the use of advanced numerical solution techniques, which are very fast and stable[3]. The TRANSURANUS code is applied for the design as well as for the licensing of the nuclear fuel, and is used by research centres, universities, industrial partners and nuclear safety authorities.

In Sub-section 1.2.1, an outline of the TRANSURANUS structure is given. Details can be found in (Lassmann et al., 2011).

1.2.1   Structure of the code

According to the geometrical representation exploited by the TRANSURANUS code, the fuel rod is divided into discrete axial positions and radial zones. At every time step, the analysis is firstly carried out for each axial position, and axial coupling is subsequently performed. Given the above approach, the structure of the problem is defined by:

- The analysis of the whole fuel rod at different times.

- The axial coupling for a specific time.

- The analysis at the single axial positions for a specific time.

---

[3] The computational time required for the analysis of a typical LWR fuel rod irradiation history by means of the TRANSURANUS code is of the order of few minutes.

The structure of the TRANSURANUS code reflects the above theoretical structure, the code being designed through the following three levels:

- The first level is the main driver of the code, in which the time integration is organised. The current time, $t_{n+1} = t_n + \Delta t$, is determined, where t_n is the previous time and Δt is the minimum time step given by stability or accuracy criteria.

- The second level controls the axial loop over all the axial positions, i.e., the axial coupling and its convergence.

- The third level controls the analysis at the single axial positions for a specific time, i.e., at this level the thermal and mechanical analyses are performed, for which all physical models are needed.

A simplified schematization of the third level is given in Fig. 1.4, which is limited to the main TRANSURANUS subprograms for the thermal analysis, the mechanical analysis, and the calculation of the fission gas swelling and release. Distinction is made between explicit and implicit models. For an explicit model, the increment during the time step depends only on results of the previous time, t_n. This numerical technique is adequate for slowly varying physical phenomena. For implicit (or mixed explicit-implicit) models, the increment depends on the results at the current time, t_{n+1}, and it is in almost all cases highly non linear. Special procedures for obtaining convergence (iteration schemes) are necessary.

A basic theoretical concept of the computational mechanics in the TRANSURANUS code is that all volume changes due to the various phenomena (e.g., swelling) are expressed via strains. The strains are calculated by means of physical models. Given the strains, the stresses are calculated by means of the equations of the mechanical analysis. This concept represents a common feature of the fuel rod analysis codes (Olander, 1976).

Numerical convergence of the whole thermo-mechanical analysis is obtained through an iteration procedure (Fig. 1.4). It is known that the volume changes related to certain phenomena (e.g., fission gas swelling) are in turn dependent on the stress. The implementation of models for these phenomena that consider the (generally non-linear) physical dependence on the stress involves difficulties concerning the numerical convergence of the fuel rod calculations.
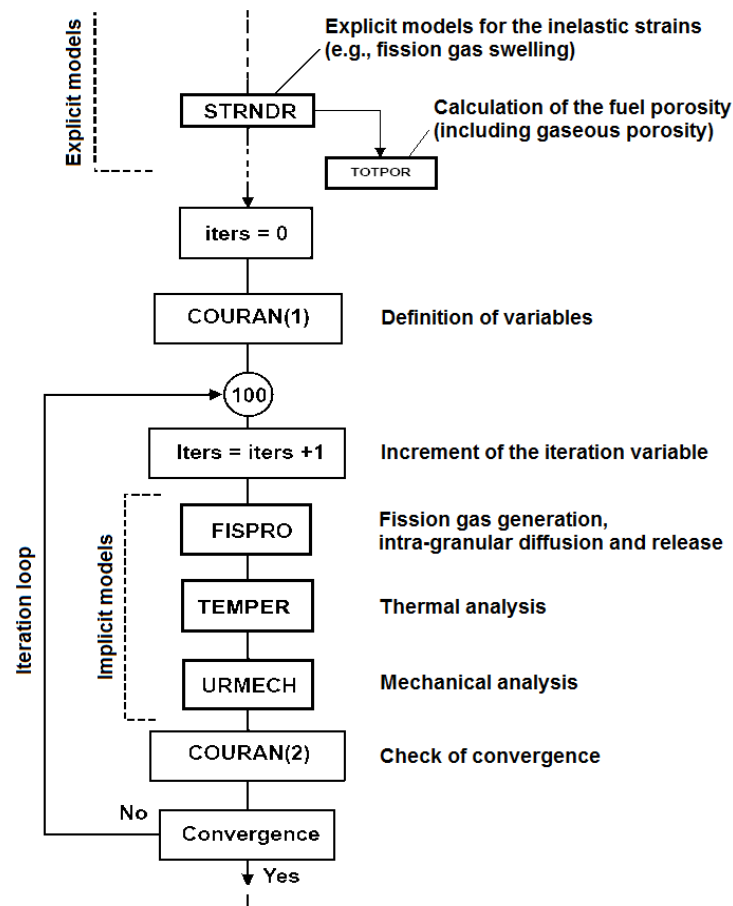
Fig. 1.4. Basic structure of the analysis at a single fuel rod axial position in the TRANSURANUS code. The scheme includes the main subprograms for the thermal analysis, the mechanical analysis, and the calculation of the fission gas swelling and release (Lassmann et al., 2011).

1.2.2   *Standard models of fission gas swelling and release*

In the current version of the TRANSURANUS code, the fission gas swelling and release are described by two distinct models. The standard model for the swelling of oxide fuels (Lassmann et al., 2011) is based on the MATPRO swelling model FSWELL (MATPRO, 1979). In particular, the correlation for the volumetric fission gas swelling reads

$$\Delta\left(\frac{\Delta V}{V}\right)_{gas} = a(T)\,exp(-c\cdot bu)\,\Delta bu\,, \tag{1.1}$$

where $\Delta(\Delta V/V)_{gas}$ [/] is the increment of volumetric fission gas swelling during a time step, *bu* [at%] the burn-up, Δbu the burn-up increment during the time step, and *a*, *c* [(at%)$^{-1}$] are empirical parameters.

The condition $\Delta(\Delta V/V)_{gas} = 0$ is applied in the TRANSURANUS code when contact pressure takes place between the fuel and the cladding. That is, a total inhibition of the fission gas swelling is considered under PCMI conditions (e.g., during a power ramp or at high burn-up), when high compressive hydrostatic stress may arise in the fuel due to cladding restraint. However, this simplified approach do not allow for the significant swelling that (although partially inhibited by the compressive hydrostatic stress) can occur during a power ramp (Arimescu, 2004; Cheon et al., 2004) and at high burn-up (Spino et al., 2005).

The standard model for FGR in oxide fuels (Lassmann et al., 2011) basically consists of two parts:

1. Solution of the equation describing the intra-granular diffusion of the fission gas.

2. Modelling of the inter-connection condition of the grain-boundary gas bubbles.

As concerns the first part, the diffusion equation describing the time evolution of the concentration of gas generated uniformly at a rate β [(at.)·m^{-3}·s^{-1}] within a spherical grain is

$$\frac{\partial C_t}{\partial t} = D_{eff}\, \frac{1}{r^2}\, \frac{\partial}{\partial r}\left(r^2\, \frac{\partial C_t}{\partial r} \right) + \beta, \qquad\qquad (1.2)$$

where C_t [(at.)·m^{-3}] is the concentration of intra-granular gas, *t* [s] the time, *r* [m] the radial co-ordinate in the spherical grain, and D_{eff} [m^2·s^{-1}] the effective diffusion coefficient of fission gas atoms in presence of intra-granular bubbles (see also Section 2.2). Efficient algorithms are implemented in the TRANSURANUS code for the numerical solution of Eq. 1.2 (Elton and Lassmann, 1987; Lassmann and Benk, 2000), allowing the rate of gas transport to the grain boundaries to be calculated. The standard TRANSURANUS option for the effective diffusion coefficient is the correlation of Matzke (1980):

$$D_{eff} = 5 \cdot 10^{-8}\, exp\!\left(-\frac{40262}{T} \right), \qquad\qquad (1.3)$$

where *T* [K] is the temperature.

As concerns the second part of the FGR model, the inter-connection condition of the gas bubbles at the grain boundaries is represented by a concept of grain boundary saturation. It is assumed that, when the concentration of gas at the grain boundaries, C_{gb} [(at.)·m^{-2}], exceeds a specific (empirical) threshold value, all the gas that further reaches the grain boundaries is released to the fuel rod free volume. As standard TRANSURANUS option, the threshold concentration of gas at the grain boundaries is

$$C_{gb,th} = 6.022 \cdot 10^{19} \text{ (at.)·m}^{-2}. \tag{1.4}$$

In addition to the standard option, an alternative treatment is available in the TRANSURANUS code, which is specific for the simulation of power ramps. In fact, enhancement of FGR is expected during rapid power changes due to pellet micro-cracking that means new paths for the release of fission gas (burst release). To allow for this effect, a model was developed, which considers a complete release of the gas inventory at the grain boundaries when empirical conditions defining the power ramp are fulfilled (Van Uffelen et al. 2008, Lassmann et al., 2011). This burst release model is based on that of Koo et al. (2000) and provided improvements in the simulation of FGR for power ramp-tested fuel rods (Van Uffelen et al. 2008, Schubert et al., 2011).

Finally, empirical models are included in the TRANSURANUS code for taking into account the athermal release mechanisms and the grain boundary sweeping effect (Section 1.1), which are not described here for brevity. Details can be found in (Lassmann et al., 2011).

1.2.3   *Previous assessments*

During the preliminary stages of the present work, the predictive capability of the TRANSURANUS code was assessed, in order to identify the main issues in view of code developments (Pastore et al., 2009a, 2009b). In particular, simulations were carried out of irradiation experiments of LWR-UO$_2$ fuel rods, power ramp-tested after base-irradiation to moderate burn-up. The results were compared with experimental data from the International Fuel Performance Experiments (IFPE) database (Sartori et al., 2010). The capabilities of the TRANSURANUS code to analyse the fission gas behaviour (swelling and release) were investigated. From these studies, the following main conclusions were drawn:

- The predictions in terms of FGR at the end-of-life suffer from a moderate but systematic under-estimation of the experimental data.

- Introducing more sophisticated models, properly taking into account the effect of the hydrostatic stress on both the fission gas swelling and the FGR, is necessary for the purpose of properly simulating these phenomena under PCMI conditions.

- In general, incorporating in the code a physics-based model of fission gas swelling and release, taking into account the intrinsic coupling between these phenomena, is advisable.

Open issues are therefore involved in the modelling of fission gas swelling and release in the TRANSURANUS code. More in general, this area currently represents a main subject of the research on fuel rod modelling, and a primary topic of International Projects supporting the development of fuel rod analysis codes, such as the Coordinated Research Project FUMEX-III (FUel Modelling at EXtended burn-up) of the IAEA (Killeen et al., 2009).

1.3   Main objectives of the work

The present work aims at providing a contribution to the modelling of fission gas swelling and release in the fuel rod analysis codes, with specific application to the TRANSURANUS code. In particular, the goals of the work include:

1. The development of a physics-based, integrated model of fission gas swelling and release in oxide fuel oriented to the application to fuel rod analysis codes, which incorporates a consistent description of the dependence of both phenomena on the hydrostatic stress.

2. The demonstration of the applicability of the developed model to the fuel rod analysis codes (hence, to fuel design and licensing) by implementation in the TRANSURANUS code and meeting of the basic requirements, in terms of numerical convergence and computational times.

3. The employment in fuel rod analyses and verification of the new model through assessment of the results against irradiation data.

The achievement of the above goals requires the construction of a modelling approach, which combines an appropriate physics-based treatment and the simplicity that is a prerequisite for the effective application to the fuel rod analysis codes. The stress-dependence represents a challenging issue in view of the implementation of the new model in the TRANSURANUS code, relating to the

implied necessity of numerically treating a mutual and non-linear dependence between stresses and strains (Sub-section 1.2.1). For the verification of the model, reference will be made to fuel irradiation data from the IFPE database (Sartori et al., 2010).

Chapter 2

An integrated model of fission gas swelling and release

Abstract. *A new model is presented for the calculation of both the fission gas swelling and release in oxide fuel during irradiation. The emphasis is on the modelling of the grain-boundary gas bubble development, which involves the basic issues in demonstrating the applicability of a physics-based, integrated and stress-dependent treatment of the fission gas swelling and release to the fuel rod analysis codes. The model incorporates the fundamental physical processes of gas diffusion and precipitation in grains, growth and coalescence of the grain-boundary bubbles, and gas release from the grain boundaries to the fuel rod free volume. Following an engineering approach, representations of the processes from the literature are revisited and combined in a treatment, characterized by a level of simplicity that allows effective application to the fuel rod analysis codes. The chapter is organized as follows. In Section 2.1, the general modelling approach is introduced. In Section 2.2, a simple and preliminary treatment of the intra-granular gas diffusion and swelling is described. In Section 2.3, the treatment of the gas behaviour at the grain boundaries is discussed, which comprises the original contributions related to the model development aspect of the present work. Conclusions are drawn in Section 2.4.*

2.1   Introduction

The fundamental physical processes, which control the kinetics of fission gas swelling and release in irradiated oxide fuel and were discussed in some detail in Section 1.1, may be summarized as follows. Fission gas atoms generated in the fuel grains partly precipitate into intra-granular bubbles, leading to intra-granular swelling (Mogensen et al., 1985; Kashibe et al., 1993). At the same time, a fraction of the gas atoms diffuse towards the grain boundaries through repeated trapping in and irradiation-induced resolution from intra-granular bubbles (Speight, 1969; Olander, 1976; Matzke, 1980; White and Tucker, 1983; Lösönen, 2000; Olander and Wongsawaeng, 2006). Although a part of the gas atoms that reach the grain boundaries are dissolved back to the grain interior by irradiation (Manley, 1968; Van Uffelen, 2002; Rest, 2003; Kim, 2004), the majority of the grain-

boundary gas precipitates and diffuses into grain-boundary bubbles acting to increase the bubble internal pressure and generally maintaining bubbles in a non-equilibrium state (White, 2004). Grain-boundary bubbles grow with inflow of gas atoms from within the grains, and with accompanying absorption of vacancies from the grain boundaries driven by the bubble over-pressure (Speight and Beere, 1975; White, 2004), thereby contributing to gas retention and swelling. Bubble growth and the associated mechanisms of bubble coalescence and inter-connection eventually lead to the formation of a tunnel network through which a fraction of the gas reaching the grain boundaries is released to the fuel rod free volume (Turnbull, 1974; Turnbull and Tucker, 1974; Tucker and White, 1979; White and Tucker, 1983; Mogensen et al., 1985). The inherently coupled kinetics of fission gas swelling and release calls for the development of physics-based, integrated models of these phenomena to be employed in fuel rod modelling (Aybar and Ortego, 2005; Calvin and Nowak, 2010). As of today, however, empirical or semi-empirical approaches are widely adopted in the fuel rod analysis codes. The model presented in this report incorporates the above processes in order to evaluate the fission gas swelling and release on a physical basis. The model is kept as simple as possible in view of (i) the efficient application to the fuel rod analysis codes and the related stringent computational cost requirements, (ii) the uncertainties pertaining to fuel rod analysis (Lassmann, 1980), and (iii) the uncertainties associated to some of the model parameters like the gas atom diffusion coefficient (at least a factor of 10) (White and Tucker, 1983; Matzke, 1980; White, 1994). The model is comprised of two modules, which describe the gas behaviour within the grains and at the grain boundaries, respectively. The main assumptions and equations of the model are discussed in the following sections.

2.2 Intra-granular gas behaviour

The first step in fission gas swelling and release consists of the mutually dependent processes of gas diffusion within the fuel grains (intra-granular diffusion) and development of the intra-granular bubble population (Section 1.1). Modelling of these two processes allows estimating the arrival rate of gas at the grain boundaries and the fission gas swelling induced by intra-granular bubbles (intra-granular swelling), the former providing the source term for the grain-boundary gas behaviour model. In the fuel rod analysis codes, the intra-granular gas diffusion is generally treated assuming the fuel grains to be spherical and making use of an effective diffusion coefficient allowing for the

effect of the intra-granular bubbles, which was firstly introduced by Speight (1969). The calculation of the effective diffusion coefficient is often based on empirical correlations, rather than on physics-based modelling of the intra-granular bubble development. Also, the intra-granular swelling contribution is usually not distinguished from the contribution due to grain-boundary bubbles, and calculated empirically. The above approach to the modelling of the intra-granular gas behaviour is adopted, for instance, in the TRANSURANUS code (Section 1.2).

The model developed in this work includes an intra-granular module, which is intended as a first step towards the physics-based description of the intra-granular bubble development and the related effects on fission gas swelling and diffusion. The proposed treatment allows to estimate in a simple way the characteristics of the intra-granular bubbles and the related impact on the effective diffusion coefficient, as well as the intra-granular swelling. However, the basic issues in demonstrating the applicability of an integrated and stress-dependent model of fission gas swelling and release to the fuel rod analysis codes concern the modelling of the gas behaviour at the grain boundaries. It is therefore underlined that a detailed description of the development of the intra-granular bubble population is beyond the scope of the present work, and the proposed treatment is to be considered as preliminary. Further developments concerning the modelling of the intra-granular gas behaviour are underway, as discussed in (Van Uffelen et al., 2011). The treatment of the intra-granular gas behaviour, as applied in the present work, is outlined in Sub-sections 2.2.1 and 2.2.2.

2.2.1   Intra-granular fission gas diffusion

The models for intra-granular diffusion of fission gas adopted in the fuel rod analysis codes almost invariably rely on the formulation of Speight for the problem of diffusion of gas atoms in presence of gas bubbles (Speight 1969). The formulation of Speight is based on the assumptions that (i) single gas atoms diffuse through the crystal lattice with a single atom diffusion coefficient, D_s [m^2·s^{-1}], (ii) gas bubbles are immobile, (iii) gas atoms are absorbed into bubbles at a rate g [s^{-1}] (trapping parameter), (iv) gas atoms are knocked back from bubbles into the lattice at a rate b [s^{-1}] (irradiation-induced resolution parameter), and (v) trapping and irradiation-induced resolution are in equilibrium (quasi-stationary approach), giving

$$\frac{C_s}{C_b} = \frac{b}{g},$$

(2.1)

where C_s [(at.)·m^{-3}] is the concentration of intra-granular gas existing as single atoms, and C_b [(at.)·m^{-3}] is the concentration of intra-granular gas residing in bubbles. In this respect, the ratio $b/(b+g)$ may be considered as the fraction of intra-granular gas that exists as single atoms and is therefore available for diffusion.

Under the above assumptions, the intra-granular diffusion in presence of bubbles may be evaluated by solving a single diffusion equation, instead of a diffusion equation for the single gas atoms coupled with an equation for the gas balance in the bubbles. The diffusion equation reads in one-dimensional spherical geometry

$$\frac{\partial C_t}{\partial t} = D_{eff} \frac{1}{r^2} \frac{\partial}{\partial r}\left(r^2 \frac{\partial C_t}{\partial r}\right) + \beta,$$

(2.2)

where C_t [(at.)·m^{-3}] is the total concentration of intra-granular gas (as single atoms + in bubbles), t [s] the time, D_{eff} [m^2·s^{-1}] the effective diffusion coefficient, and r [m] the radial co-ordinate in the spherical grain. The gas generation rate, β [(at.)·m^{-3}·s^{-1}], is given by $Y_{fg}F$, where Y_{fg} [(at.)·(fiss.)$^{-1}$] is the yield of fission gas atoms and F [(fiss.)·m^{-3}·s^{-1}] the fission rate density. Eq. 2.2 is formally identical to the equation solved by Booth (1957) for the case of diffusion of single gas atoms in absence of bubbles, where the single atom diffusion coefficient is replaced by the effective diffusion coefficient (Speight, 1969)

$$D_{eff} = \frac{b}{b+g} D_s.$$

(2.3)

Considering the effects of trapping in and irradiation-induced resolution from intra-granular bubbles, the *apparent* diffusion rate of gas atoms under irradiation is therefore described by a lower (effective) diffusion coefficient, since only a fraction $b/(b+g)$ of the gas – namely, the fraction existing as single atoms – contributes to diffusion, while the remaining fraction $g/(b+g)$ is trapped into immobile bubbles. Adopting Eqs. 2.2 and 2.3 implies considering the parameters g, b and D_s as spatially independent within a grain (Speight, 1969; Wood and Matthews, 1980). Also, when

adopting the quasi-stationary approach (Eq. 2.1), one assumes that equilibrium between trapping and resolution occurs on a shorter time scale than that of variation of the parameters g and b. This assumption is graver for rapidly changing power or temperature conditions.

The effective diffusion coefficient is often considered as a parameter in the fuel rod analysis codes (e.g., Lassmann, 1992, 2001). In order to obtain a more physical treatment, the effective diffusion coefficient may be calculated from the single atom diffusion coefficient, D_s, by means of Eq. 2.3. In this case, modelling is needed of the intra-granular bubble population, whose characteristics determine the magnitudes of the parameters g and b. As resulting from transmission electron microscopy (TEM) examinations of irradiated oxide fuel, the salient characteristics of the intra-granular bubble population are the high concentration ($\sim 10^{23}$-10^{24} (bub.)·m^{-3}) and the small, nearly-uniform size of the bubbles (typically $\sim$ 2 nm diameter). In the present work, a preliminary approach to the modelling of the intra-granular bubble development is attempted, by adopting the following simplifying assumptions:

- Intra-granular bubbles are spherical, homogeneously distributed and of equal size (Ham, 1958; Cornell, 1971; Turnbull, 1971; White and Tucker, 1983; Lösönen, 2002; Massih and Forsberg, 2008).

- The gas residing in the intra-granular bubbles is equally distributed in the bubbles.

- The number density of the intra-granular bubbles, N_{ig}, remains constant throughout irradiation at an initially nucleated level. A value $N_{ig} = 7 \cdot 10^{23}$ (bub.)·m^{-3} (Olander and Wongsawaeng, 2006) is adopted. Considering a fixed number density of bubbles is consistent with the model of Speight (1969). Nevertheless, this assumption may be questioned, since dependence of the bubble number density on both burn-up and temperature was experimentally observed (Baker, 1977a; Mogensen et al, 1985; Kashibe et al., 1993). However, the bubble number density is approximately constant for temperatures up to about 1600°C (Cornell et al., 1969; Cornell, 1971), pertaining to LWR fuel under normal operating conditions.

- The volume occupied by each gas atom inside the intra-granular bubbles, Ω_{ig}, is constant and equal to $3 \cdot 10^{-29}$ m^3, which corresponds to a constant gas density of $\sim 7 \cdot 10^3$ kg·m^{-3} and is appropriate for bubble radii ranging from 0.5 to 2 nm (Olander and Wongsawaeng, 2006). The assumption of constant gas density follows from the observation that the intra-granular bubbles

are small enough that the surface-tension stress keeps the gas density near that of solid xenon (Lösönen, 2000; Olander and Wongsawaeng, 2006).

Under the above assumptions, the radius of a bubble containing m fission gas atoms is given by

$$R_{ig} = Bm^{1/3},$$
(2.4)

where $B = (3\Omega_{ig}/4\pi)^{1/3} = 2\cdot10^{-10}$ m. The number of fission gas atoms contained in each bubble, m, is calculated as

$$m = \frac{C_b}{N_{ig}},$$
(2.5)

where, considering that $C_t = C_s + C_b$ and adopting the quasi-stationary approach (Eq. 2.1), C_b is given by

$$C_b = \frac{g}{g+b} C_t.$$
(2.6)

In order to evaluate the effective diffusion coefficient consistently with the above treatment of the intra-granular bubbles, analytical descriptions are needed of the three parameters appearing in the right-hand side of Eq. 2.3. In the present model, the three-term formulation for the single atom diffusion coefficient, D_s, proposed by Turnbull et al. (1982, 1988) and used by many authors (e.g., White and Tucker, 1983; Bernard et al., 2002; Lösönen, 2000) is adopted:

$$D_s = D_1 + D_2 + D_3,$$
(2.7)

where D_1 represents high temperature intrinsic diffusion by means of thermally activated vacancies, and D_2 and D_3 represent the effect of irradiation enhancement. The first two terms are calculated as

$$D_1 = 7.6\cdot10^{-10} \, exp\left(-\frac{4.86\cdot10^{-19}}{kT}\right),$$
(2.8)

$$D_2 = 3.22\cdot10^{-16} \sqrt{q_s} \, exp\left(-\frac{1.90\cdot10^{-19}}{kT}\right),$$
(2.9)

where k [J·K^{-1}] is the Boltzmann constant, T [K] the temperature, and q_s [W·g^{-1}] the specific power. The purely rating dependent term, D_3, is not taken into account, since it has no visible effect on the diffusion of stable gas atoms (White, 1994, Lösönen, 2002). Applying q_s = 30 W·g^{-1} produces the single atom diffusion coefficient as a function of the temperature presented in Fig. 2.1, where experimental data from Matzke (1980) and White (1994) are also shown. It can be noticed that the uncertainties related to the experimental data are extremely high, which unavoidably limits the accuracy of fission gas behaviour calculations. This may justify the adoption of simple models of fission gas swelling and release in the fuel rod analysis codes.

The following expressions are adopted for the trapping and the irradiation-induced resolution parameters (Ham, 1958; White and Tucker, 1983):

$$g = 4\pi D_s R_{ig} N_{ig} , \tag{2.10}$$
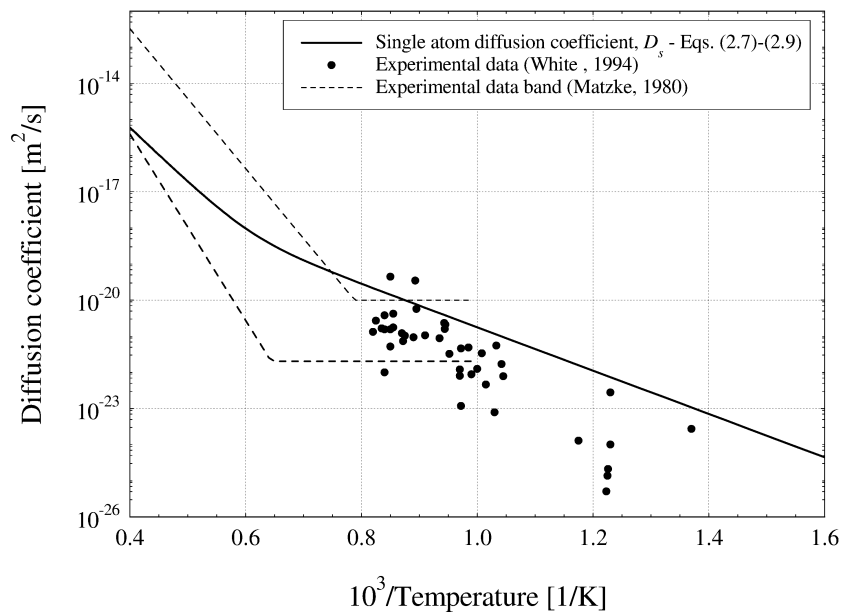
$$b = 3.03 F \pi l_f \left(R_{ig} + Z_0 \right)^2 , \tag{2.11}$$

Fig. 2.1. Single atom diffusion coefficient according to Turnbull et al. (1982, 1988) (q_s = 30 W·g^{-1}) and experimental data from White (1994) and Matzke (1980).

where l_f [m] is the length of a fission fragment track and Z_0 [m] the radius of influence of a fission fragment track. The values l_f =6·10^{-6} m and Z_0=10^{-9} m (White and Tucker 1983) are used in the new model, while the calculation of N_b and R_b is performed as described above.

Figure 2.2 shows an analytical study of the effective diffusion coefficient, D_{eff}, as a function of the temperature, obtained by introducing Eqs. 2.7-2.11 in Eq. 2.3. Only for the purpose of this analytical study, typical LWR values are used for the specific power and fission rate density. Moreover, an empirical correlation proposed by White and Tucker (1983) and based on the experimental data of Baker (1977a) is used for the intra-granular bubble radius, which reads R_{ig} = 5·10^{-10}[1+106exp(1.2·10^{-19}/(kT))]. The study is therefore aimed at giving a qualitative account of the effect of the intra-granular bubbles on gas atom diffusion, rather than at accurately assessing the effective diffusion coefficient as calculated by the model (that depends on the specific irradiation conditions to which the model is applied). For this purpose, the single atom diffusion coefficient, D_s (Eqs. 2.7-2.9) and the fraction of gas existing as single atoms, $b/(b+g)$, are also shown. With increasing temperature, D_{eff} (full grey line) is increasingly attenuated compared to D_s. The attenuation corresponds to the decrease of the fraction of gas that exist as single atoms and is therefore available for diffusion, which is due to enhancement of the trapping effect with increasing temperature.

The formulation of Speight for the effective diffusion coefficient, which is adopted here, has a tendency to under-predict the rate of gas transport to the grain boundaries during irradiation at high temperature (Lassmann and Benk, 2000). Under these conditions, a considerable fraction of the intra-granular gas is trapped into bubbles (Fig. 2.2), and bubble motion (not considered in the formulation of Speight) may significantly contribute to intra-granular gas diffusion (see also Section 1.1). The model presented in (Van Uffelen et al., 2011), which is a development of the preliminary treatment of the intra-granular gas behaviour described in this section, comprises an extension of the formulation of Speight, including an estimation of the contribution of bubble motion to fission gas diffusion.
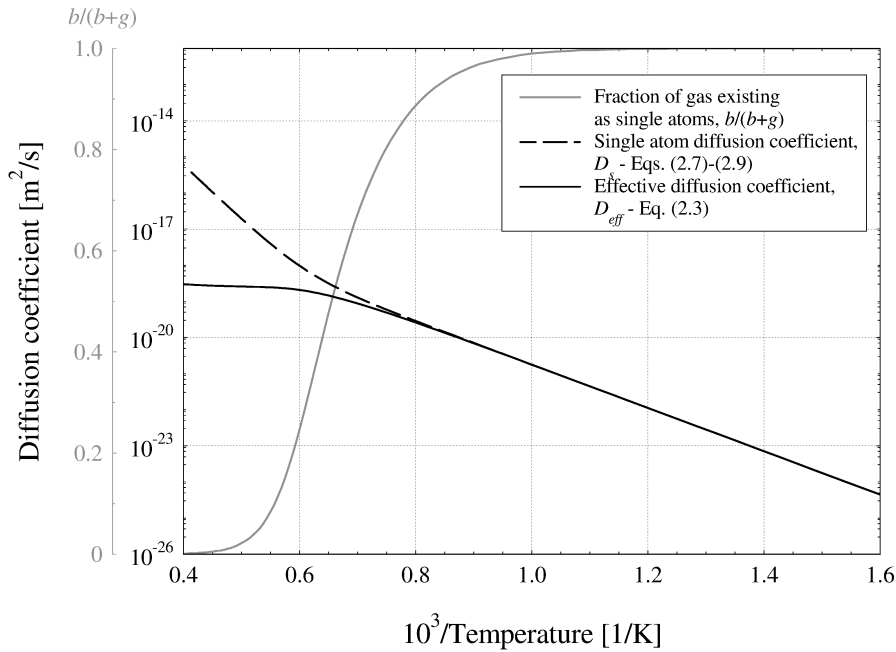
Fig. 2.2. Single atom diffusion coefficient according to Turnbull et al. (1982, 1988) compared with the effective diffusion coefficient. The calculated fraction of gas existing as single atoms is also shown. Values adopted for the parameters: $q_s = 30$ W·g^{-1}, $F = 10^{19}$ (fiss.)·m^{-3}·s^{-1}, $R_{ig} = 5\cdot10^{-10}[1+106\exp(1.2\cdot10^{-19}/(kT))]$ (White and Tucker, 1983).

2.2.2   Intra-granular fission gas swelling

The simple treatment of the intra-granular bubble development described in Sub-section 2.2.1 allows to estimate, in a preliminary way, the intra-granular contribution to the swelling. Under the assumptions discussed in Sub-section 2.2.1, the volumetric intra-granular fission gas swelling, normalized to the unit volume of fuel, is given by

$$\left(\frac{\varDelta V}{V}\right)_{ig} = N_{ig}\left(\frac{4}{3}\pi R_{ig}^3\right). \tag{2.12}$$

2.2.3   Calculation sequence

The following calculation sequence is adopted in applying the intra-granular module at each computational time step:

(i)   The trapping and irradiation-induced resolution parameters are estimated by means of Eqs. 2.10 and 2.11, using the intra-granular bubble radius calculated at the previous time step. At

the first time step, an initial bubble radius R_{ig} = 0.5 nm (lower limit) is adopted (e.g., Govers et al., 2008).

(ii)   The effective diffusion coefficient is calculated by means of Eq. 2.3.

(iii)   The variation of the intra-granular gas concentration during the time step is calculated by numerical solution of Eq. 2.2, thus allowing calculation of both the intra-granular and grain-boundary gas concentrations at the current time step.

(iv)   The concentration of intra-granular gas residing in bubbles is calculated by means of Eq. 2.6.

 (v)   The number of gas atoms contained in each bubble is calculated by means of Eq. 2.5.

(vi)   The bubble radius is calculated by means of Eq. 2.4.

(vii)   The intra-granular fission gas swelling is calculated by means of Eq. 2.12.

2.3   Grain-boundary gas behaviour

The intra-granular diffusion of fission gas determines the arrival rate of gas at the grain boundaries, thus driving the development of the grain-boundary bubble population. The development of the grain-boundary bubbles in turn determines the kinetics of both the grain-boundary contribution to the swelling and the FGR (Section 1.1). The fission gas swelling induced by grain-boundary bubbles (grain-boundary swelling) is generally more important than the intra-granular swelling, at least for burn-ups below about 45 GWd·(tM)$^{-1}$ (White and Tucker, 1983; Mogensen et al., 1985; Kashibe et al., 1993).

The grain-boundary module of the new model consists of a conveniently simple description of the fundamental processes governing the development of the grain-boundary bubble population, allowing the physics-based and integrated calculation of the fission gas swelling and release, as inherently coupled phenomena. The dependence of the processes on the compressive hydrostatic stress in the fuel, acting to constrain bubble growth and consequently affecting both the swelling and the FGR (Turnbull and Tucker, 1974; Zimmermann, 1978; Kogai et al., 1988; Walker et al., 1988, Mogensen et al., 1993; Kashibe and Une, 1997), is consistently considered. Properly taking into account the role of the hydrostatic stress in fission gas swelling and release is of particular importance for the analysis of the fuel rod behaviour at extended burn-up or during power ramps (when high compressive hydrostatic stress may develop in the fuel due to strong PCMI) and of the related, safety-relevant issues in terms of fuel rod structural integrity (OECD/NEA, 2004).

Nevertheless, introducing the stress-dependence of the swelling in a model to be applied to the fuel rod analysis codes represents a major challenge from the viewpoint of the numerical stability of the fuel rod calculations.

2.3.1   Main assumptions

In order to simplify the problem, the developed model involves the following main assumptions:

- The grain-boundary gas bubbles are considered to reside at the interfaces between two grains (grain faces). Peculiarities related to the presence of grain edges (where three grains meet) are neglected (e.g., Kogai, 1997; Massih and Forsberg, 2008).

- An initial concentration of grain-boundary bubbles (nucleation centres), $N_{gb,0}$ [(bub.)·m^{-2}], is given, and no further nucleation is considered during the irradiation. This corresponds to the assumption that the geometric size of the initial population leads to absorption of any newly nucleated bubble, giving the effect that the nucleation is a one-off process (White, 2004). The choice of $N_{gb,0}$ is not too critical since the concentration of bubbles falls very quickly once bubble growth and coalescence commence (White, 2004). In the present model, a value $N_{gb,0}=$ $4 \cdot 10^{13}$ (bub.)·m^{-2} is adopted, in line with Cheon et al. (2004) and consistently with experimental observations pointing out bubble number densities between $1 \cdot 10^{13}$ (bub.)·m^{-2} and $5 \cdot 10^{13}$ (bub.)·m^{-2} (White, 2004).

- The absorption rate of gas at the grain-boundary bubbles equals the rate of gas transport to the grain boundaries. This corresponds to the hypothesis of instantaneous absorption at the bubbles of the gas atoms reaching the grain boundaries. A more accurate description could be obtained by solution of the full time-dependent diffusion equation, but numerical solutions indicate this to be an unnecessary refinement (White, 2004). The validity of this approximation follows from the large difference between the lattice and grain boundary diffusivities of gas atoms (a factor of 10^2-10^6 in the temperature range from 1000°C to 1700°C (Olander and Van Uffelen, 2001)).

- The gas on the grain boundaries is equally distributed in the grain-boundary bubbles.

- The gas residing in the grain-boundary bubbles obeys the Van der Waals' equation of state.

- All the grain-boundary bubbles have, at any instant, equal size and equal lenticular shape of circular projection. A uniform, average bubble size is therefore considered at any instant (mean-field approximation, e.g., Veshchunov, 2008).

- The flux of gas atoms dissolved from the grain boundaries back to the grain interior by irradiation is neglected (Rest, 2003; Spino et al., 2005).

- The athermal (recoil and knock-out) release mechanisms (Section 1.1), which contribute less than 1% to the release of the generated gas (Wise, 1985; Lewis, 1987), are not considered.

The new model describes the grain-boundary bubble growth, coalescence and inter-connection in order to estimate the kinetics of the bubble size and number density, allowing for their time dependence and interrelation. For this purpose, the development of the grain-boundary bubbles may be conveniently considered as resulting from the following processes:

1. The growth of bubbles through the collection of fission gas atoms and vacancies.

2. The mutual interaction between bubbles through coalescence leading to larger but fewer bubbles.

3. The release of fission gas from the grain boundaries to the fuel rod free volume.

The modelling of these processes is discussed in Sub-sections 2.3.2, 2.3.3 and 2.3.4.

2.3.2   Bubble growth

Mechanical equilibrium requires that the pressure of the gas in the bubble is balanced by the surface tension force and the hydrostatic stress. The mechanical equilibrium pressure, p_{eq} [Pa], of the gas in a lenticular bubble of circular projection is given by

$$p_{eq} = \frac{2\gamma}{R_{gb}} - \sigma_h, \tag{2.13}$$

where γ [J·m^{-2}] is the fuel/gas specific surface energy, R_{gb} [m] the bubble radius of curvature, and σ_h [Pa] the hydrostatic stress (considered to be negative if the solid medium is under compression). Although the assumption that the grain-boundary bubbles are always in mechanical equilibrium has been largely adopted in fission gas behaviour models (e.g., Koo et al., 2000; Massih and Forsberg, 2008; Veshchunov, 2008), in general the grain-boundary gas bubbles exist in a non-equilibrium state and tend to restore equilibrium by absorption or emission of vacancies. The model of Speight and Beere (1975) describes the growth (or shrinkage) of the grain-boundary bubbles as proceeding

by absorption (or emission) of vacancies in grain boundaries, induced by the difference between the pressure of the gas in the bubble, p [Pa], and the mechanical equilibrium pressure. The vacancy absorption/emission rate at a bubble is given by

$$\frac{dn_v}{dt} = \frac{2\pi D_v \delta_{gb}}{kTS}\left(p - p_{eq}\right), \tag{2.14}$$

where n_v [(vac.)] is the number of vacancies in the bubble, D_v [$m^2 \cdot s^{-1}$] the vacancy diffusion coefficient in grain boundaries, δ_{gb} [m] the thickness of the diffusion layer in grain boundaries, and S [-] is calculated as (White, 2004)

$$S = -\frac{1}{4}\left[\left(3 - F_c\right)\cdot\left(1 - F_c\right) + 2\,ln\left(F_c\right)\right], \tag{2.15}$$

with F_c (/) being the fraction of grain boundaries covered by bubbles (fractional coverage). The following expression is used in the developed model for the vacancy diffusion coefficient in grain boundaries (Reynolds and Burton, 1969; Kogai, 1997):

$$D_v = 6.9\cdot 10^{-4}\,exp\left(-\frac{5.35\cdot 10^{-19}}{kT}\right), \tag{2.16}$$

and a value $\delta_{gb} = 5\cdot 10^{-10}$ m is used in line with Kogai (1997).

For describing the thermodynamic state of the grain-boundary bubbles, the Van der Waals' equation of state is adopted[4]:

$$p\left(V_{gb} - n_g\omega\right) = n_g kT\,, \tag{2.17}$$

where n_g [(at.)] is the number of fission gas atoms per bubble, k [$J\cdot K^{-1}$] the Boltzmann constant, T [K] the temperature, V_{gb} [m^3] the bubble volume, and ω [$m^3\cdot(at.)^{-1}$] the Van der Waals' volume of a fission gas atom. Given that each bubble consists of vacancies and gas atoms, the volume of a bubble comprising n_g fission gas atoms and n_v vacancies is given by

$$V_{gb} = n_g\omega + n_v\Omega_{gb}, \tag{2.18}$$

---

[4] For gases such as Xe and Kr, which are of interest here, the correction for the pressure in the Van der Waals' equation of state is relatively small and can be neglected (e.g., Olander, 1976; Massih and Forsberg, 2008). This simplification was introduced in Eq. (2.17).

where Ω_{gb} [m^3] is the atomic (vacancy) volume in the bubble. A value $\Omega_{gb} = 4.09 \cdot 10^{-29}$ m^3 is adopted in the model (Kogai, 1997). Combination of Eqs. 2.17 and 2.18 gives for the pressure of the gas in the bubble

$$p = \frac{kT}{\Omega_{gb}} \frac{n_g}{n_v},$$

(2.19)

The above approach was proposed earlier by White (2004) and allows to calculate the bubble growth rate from the rate of inflow of gas atoms along with the rate of absorption (emission) of vacancies in the bubble. The combined effects of gas atom inflow and vacancy absorption (emission) are interactive, since the addition of fission gas atoms gives rise to a change in the bubble pressure via Eq. 2.19, which immediately affects the propensity of the bubble to absorb (or emit) vacancies through Eq. 2.14. Also, the hydrostatic stress, σ_h, affects the mechanical equilibrium pressure (Eq. 2.13) and hence the bubble growth rate through Eq. 2.14.

Given the volume, V_{gb}, of a lenticular bubble of circular projection, the bubble radius of curvature is calculated as

$$R_{gb} = \left(\frac{3V_{gb}}{4\pi\varphi(\Theta)} \right)^{1/3}.$$

(2.20)

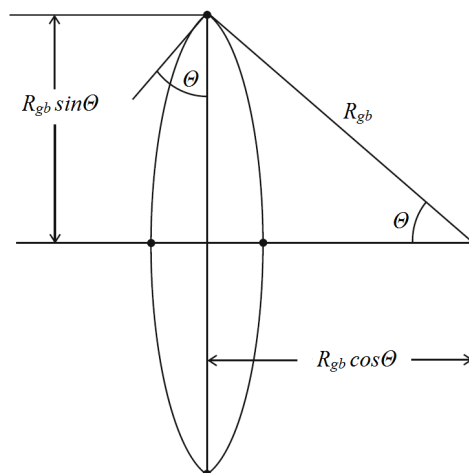where Θ is the semi-dihedral angle of the bubble.

Fig. 2.3. Schematic representation (cross-sectional view) of a lenticular grain-boundary bubble with radius of curvature R_{gb}.

The geometric factor, $\varphi(\Theta)$, relating the volume of a lenticular-shape bubble to that of a sphere, is given by

$$\varphi(\Theta) = 1 - 1.5\cos\Theta + 0.5(\cos\Theta)^3. \tag{2.21}$$

The conventionally accepted value for Θ is 50°. Figure 2.3 shows a schematic of a grain-boundary bubble as represented in the model. The projected area of the bubble, A_{gb} [m^2], is given by

$$A_{gb} = \pi(\sin\Theta)^2 R_{gb}^2, \tag{2.22}$$

and the fractional coverage, F_c [/], is given by

$$F_c = A_{gb}N_{gb}, \tag{2.23}$$

where N_{gb} [(bub.)·m^{-2}] is the number density of grain-boundary bubbles. In view of the experimental observations showing that N_{gb} markedly varies throughout the irradiation (Section 1.1), a variable bubble number density model is introduced. The time evolution of the bubble number density is evaluated on a physical basis, by describing the underlying processes of bubble coalescence and FGR, as discussed in the following sub-sections.

2.3.3 Bubble coalescence

In the coalescence process, grain-boundary bubbles intersect and merge into larger but fewer bubbles. Bubble growth brings about mechanical interference between bubbles and coalescence, and consequent progressive reduction in the bubble number density and increase in the average bubble size (Section 1.1). Given that each bubble consists of vacancies and gas atoms, the coalescence event must preserve the volume of the interacting bubbles. In line with White (2004), the coalescence rate may be considered as related to the rate of increase of the bubble projected area, A_{gb}, resulting from bubble growth. In this respect, an increase in the bubble area by an amount ∂A_{gb} leads to interaction of the bubble with $4N_{gb}\partial A_{gb}$ surrounding bubbles. It is easy to demonstrate that this is correct for circular bubbles of the same size in a regular square lattice. Considering each bubble in turn, the total rate of loss of bubbles by coalescence following an increase in the bubble projected area, A_{gb}, due to bubble growth is given by (White, 2004)

$$\frac{dN_{gb}}{dt} = -2N_{gb}^2 \left(\frac{\partial A_{gb}}{\partial t}\right)_g, \tag{2.24}$$

where the factor of 4 is reduced to 2 to avoid counting each interaction twice, and $(\partial A_{gb}/\partial t)_g$ denotes the variation of the bubble area owing solely to bubble growth. Under the assumption of White that the newly coalesced bubble retains the same area of the two individual parent bubbles (White, 2004), the coalescence event has no impact on the average bubble area. Hence, in the model of White the total rate of increase in the average bubble area is given by $dA_{gb}/dt = (\partial A_{gb}/\partial t)_g$, and Eq. 2.24 gives the relationship between the total rate of loss of bubbles and the total rate of increase in bubble area.

Veshchunov (2008) modified the model of White by introducing the variation of the average bubble area associated with the coalescence mechanism. Veshchunov assumed the bubbles to be always in mechanics equilibrium, and that the surrounding solid medium is stress-free ($\sigma_h = 0$). Moreover, he assumed that the gas in the bubbles obeys the perfect gas law. It can be demonstrated that, under these assumptions, the area of a newly coalesced bubble that retains the gas content of the two parent bubbles equals the summation of the areas of the parent bubbles. Hence, according to the approach of Veshchunov, the total bubble area (summation of the areas of all the bubbles) or, equivalently, the total bubble area per unit grain boundary area (fractional coverage, Eq. 2.23) is conserved through coalescence. Given that the bubble number density, N_{gb}, decreases through coalescence, the conservation of the fractional coverage, $N_{gb}A_{gb}$, implies a variation of the average bubble area, A_{gb}, due to coalescence. As a result, the total rate of increase in the average bubble area may be expressed as

$$\frac{dA_{gb}}{dt} = \left(\frac{\partial A_{gb}}{\partial t}\right)_g + \left(\frac{\partial A_{gb}}{\partial t}\right)_c, \qquad (2.25)$$

where $(\partial A_{gb}/\partial t)_c$ denotes the variation of the average bubble area owing solely to coalescence.

The variation of the fractional coverage is due solely to bubble growth and may be expressed as

$$\frac{d(N_{gb}A_{gb})}{dt} = N_{gb}\left(\frac{\partial A_{gb}}{\partial t}\right)_g, \qquad (2.26)$$

where

$$\frac{d(N_{gb}A_{gb})}{dt} = N_{gb}\frac{dA_{gb}}{dt} + A_{gb}\frac{dN_{gb}}{dt}. \qquad (2.27)$$

Superposition of Eqs. 2.25, 2.26 and 2.27 yields

$$\left(\frac{\partial A_{gb}}{\partial t} \right)_c = - \frac{A_{gb}}{N_{gb}} \frac{dN_{gb}}{dt},$$

(2.28)

Combining Eqs. 2.24, 2.25 and 2.28, one obtains for the total rate of loss of bubbles by coalescence according to the model of Veshchunov (2008)

$$\frac{dN_{gb}}{dt} = - \frac{2N_{gb}^2}{1 + 2N_{gb}A_{gb}} \frac{dA_{gb}}{dt}$$

(2.29)

In the present work, the model of Veshchunov is revisited by removing – consistently with the assumptions discussed in Sub-section 2.3.1 – the hypotheses of bubbles in mechanical equilibrium, stress-free solid, and perfect gas. It is considered that the newly coalesced bubble retains the gas atom and vacancy content of the two parent bubbles, which entails that the volume of the newly coalesced bubble equals the sum of the volumes of the parent bubbles. Hence, according to the new model, the total bubble volume (summation of the volumes of all the bubbles) or, equivalently, the total bubble volume per unit grain boundary area is conserved through coalescence. Given that the bubble number density, N_{gb}, decreases through coalescence, the conservation of the total bubble volume per unit grain boundary area, $N_{gb}V_{gb}$, implies a variation of the average bubble volume, V_{gb}, due to coalescence. Then, the total rate of increase in the average bubble volume may be expressed as

$$\frac{dV_{gb}}{dt} = \left(\frac{\partial V_{gb}}{\partial t} \right)_g + \left(\frac{\partial V_{gb}}{\partial t} \right)_c,$$

(2.30)

where $(\partial V_{gb}/\partial t)_g$ denotes the variation of the bubble volume owing solely to bubble growth, and $(\partial V_{gb}/\partial t)_c$ the variation of the average bubble volume owing solely to coalescence.

The variation of the total bubble volume per unit grain boundary area is due solely to bubble growth and may be expressed as

$$\frac{d(N_{gb}V_{gb})}{dt} = N_{gb} \left(\frac{\partial V_{gb}}{\partial t} \right)_g,$$

(2.31)

where

$$\frac{d(N_{gb}V_{gb})}{dt} = N_{gb} \frac{dV_{gb}}{dt} + V_{gb} \frac{dN_{gb}}{dt}.$$

(2.32)

Superposition of Eqs. 2.30, 2.31 and 2.32 yields

$$\left(\frac{\partial V_{gb}}{\partial t}\right)_c = -\frac{V_{gb}}{N_{gb}}\frac{dN_{gb}}{dt}, \tag{2.33}$$

Given that $V_{gb} \sim A_{gb}^{3/2}$, the validity of Eq. 2.30 implies the validity of Eq. 2.25, and Eq. 2.33 can be written in terms of average bubble area as

$$\left(\frac{\partial A_{gb}}{\partial t}\right)_c = -\frac{2}{3}\frac{A_{gb}}{N_{gb}}\frac{dN_{gb}}{dt}, \tag{2.34}$$

Combining Eqs. 2.24, 2.25 and 2.34, one obtains for the total rate of loss of bubbles by coalescence according to the new model

$$\frac{dN_{gb}}{dt} = -\frac{6N_{gb}^2}{3+4N_{gb}A_{gb}}\frac{dA_{gb}}{dt} \tag{2.35}$$

2.3.4   Fission gas release

The release of fission gas from the grain boundaries following inter-connection of grain-boundary bubbles (Section 1.1) is usually modelled based on a principle of grain boundary saturation. Models adopted in the fuel rod analysis codes often consider an empirical saturation concentration of gas at the grain boundaries (e.g., Bernard et al., 2002; Lassmann et al., 2011), i.e., when the concentration of gas at the grain boundaries exceeds a threshold value, all the gas that further reaches the grain boundaries is assumed to be released to the fuel rod free volume. This treatment does not consider, however, the dependence of the grain-boundary bubble growth and subsequent inter-connection on the temperature and the hydrostatic stress through the equation of state of the gas. This can be allowed for in a physics-based model that directly describes the grain-boundary bubble development.

In the new model, rather than considering a saturation concentration of gas at the grain boundaries, a saturation fraction of grain boundary surface covered by bubbles (saturation coverage) is introduced. It is considered that once the fractional coverage attains the saturation value, $F_{c,sat}$, the bubble number density and projected area obey the saturation coverage condition (Veshchunov, 2008)

$$F_c = N_{gb}A_{gb} = F_{c,sat}. \tag{2.36}$$

This implies that a fraction of the gas reaching the grain boundaries is transferred to the fuel exterior to compensate for bubble growth. More precisely, it is considered that any further bubble growth is balanced by loss (venting) of bubbles through gas release in order to maintain the saturation coverage condition, that is, $dF_c/dt = 0$. It follows that the rate of variation of the bubble number density
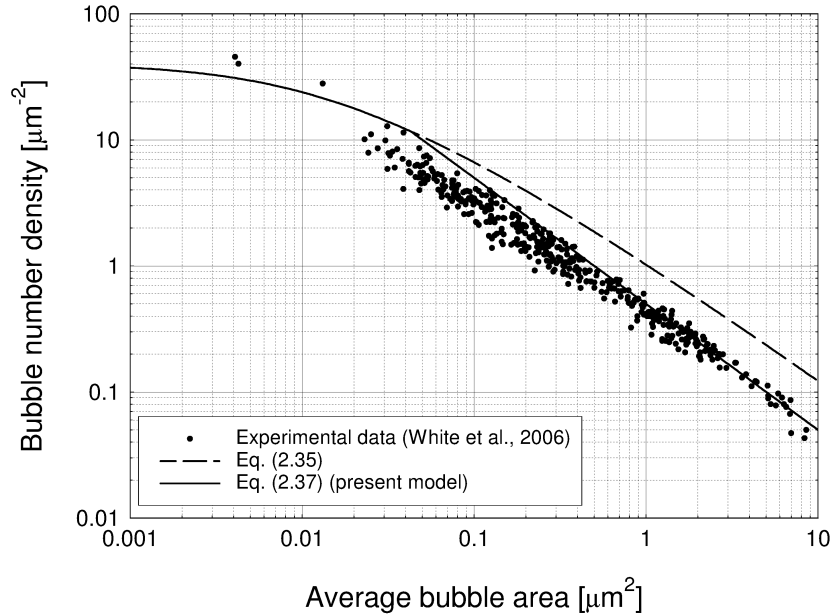
Fig. 2.4. Variation of the bubble number density with the bubble projected area according to the developed model. Eq. 2.37 is compared with experimental data (White et al., 2006). Eq. 2.35 is also shown. An initial bubble number density $N_{gb,0} = 4 \cdot 10^{13}$ (bub.)·m^{-2} is considered.

is governed by coalescence (Sub-section 2.3.3) for $F_c < F_{c,sat}$, and by gas release after attainment of the saturation coverage, and is described by

$$\frac{dN_{gb}}{dt} = -\frac{6N_{gb}^2}{3 + 4N_{gb}A_{gb}}\frac{dA_{gb}}{dt} \qquad \text{if } N_{gb}A_{gb} < F_{c,sat}$$

$$\frac{dN_{gb}}{dt} = -\frac{N_{gb}}{A_{gb}}\frac{dA_{gb}}{dt} \qquad \text{if } N_{gb}A_{gb} = F_{c,sat} \tag{2.37}$$

The adopted value for $F_{c,sat}$ is 0.5 (e.g., Koo et al., 2000; White, 2004; Veshchunov, 2008). Eq. 2.37 allows evaluating the observed reduction in the number density of grain-boundary bubbles in the fuel throughout irradiation (White, 2004). Figure 2.4 compares Eq. 2.37 with the experimental data of bubble number density and corresponding average bubble projected area from (White et al., 2006). The bifurcation between the dashed line (Eq. 2.35) and the full line (Eq. 2.37) corresponds to the attainment of the saturation coverage. The developed variable bubble number density model (Eq. 2.37) appears to reasonably conform to the data.

According to the above discussed description, and considering that each bubble contains n_g fission gas atoms, the FGR is calculated by means of

$$\frac{dn_{fgr}}{dt} = 0 \qquad \qquad \text{if } N_{gb}A_{gb} < F_{c,sat}$$

$$\frac{dn_{fgr}}{dt} = n_g \frac{N_{gb}}{A_{gb}} \frac{dA_{gb}}{dt} \qquad \qquad \text{if } N_{gb}A_{gb} = F_{c,sat} \qquad \qquad (2.38)$$

where n_{fgr} is the number of gas atoms released to the fuel rod free volume. This simple approach allows reproducing the incubation behaviour (Vitanza et al., 1978) and the dependence of the FGR on the hydrostatic stress (Kogai et al., 1988; Walker et al., 1988; Mogensen et al., 1993), as well as the coupling between the fission gas swelling and release, on a physical basis.

2.3.5   Grain-boundary swelling

The equations presented in the previous sub-sections allow to calculate the evolution of the number density and the size of the grain-boundary bubbles, as well as the amount of fission gas released to the fuel rod free volume. Since a uniform population of bubbles is considered (Sub-section 2.3.1), the volumetric grain-boundary fission gas swelling, normalized to the unit volume of fuel, is calculated as

$$\left(\frac{\Delta V}{V} \right)_{gb} = \frac{1}{2} \frac{N_{gb}}{(1/3) r_{gr}} \left(\frac{4}{3} \pi R_{gb}^3 \, \varphi(\Theta) \right), \qquad \qquad (2.39)$$

where r_{gr} [m] is the radius of the spherical fuel grains, $(1/3) r_{gr}$ is the grain volume to surface ratio, and the factor 1/2 is introduced because a grain-boundary bubble is shared by two neighbouring grains.

2.3.6   Calculation sequence

The following calculation sequence is adopted in applying the grain-boundary module at each computational time step:

(i)   The inflow of gas atoms in the grain-boundary bubbles is calculated as the arrival rate of gas at the grain boundaries provided by the intra-granular module (Sub-section 2.2.1). At the first time step, an initial bubble radius $R_{gb} = 10$ nm is used.

(ii)   The bubble growth rate is calculated on the basis of the Speight and Beere model by solving incrementally Eq. 2.14, giving the time evolution of the temperature and hydrostatic stress-dependent bubble size.

(iii)   The decrease of bubble number density through coalescence/FGR, as well as the FGR rate, are calculated by solving incrementally Eqs. 2.37 and 2.38, using the new projected area after the effect of bubble growth.

(iv)   The grain-boundary fission gas swelling is calculated by means of Eq. 2.39.

The (total) volumetric fission gas swelling, $(\Delta V/V)_{gas}$, is calculated as the summation of the intra-granular swelling and the grain-boundary swelling:

$$\left(\frac{\Delta V}{V}\right)_{gas} = \left(\frac{\Delta V}{V}\right)_{ig} + \left(\frac{\Delta V}{V}\right)_{gb}. \tag{2.40}$$

Given the isotropic nature of the swelling, the strains due to fission gas swelling are calculated as (Lassmann et al., 2011)

$$\varepsilon_{r,\theta,z}^{gas} = \frac{1}{3}\left(\frac{\Delta V}{V}\right)_{gas}. \tag{2.41}$$

The values adopted for the model parameters are summarized in Table 2.1.

Table 2.1 - Values adopted for the model parameters.

Symbol	Definition	Value / expression
D_s	Gas atom diffusion coefficient in grains	$D_1+D_2+D_3$ (m$^2\cdot$s^{-1})
		$D_1=7.6\cdot10^{-10}\cdot exp(-4.86\cdot10^{-19}/kT)$
		$D_2=3.22\cdot10^{-16}\cdot q_s^{1/2}\cdot exp(-1.90\cdot10^{-19}/kT)$
		D_3 not considered
		T: temperature (K)
		q_s: specific power (W$\cdot$g^{-1})
D_v	Vacancy diffusion coefficient in grain boundaries	$6.9\cdot10^{-4}\cdot exp(-5.35\cdot10^{-19}/kT)$ m$^2\cdot$s^{-1}
$F_{c,sat}$	Fractional coverage at grain boundary saturation	0.5
k	Boltzmann constant	$1.38\cdot10^{-23}$ J$\cdot$K^{-1}
l_f	Length of a fission fragment track	$6\cdot10^{-6}$ m
$N_{gb,0}$	Initial number density of grain-boundary bubbles	$4\cdot10^{13}$ (bub.)$\cdot$m^{-2}
N_{ig}	Number density of intra-granular bubbles	$7\cdot10^{23}$ (bub.)$\cdot$m^{-3}
Z_0	Radius of influence of a fission fragment track	10^{-9} m
γ	fuel/gas specific surface energy	1 J$\cdot$m^{-2}
δ_{gb}	Thickness of the diffusion layer in grain boundaries	$5\cdot10^{-10}$ m
Θ	Semi-dihedral angle of grain-boundary bubbles	50°
ω	Van der Waals' volume of a fission gas atom	$8.5\cdot10^{-29}$ m$^3\cdot$(at.)$^{-1}$
Ω_{gb}	Vacancy volume in grain-boundary bubbles	$4.09\cdot10^{-29}$ m^3
Ω_{ig}	Volume per gas atom in intra-granular bubbles	$3\cdot10^{-29}$ m^3

2.4   Concluding remarks

A model was developed for the analysis of the fission gas swelling and release in oxide fuel during irradiation as inherently coupled phenomena, which represents a pragmatic compromise between the strength of a physics-based description and the simplicity required for application to the fuel rod analysis codes. The model is based on concepts presented earlier by Speight, Beere, White, Tucker, Veshchunov, which are revisited and combined in a practical treatment, aimed to grasp the fundamental peculiarities of the fission gas behaviour. In particular, a simple approach is adopted to describe the development of the intra-granular bubbles, which determine the intra-granular contribution to the swelling and affect the diffusion of gas to the grain boundaries. This treatment of the intra-granular gas behaviour is preliminary and being further developed, starting from the approach presented in (Van Uffelen et al., 2011). The main and most innovative part of the model describes the development of the grain-boundary bubbles, which determines the kinetics of both the grain-boundary contribution to the swelling and the fission gas release. In particular, the mutually dependent processes of grain-boundary bubble growth, coalescence and inter-connection are described. In outline:

- The Speight and Beere model is adopted for describing the growth of the grain-boundary bubbles, and its dependence on the hydrostatic stress in the fuel. The latter aspect is of particular importance for the analysis of the fuel rod behaviour at extended burn-up or during power ramps and of the related, safety-relevant issues.
- Bubble coalescence is described by means of a revisited model of White.
- Bubble inter-connection and the subsequent gas release from the grain boundaries are modelled by adopting a concept of fractional coverage saturation.

The model is intended to provide a contribution to the development of the fuel rod analysis codes for application in both research and industrial frameworks, since it offers the advantages of a physics-based treatment in terms of flexibility in comparison with widely used semi-empirical models of fission gas behaviour. To this purpose, testing, implementation in a fuel rod analysis code, and evaluation of the model were carried out, as discussed in the next chapters.

Chapter 3

Model testing as stand-alone version

Abstract. *In this chapter, calculations performed using the stand-alone version of the new integrated model of fission gas swelling and release are presented. In particular, the model was applied to the analysis of either power ramped or power cycled fuel specimens. Despite its simplicity, the model was proven to reproduce the main peculiarities of the fission gas behaviour, consistently with the observations reported in the literature. The comparison of the results with an extensive dataset of fission gas swelling measurements is presented as a first step of verification. The predictive accuracy for different irradiation conditions is reasonable, without applying any fitting to the model parameters. The chapter is organized as follows. In Section 3.1, the stand-alone version of the model is briefly described. In Section 3.2, the experimental database is presented, which is adopted for the model evaluation. In Section 3.3, details are given about the set-up of the calculations. In Section 3.4, the results are discussed, both in terms of model capabilities to represent the relevant processes and assessment of the predictions against experimental data from the IFPE database. Conclusions are drawn in Section 3.5.*

3.1   Introduction

Specific test programs are to be developed for the physical models before implementation in a fuel rod analysis code. A test program (or stand-alone model version) is generally designed to perform a zero-dimensional ('point') analysis. Moreover, the input parameters of the model (e.g., specific power, temperature, stress) are defined by the user. Differently, when implemented in a fuel rod analysis code, the model is called for every node of the computational domain, and it is integrated in a consistent fuel rod analysis. In this respect, the construction of a test program may be considered as an intermediate step of the work of development and application of a new model, lying between the definition of the mathematical formulation of the model and its implementation in a fuel rod analysis code. The importance of this intermediate step is twofold:

• It allows to assess the model capabilities to represent the relevant processes and to evaluate the

quantities of interest, decoupled from the multiple interrelations with the other aspects of the thermo-mechanical analysis.

- It allows to address the basic numerical issues, decoupled from those related to the incorporation of the model in a pre-existing, complex numerical framework.

In this work, a test program was developed for the new integrated model of fission gas swelling and release in oxide fuel described in Chapter 2. The program receives the fuel fabrication data (porosity and grain size) and the time-dependent specific power, temperature and hydrostatic stress as input. Linear interpolation is performed of the time-dependent quantities within the user-defined time steps. The program consists of Fortran 95 subroutines designed to consistently calculate the fuel density, power density, fission gas generation rate, fission gas concentrations within the grains, at the grain boundaries and released to the fuel rod free volume, and the fission gas swelling. The 'point' analysis is surrounded by a time loop, and a simple time step control was developed and implemented in order to assure adequate numerical accuracy.

Besides representing the first step towards the incorporation of the model in a fuel rod analysis code, the stand-alone version of the model allowed to investigate the model capabilities for the simulation of real irradiation histories and to perform a first verification of the predictions against experimental data from the IFPE database, as discussed in the next sections.

3.2   Experimental database

The experiments of the AGR/Halden Ramp Test Programme (White et al., 2006) involved the power ramp test of Advanced Gas-cooled Reactor (AGR) UO_2 fuel rods in the Halden Reactor, after base-irradiation in the Hinkley Point, Torness and Halden Reactors up to burn-ups of around 21 $GWd\cdot(tM)^{-1}$. Extensive post-irradiation examinations (PIE) of the irradiated fuel by scanning electron microscopy (SEM) were performed to measure the fission gas swelling due to grain-boundary gas bubbles. The results of the study were made available through the IFPE database (Sartori et al., 2010). Some details of the different irradiation tests and SEM examinations, on which the experimental data of grain-boundary swelling considered in the present work are referred to, are given in Table 3.1. The fuel rods were subject to either power ramps or power cycling. The schematic of the ramp tests is presented in Fig. 3.1 and the times and powers of each stage are summarized in Table 3.2. The ramp test consists of a conditioning time, τ_1, and a subsequent power

ramp, followed by a holding time (if any) at the ramp terminal power level, τ_{2b}, and reactor scram. The ramps denoted as slow are those in which the power increasing time, τ_{2a}, is of the order of 45 min and the fast ramps are those for which τ_{2a} lies within the range 1-2 min. The two power-cycled fuel rods were subjected to 115 four-hour cycles, the details of which are summarized in Table 3.3. For each irradiation test, the PIE/SEM examinations were performed at different zones of the fuel specimen, allowing the construction of an extensive database of grain-boundary swelling measurements. Moreover, the specific power, temperature, and hydrostatic stress for each SEM zone were evaluated by means of the ENIGMA code (White et al., 2006), thus providing the basis for reconstruction of the experiments and verification of fission gas swelling models. In Table 3.4, a summary of the post-irradiation experimental data of volumetric grain-boundary swelling, $(\Delta V/V)_{gb}$, for each SEM zone is given. All the available grain-boundary swelling data are reported, except for that related to the SEM zone 4160-G, which was not used in the present work in view of the lack of information on the fuel grain size during the ramp test (White et al., 2006).

Table 3.1 - Details of considered irradiation tests and PIE/SEM examinations from the AGR/Halden Ramp Test Programme.

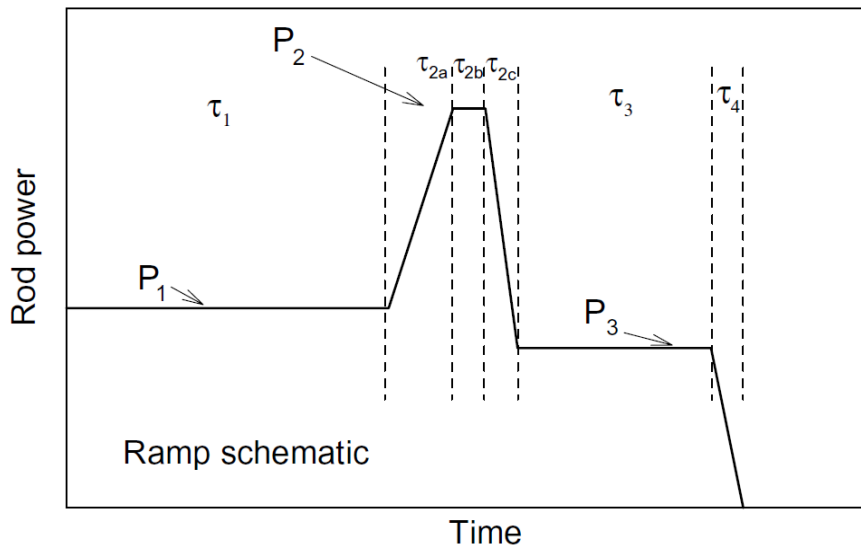| Rod identifier	Burn-up [GWd·(tM)$^{-1}$]	Ramp type	Peak rating [kW·m^{-1}]	Holding time	SEM zones	Boundaries measured
4000	20.7	Fast	40	30.0 min	5	48
4004	20.5	Fast	40	2.38 min	6	44
4005	20.8	Fast	40	2.0 min	5	39
4064	20.1	Slow	43	–	5	63
4065	9.3	Slow	41.8	–	5	43
4159	20.2	Cycles	18-26	115·4 h	5	56
4160	20.1	Cycled	18-26	115·4 h	6	45
4162	12.6	Slow	40	–	4	47
4163	12.6	Fast	40	2.0 min	5	37
					46	422

Fig. 3.1. Schematic of a generic ramp test of the AGR/Halden Ramp Test Programme – from (White et al., 2006). The parameters for each case are reported in Table 3.2.

Table 3.2 - Details of power ramps in the irradiation tests of the AGR/Halden Ramp Test Programme.

Rod identifier	Power 1 [kW·m^{-1}]	τ_1	τ_{2a} [min]	Power 2 [kW·m^{-1}]	τ_{2b} [min]	τ_{2c} [s]	Power 3 [kW·m^{-1}]	τ_3 [min]	τ_4
4000	14.0	12d	1.52	40.0	30.0	100	14.0	99.0	SCRAM
4004	14.0	12d	1.97	40.0	2.38	90	14.0	99.0	SCRAM
4005	14.0	12d	1.32	40.0	2.0	–	SCRAM	–	–
4064	20.0	15wk	47.0	43.0	0.0	–	SCRAM	–	–
4065	19.3	3wk	47.0	41.8	0.0	–	SCRAM	–	–
4162	18.0	3wk	45.0	40	0.0	40	18.0	6	–
4163	18.0	3wk	2.0	40.0	2.0	80	SCRAM	–	–

Table 3.3 - Details of power cycles in the irradiation tests of the AGR/Halden Ramp Test Programme.

Rod identifier	Power 1 [kW·m^{-1}]	Time 1	Ramp up	Power up [kW·m^{-1}]	Ramp down	Power down [kW·m^{-1}]	De-conditioning [kW·m^{-1}]	Last phase
4159 and 4160	18.0	7d	30 min	26.0 for 1h	30 min	18.0 for 2h	18.0 for 2d	Shut-down
			115 – 4h cycles					

Table 3.4 - Summary of the post-irradiation experimental data of grain-boundary swelling considered in the present work.

SEM zone	$(\Delta V/V)_{gb}$ [%]	SEM zone	$(\Delta V/V)_{gb}$ [%]	SEM zone	$(\Delta V/V)_{gb}$ [%]
4000-A	0.97±0.35	4064-A	1.07±0.58	4160-A	2.61±0.57
4000-B	0.68±0.12	4064-B	0.86±0.32	4160-B	2.30±0.56
4000-C	0.53±0.10	4064-C	0.63±0.22	4160-C	2.60±0.36
4000-D	0.46±0.10	4064-D	0.74±0.19	4160-D	1.64±0.20
4000-F	0.17±0.4	4064-E	0.59±0.26	4160-E	1.22±0.21
				4160-F	0.74±0.09
4004-A	0.62±0.13	4065-A	1.25±0.43	4162-A	0.70±0.26
4004-B	0.70±0.26	4065-B	1.35±0.30	4162-B	0.46±0.17
4004-C	0.44±0.11	4065-C	0.97±0.26	4162-C	0.43±0.18
4004-D	0.56±0.15	4065-D	0.79±0.15	4162-D	0.43±0.22
4004-E	0.27±0.07	4065-E	0.21		
4004-F	0.16				
4005-A	0.94±0.16	4159-A	1.85±0.22	4163-A	0.60±0.20
4005-B	0.57±0.20	4159-B	1.67±0.26	4163-B	0.59±0.18
4005-C	0.42±0.12	4159-C	1.37±0.16	4163-C	0.35±0.10
4005-D	0.54±0.15	4159-D	1.06±0.15	4163-D	0.40±0.06
4005-E	0.27±0.02	4159-E	0.91±0.28	4163-E	0.26±0.13

3.3 Set-up of calculations

Simulations of the ramp tests from the AGR/Halden Ramp Test Programme were performed by means of the stand-alone version of the new integrated model of fission gas swelling and release. 46 SEM zones (Table 3.4) were analysed. The calculations were carried out coherently with the fuel fabrication data and the details of the irradiation histories provided in (White et al., 2006). Moreover, the following assumptions were made in order to assess the initial conditions for the analysis of the ramp tests:

- All the fission gas generated during the base-irradiation is considered to be retained inside the fuel grains at the beginning of the calculation. This hypothesis is consistent with the observation that, in all of the cases studied, the base-irradiation resulted in negligible fission gas release and microstructural changes (White et al., 2006).

- The fuel grain size is assumed to remain constant at the final (measured) value throughout the ramp test. Grain growth calculations based on the model of Ainscough et al. (1973) showed that the predicted grain growth is lower than or comparable to the experimental scatter for the grain size measurements (White et al., 2006) in all the analysed cases.

3.4   Results and discussion

3.4.1   Model capabilities

The results of the calculations are firstly presented for the exemplifying case of the SEM zone 4000-A. The fuel specimen was characterized by a burn-up of 20.7 GWd·(tM)$^{-1}$ and was subject to a fast ramp followed by a holding time at the ramp terminal power level of 30 min duration (Table 3.1). The time-dependent input quantities (specific power, temperature and hydrostatic stress) are presented in Fig. 3.2. The specific power was maintained at about 13 W·g^{-1} during the conditioning time, and raised up to about 32 W·g^{-1} during the power ramp[5]. The fuel temperature and the compressive hydrostatic stress reached values of about 1775°C and 15 MPa, respectively, at the top of the ramp.

The output of the stand-alone model version is shown in Fig. 3.3 in terms of intra-granular bubble radius and volumetric intra-granular swelling as a function of the time. A slight increase of the intra-granular bubble radius is observed during the conditioning time. This behaviour is ascribed to the moderate temperature (about 880°C) and the associated slight trapping effect of the gas atoms in the bubbles (Section 2.2). Following the temperature rise during the ramp, the intra-granular bubbles rapidly grow, and the intra-granular swelling correspondingly increases.

The results in terms of grain-boundary bubble radius of curvature and volumetric grain-boundary swelling as a function of the time are shown in Fig. 3.4. The grain-boundary bubbles grow throughout the irradiation by diffusional inflow of gas atoms and vacancies. Also, bubble growth brings about bubble coalescence and the related increase in the bubble radius (Section 2.3). During the ramp, the bubble growth rate increases as a consequence of the temperature rise, and the grain-boundary swelling correspondingly accelerates. To give more details about the model capabilities to simulate the growth kinetics of the grain-boundary bubbles, Fig. 3.5 shows the ratio of the gas pressure in the grain-boundary bubbles (bubble pressure) to the mechanical equilibrium pressure as a function of the time (full black line). During the conditioning time at moderate temperature, the bubble over-pressure is high ($p/p_{eq} \approx 30$) due to the low vacancy mobility and consequent low vacancy absorption rate at the bubbles. Subsequent excursion to higher temperatures during the

---

[5] The specific power is a prescribed quantity for the 'point' analyses presented in this chapter, while the linear heat rate is generally prescribed for fuel rod analyses.

power ramp brings about (i) a further increase of the bubble over-pressure, which drives the absorption of vacancies at the bubbles, and (ii) an enhanced mobility of vacancies and gas atoms (Section 2.3). Both these effects favour the bubble growth during the ramp and the subsequent holding
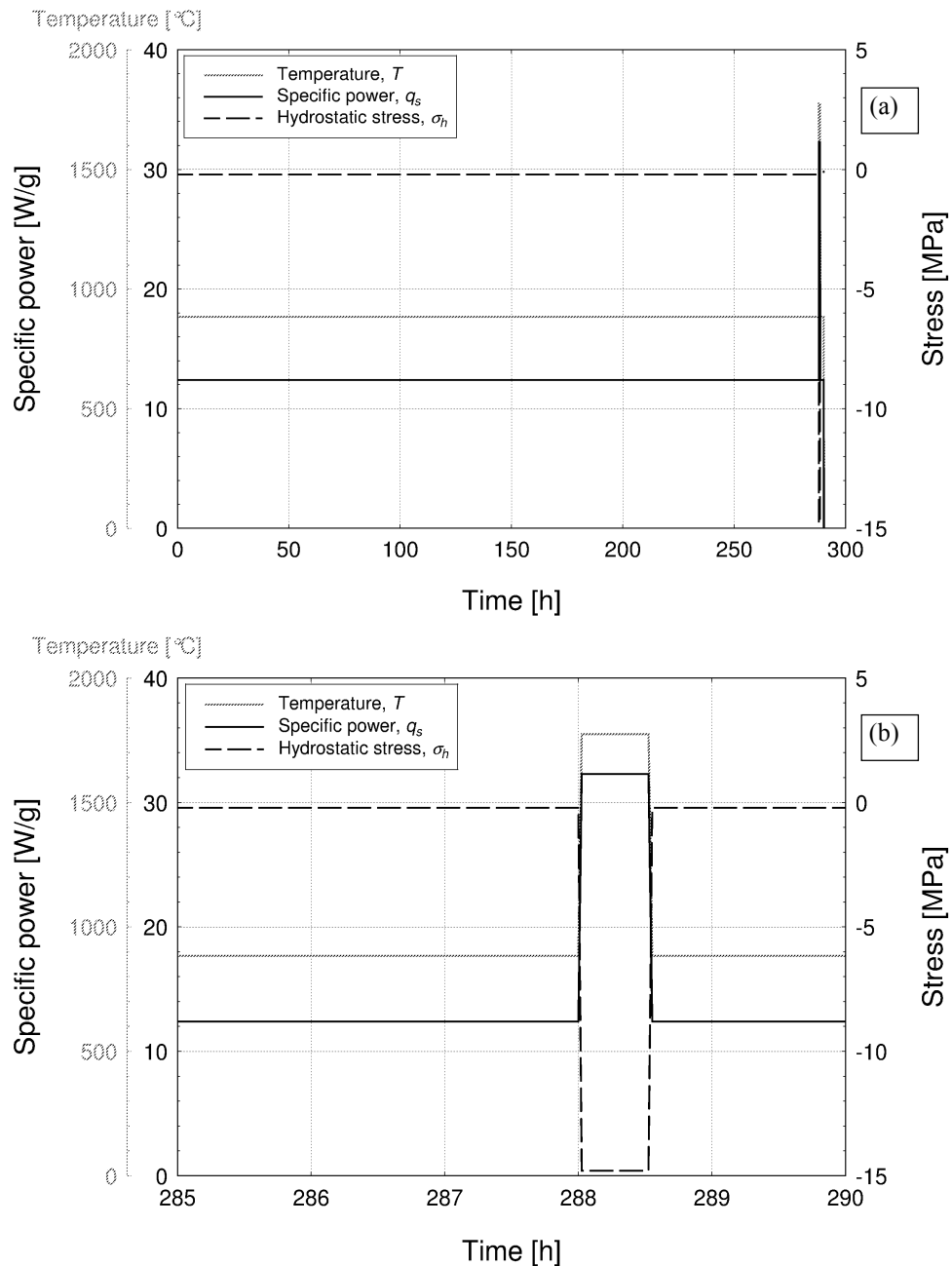

Fig. 3.2. Temperature, specific power, and hydrostatic stress as a function of the time for the SEM zone 4000-A. (a) Entire ramp test, (b) zoom on the ramp.
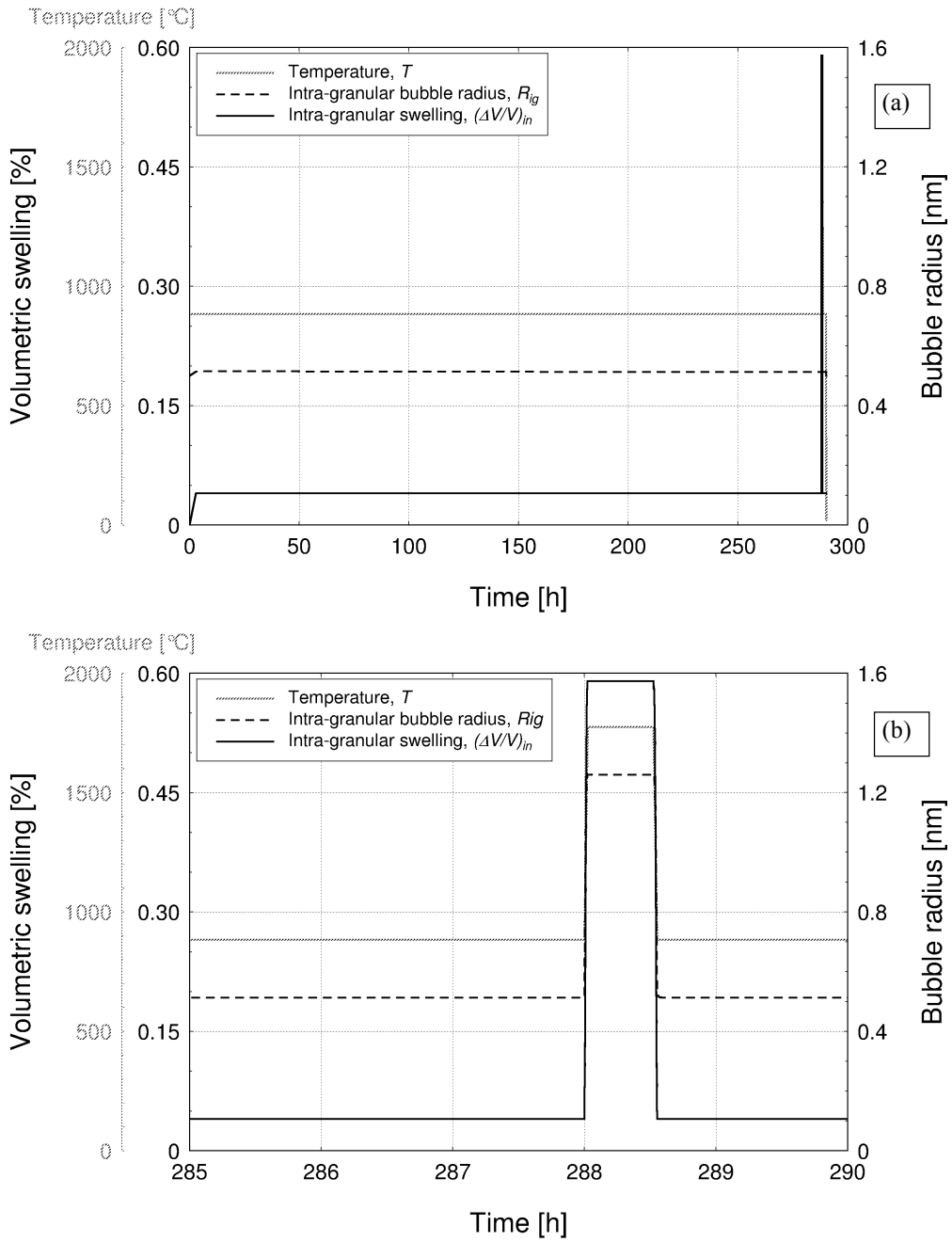
Fig. 3.3. Calculated intra-granular bubble radius and intra-granular swelling as a function of the time for the SEM zone 4000-A. The temperature is also shown. (a) Entire ramp test, (b) zoom on the ramp.
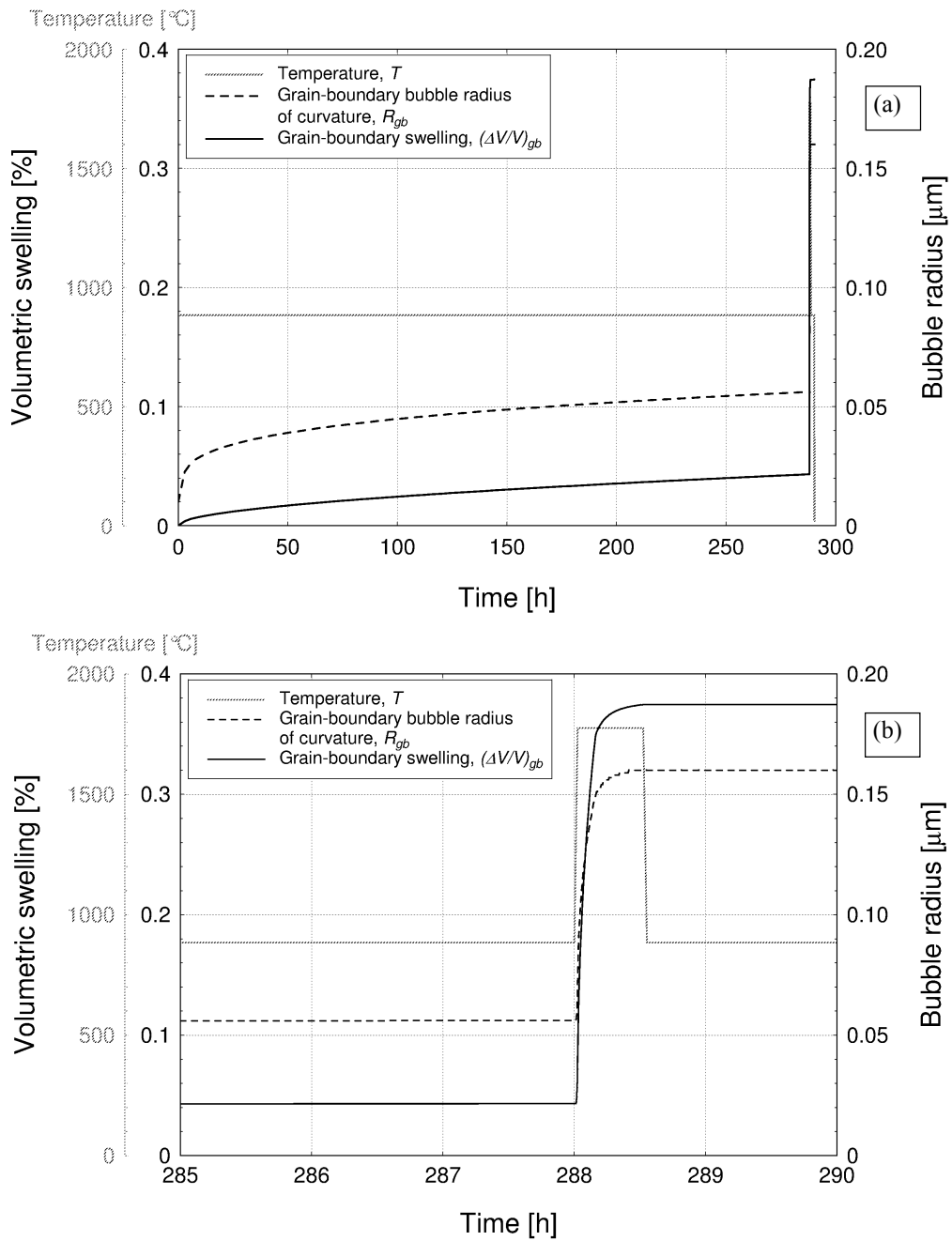
Fig. 3.4. Calculated grain-boundary bubble radius of curvature and grain-boundary swelling as a function of the time for the SEM zone 4000-A. The temperature is also shown. (a) Entire ramp test, (b) zoom on the ramp.
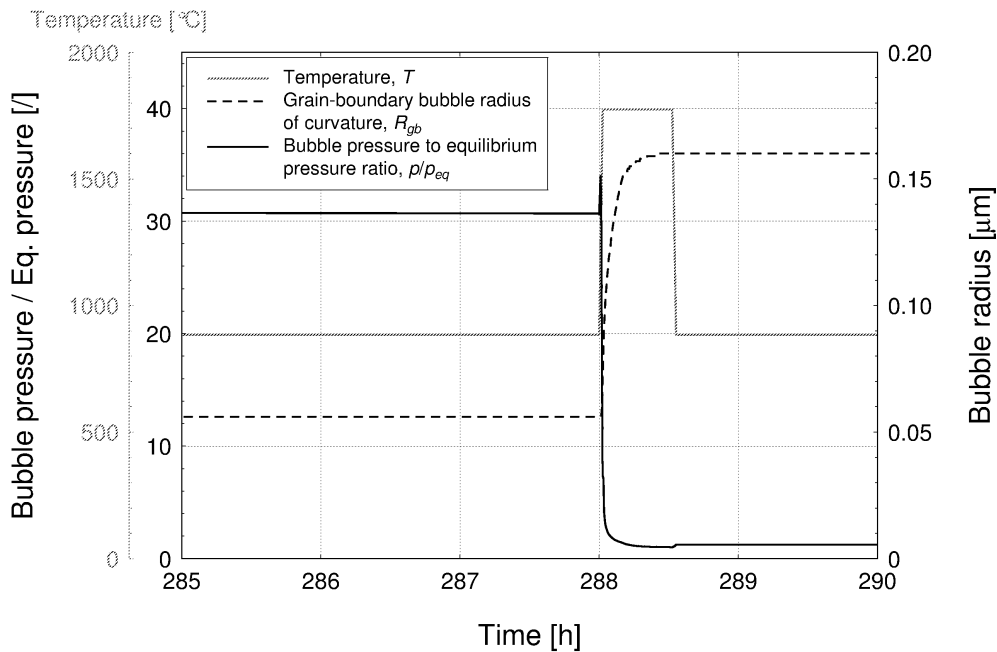
Fig. 3.5. Calculated grain-boundary bubble radius of curvature and ratio of the gas pressure in the bubble to the mechanical equilibrium pressure as a function of the time for the SEM zone 4000-A. The temperature is also shown. Zoom on the ramp is displayed.

time at high temperature. Following the ramp, the rapid vacancy absorption acts to decrease the bubble over-pressure, thus progressively decreasing the bubble growth rate. However, the ratio of the bubble pressure to the equilibrium pressure remains > 1 (over-pressurized bubbles) even at high temperature. The finding that the grain-boundary bubbles are generally over-pressurized in irradiated oxide fuel is consistent with the results reported in (White, 2004).

Owing to significant bubble growth during the ramp and the subsequent holding time, the fractional coverage increases to the saturation value of 0.5 (saturation coverage). In accordance with the concept of grain boundary saturation included in the model, a constant fractional coverage condition is maintained after attainment of the saturation coverage, compensating for bubble growth by FGR from the grain boundaries (Section 2.3). This behaviour is shown in Fig. 3.6. FGR starts at the attainment of the saturation coverage and rapidly increases as the bubbles grow. Hence, the model reproduces the experimentally observed incubation behaviour of the FGR (Vitanza et al., 1978), on a physical basis.
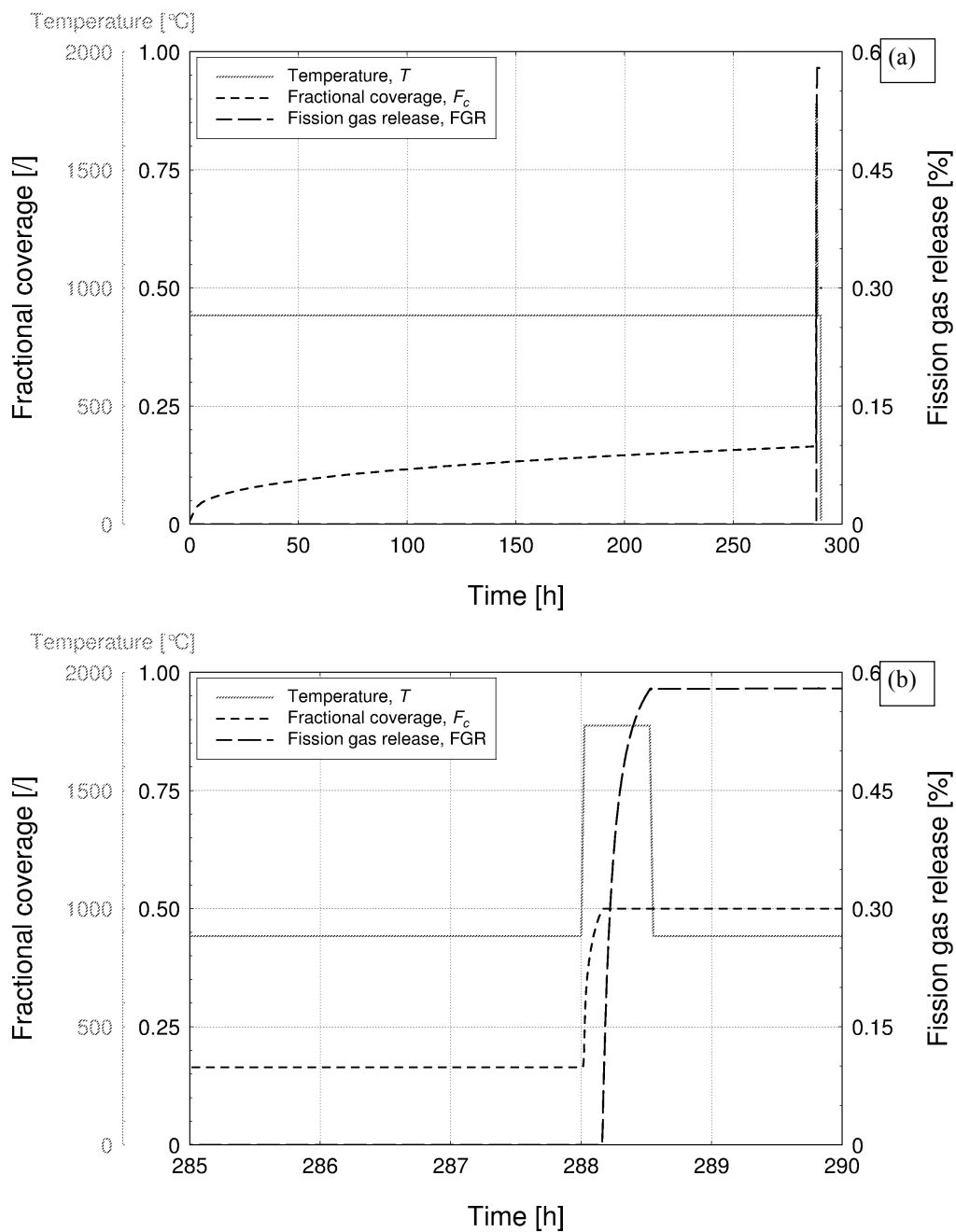
Fig. 3.6. Calculated fractional coverage and fission gas release (defined as the ratio of the released to the generated gas) as a function of the time for the SEM zone 4000-A. The temperature is also shown. (a) Entire ramp test, (b) zoom on the ramp.

Figure 3.7 displays the evolution of the radius of curvature (dashed black line) and the number density (full black line) of the grain-boundary bubbles. The number density progressively decreases throughout the irradiation by coalescence and (once FGR commences) by gas venting from the

grain boundaries (Section 2.3). The decrease of the bubble number density accelerates during the power ramp, when rapid bubble growth brings about strong coalescence and subsequent onset of the
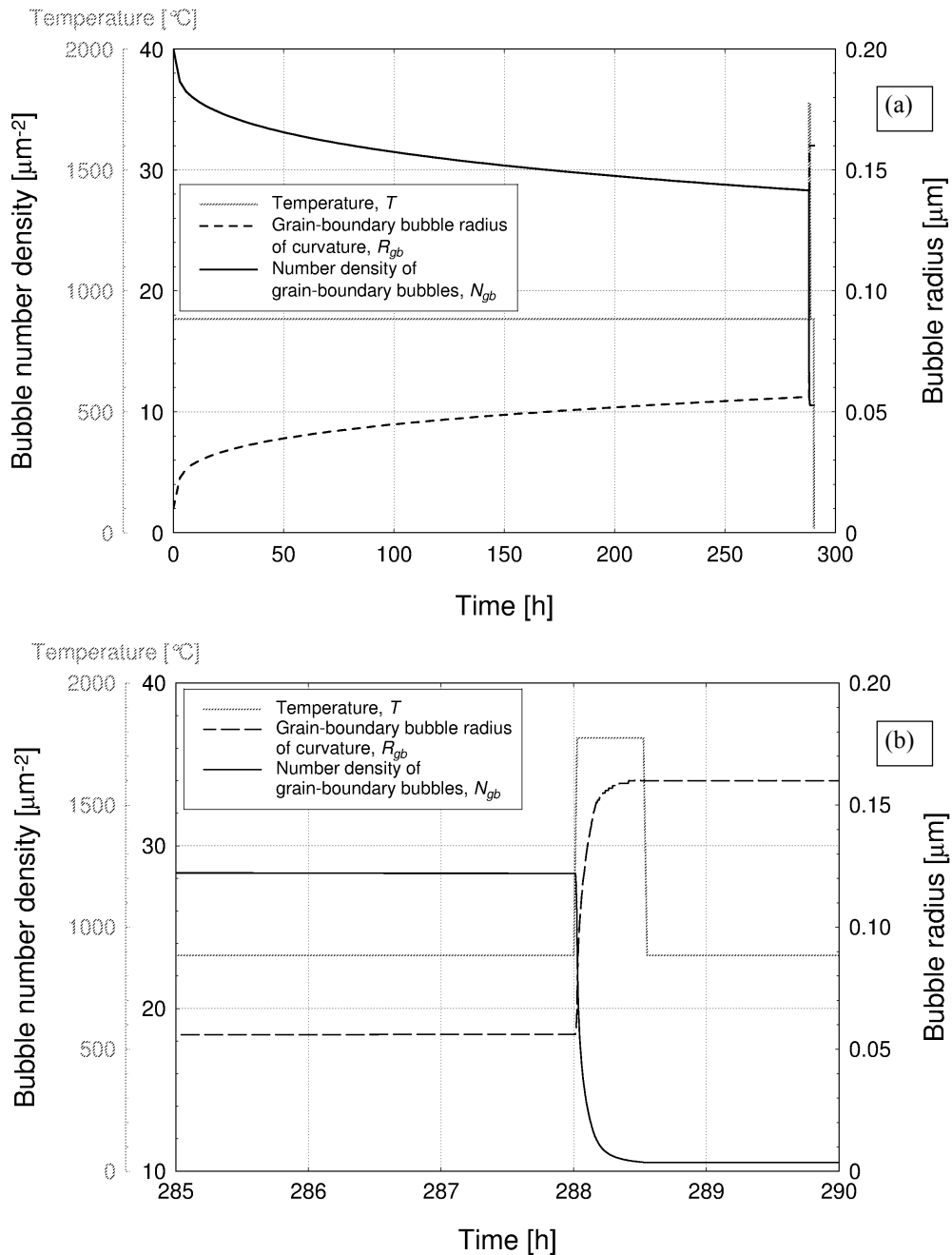
Fig. 3.7. Calculated grain-boundary bubble radius of curvature and number density as a function of the time for the SEM zone 4000-A. The temperature is also shown. (a) Entire ramp test, (b) zoom on the ramp.

FGR. The simple but physics-based representation of bubble coalescence and FGR included in the model therefore allows to reproduce the experimentally observed decrease of the number density of the grain-boundary bubbles as the irradiation proceeds (White, 2004).

The calculated grain-boundary swelling and FGR for the SEM zone 4000-A are shown together in Fig. 3.8 (black lines). It can be noted that the coupling between swelling and FGR is consistently reproduced by the model, since the swelling rate is reduced by loss of gas from the grain boundaries as FGR takes place. The comparison with the results obtained by neglecting the stress-dependence (grey lines in Fig. 3.8) points out the role of the hydrostatic stress in affecting the fission gas swelling and release by inhibiting the growth of the grain-boundary bubbles. Both the swelling and the FGR are reduced by the compressive stress. Also, the stress delays the FGR by slowing down the bubble growth and consequently retarding the attainment of the saturation coverage. The effect of the hydrostatic stress is relevant during the power ramp, when (i) the stress is higher due to the onset of pellet-cladding mechanical interaction, and (ii) the bubble radius is larger, meaning that the surface tension force – that competes with the hydrostatic stress in affecting the bubble growth rate
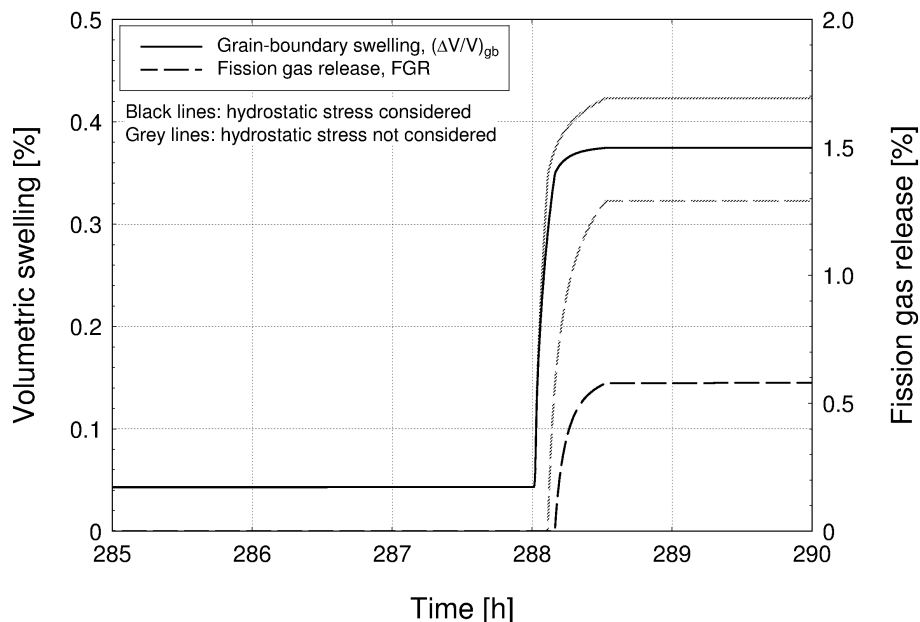

Fig. 3.8. Calculated grain-boundary swelling and fission gas release (defined as the ratio of the released to the generated gas) as a function of the time for the SEM zone 4000-A. The grey lines correspond to the results obtained by neglecting the stress-dependence in the model. Zoom on the ramp is displayed.

(Section 2.3) – is lower. The results are therefore in qualitative agreement with the experimental observations pointing out the above effects of the hydrostatic stress on the fission gas swelling and release (Zimmermann, 1978; Kogai et al., 1988; Walker et al., 1988, Mogensen et al., 1993; Kashibe and Une, 1997).
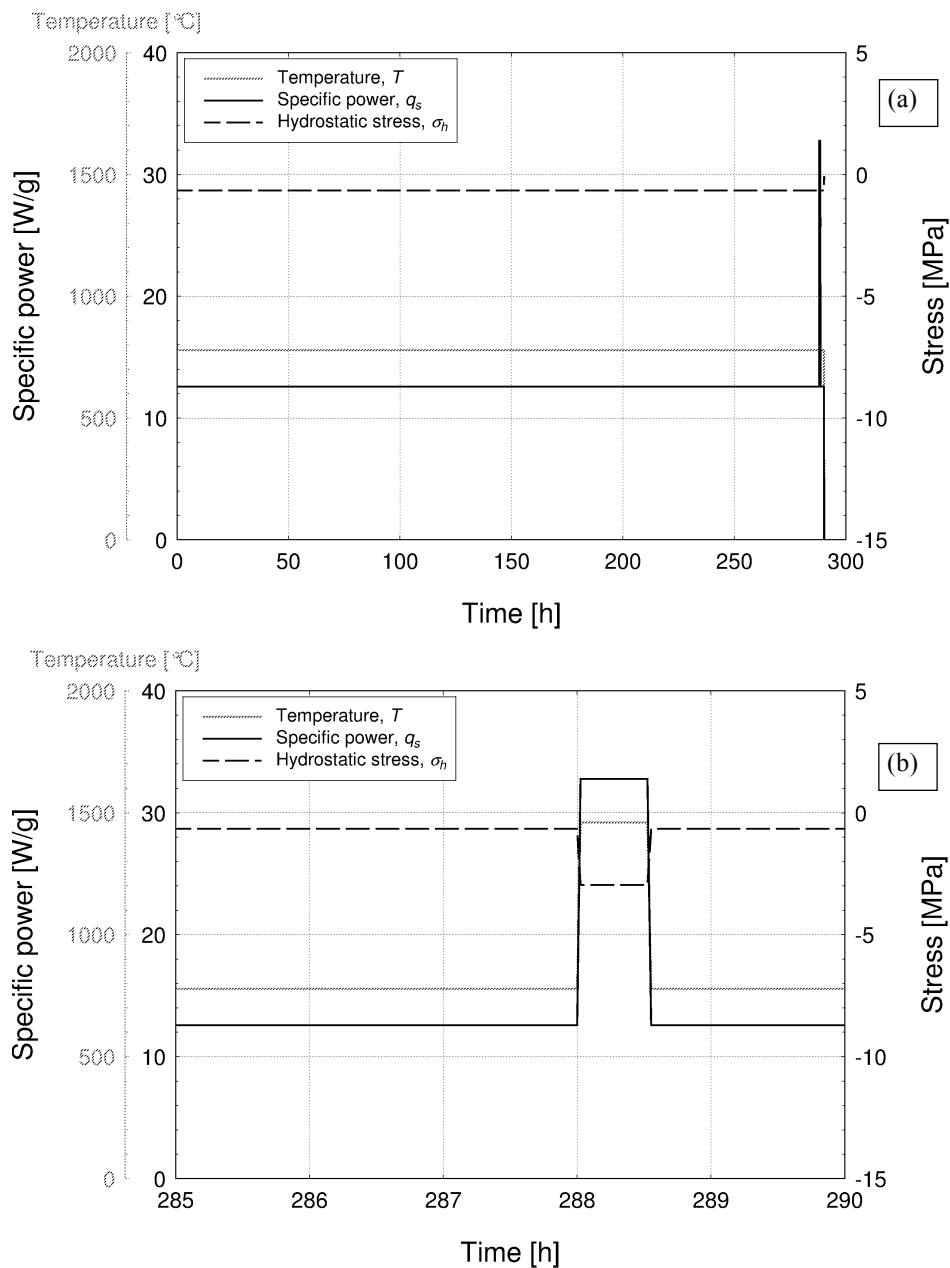

Fig. 3.9. Temperature, specific power, and hydrostatic stress as a function of the time for the SEM zone 4000-F. (a) Entire ramp test, (b) zoom on the ramp.

The time-dependent input quantities are presented in Fig. 3.9 for the SEM zone 4000-F, which belongs to the same fuel rod as the SEM zone 4000-A but lies in a colder (more peripheral) region of the fuel pellet. The temperature was maintained at about 780°C during the conditioning time, and raised to 1460°C during the power ramp. The compressive hydrostatic stress reached a value of about 3 MPa at the top of the ramp.

The output of the stand-alone model version is shown in Fig. 3.10 in terms of grain-boundary bubble radius of curvature and volumetric grain-boundary swelling as a function of the time.

Due to the lower temperature, the bubble radius and the swelling are lower compared to the SEM zone 4000-A. Also, the bubble over-pressure (Fig. 3.11) is generally higher compared to the SEM zone 4000-A, due to the lower vacancy mobility at lower temperature.

FGR does not occur in this case, since the fractional coverage does not reach the saturation value owing to the reduced bubble growth. When applied to fuel rod analyses, it is therefore expected that the model predicts lower grain-boundary swelling and FGR with increasing distance from the pellet centre, reflecting the spatial dependence of the temperature in the fuel and consistently with the experimental observations (White et al., 2006).

Figure 3.12 shows the grain-boundary swelling for the SEM zone 4000-F, calculated both considering (black line) and neglecting (grey line) the hydrostatic stress. The dependence of the calculated swelling on the stress is almost negligible in this case, as a consequence of the low stress and the small bubble radius (that is, the surface tension force is dominant in comparison with the hydrostatic stress).

The time-dependent input quantities are presented in Fig. 3.13 for the SEM zone 4064-A. The fuel specimen was characterized by a burn-up of 20.1 GWd·(tM)$^{-1}$ and was subject to a slow ramp followed by reactor scram (Tables 3.1 and 3.2). The specific power was maintained at about 16 W·g^{-1} during the conditioning time, and raised up to about 35 W·g^{-1} during the power ramp. The fuel temperature and the compressive hydrostatic stress reached values of about 1870°C and 10 MPa, respectively, at the top of the ramp.
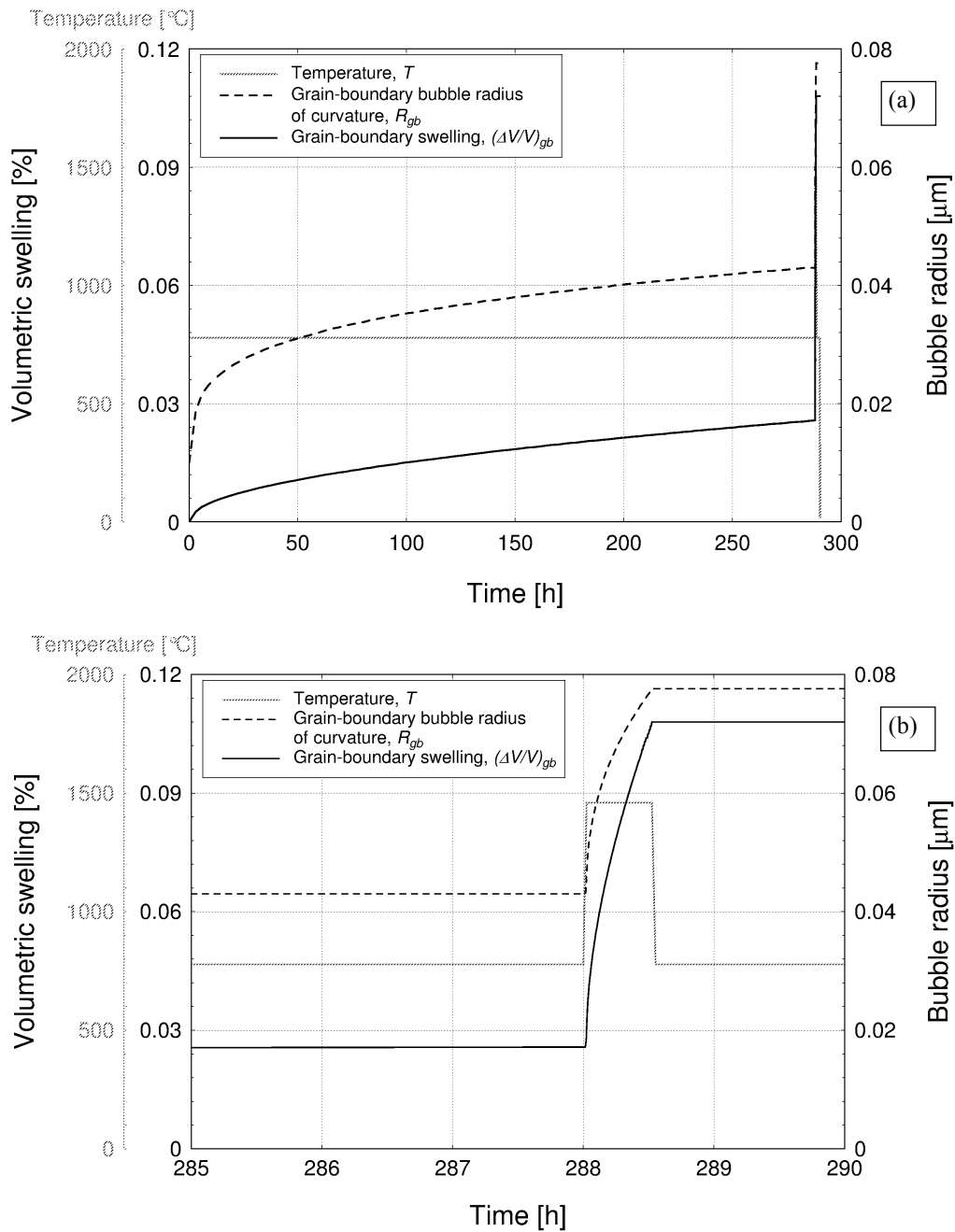
Fig. 3.10. Calculated grain-boundary bubble radius of curvature and grain-boundary swelling as a function of the time for the SEM zone 4000-F. The temperature is also shown (a) Entire ramp test, (b) zoom on the ramp.
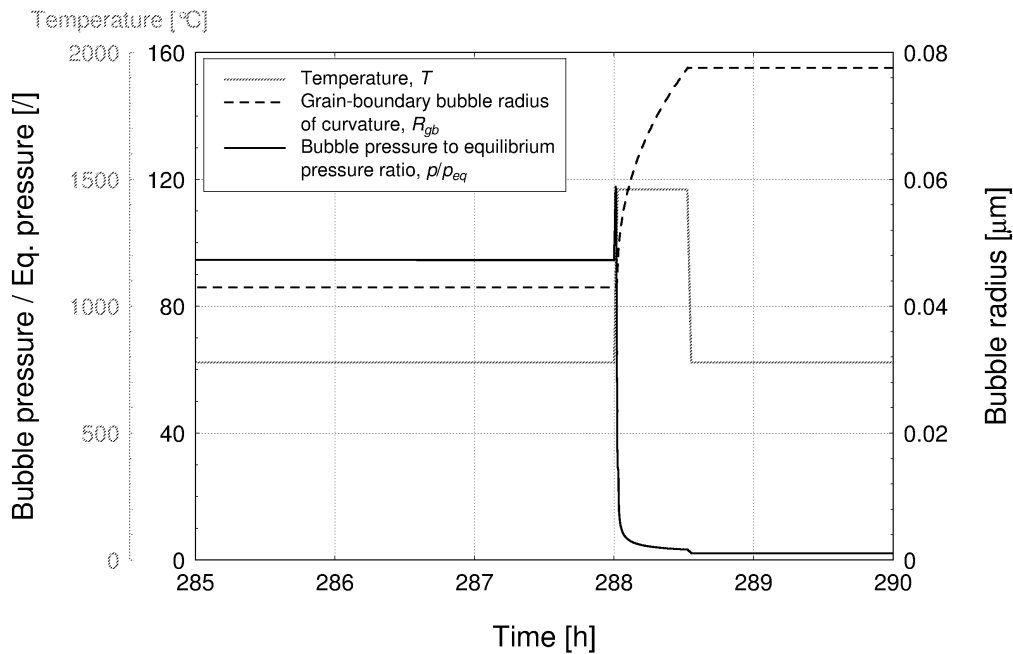
Fig. 3.11. Calculated grain-boundary bubble radius of curvature and ratio of the gas pressure in the bubble to the mechanical equilibrium pressure as a function of the time for the SEM zone 4000-F. The temperature is also shown. Zoom on the ramp is displayed.
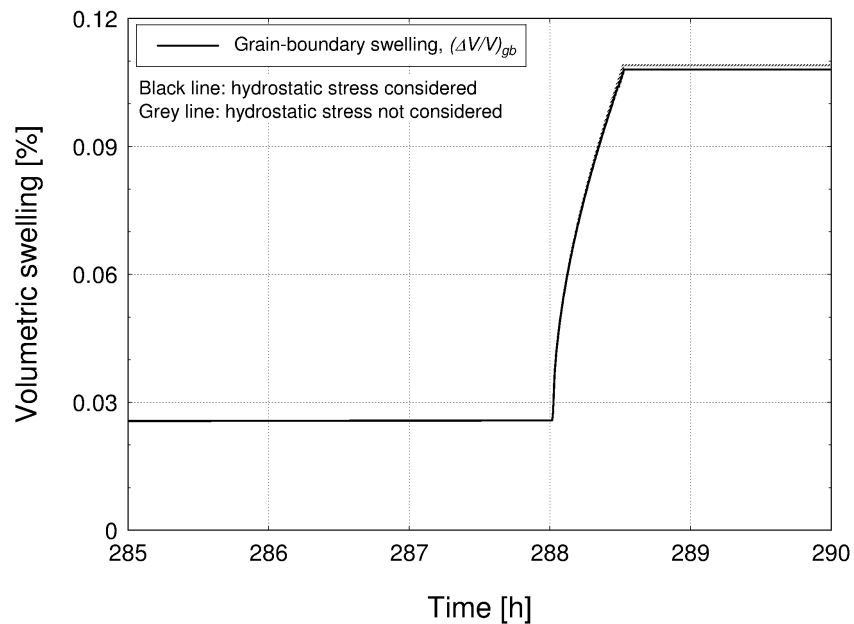

Fig. 3.12. Calculated grain-boundary swelling as a function of the time for the SEM zone 4000-F. The grey line corresponds to the swelling obtained by neglecting the stress-dependence in the model. Zoom on the ramp is displayed.
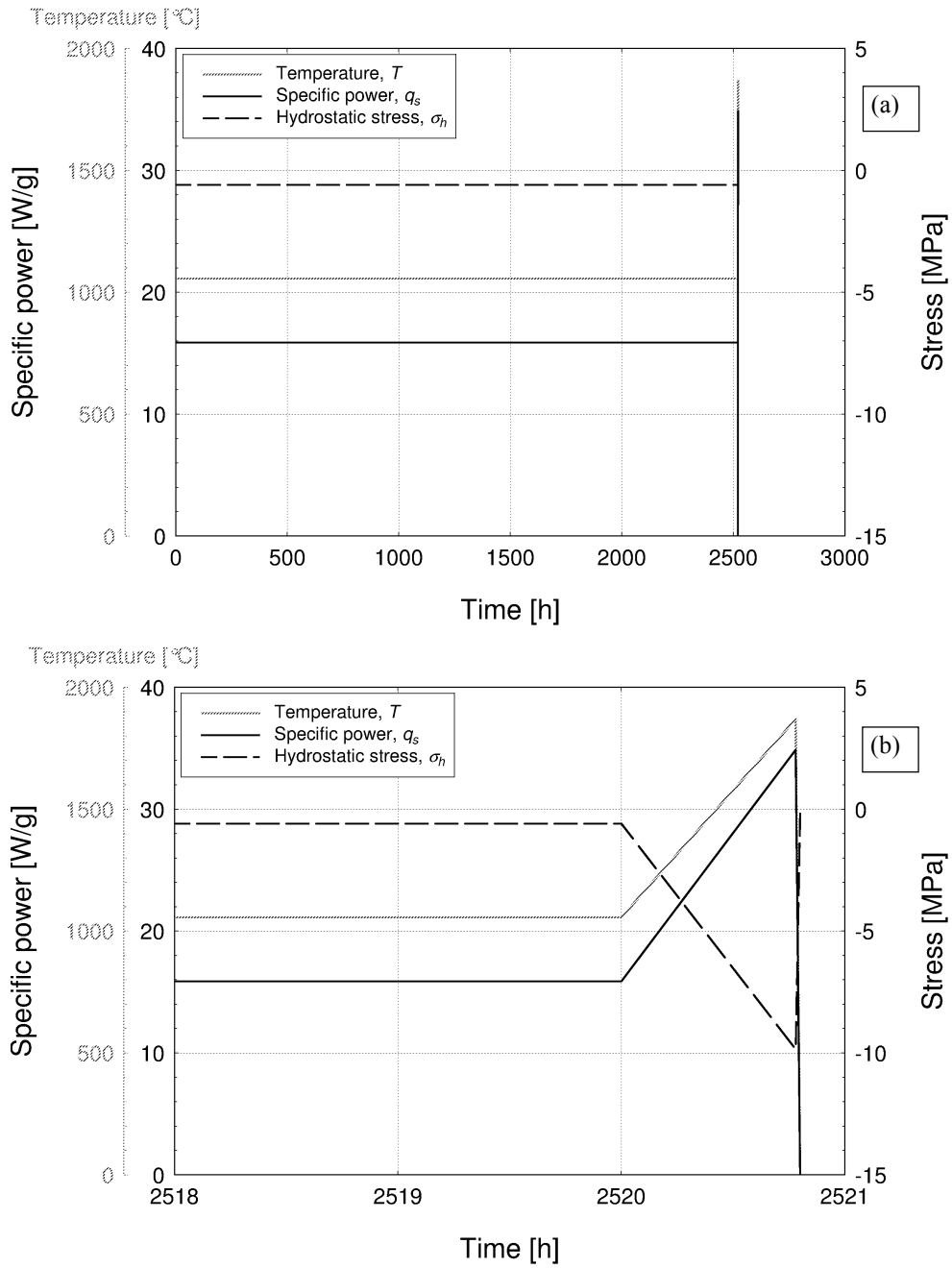
Fig. 3.13. Temperature, specific power, and hydrostatic stress as a function of the time for the SEM zone 4064-A. The temperature is also shown. (a) Entire ramp test, (b) zoom on the ramp.
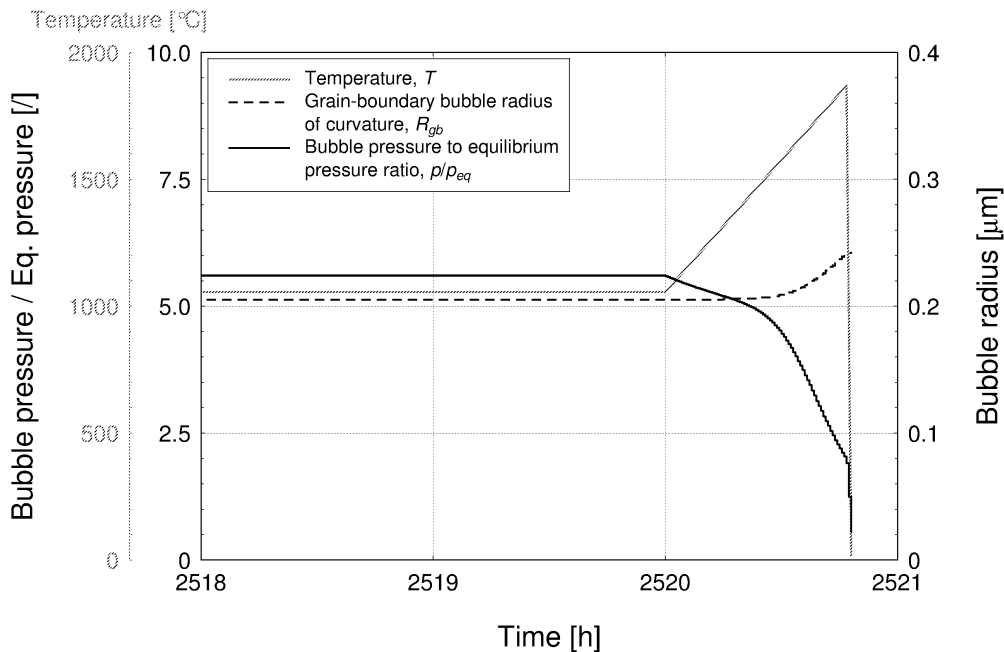
Fig. 3.14. Calculated grain-boundary bubble radius of curvature and ratio of the gas pressure in the bubble to the mechanical equilibrium pressure as a function of the time for the SEM zone 4064-A. The temperature is also shown. Zoom on the ramp is displayed.

Figure 3.14 shows the calculated radius of curvature of the grain-boundary bubbles as a function of the time, along with the ratio of the bubble pressure to the mechanical equilibrium pressure. The results confirm the dependence of the grain-boundary bubble growth rate on the temperature, and the general over-pressurization of the grain-boundary bubbles.

Figure 3.15 reports the calculated grain-boundary swelling and FGR as a function of the time. Figure 3.15-a confirms that the model consistently couples the swelling and the FGR, since the swelling rate decreases due to loss of gas from the grain boundaries when FGR commences. The capability of the model to reproduce the incubation behaviour of the FGR can also be appreciated. Figure 3.15-b shows the expected rapid increase of both the swelling and the FGR following the temperature rise during the power ramp.
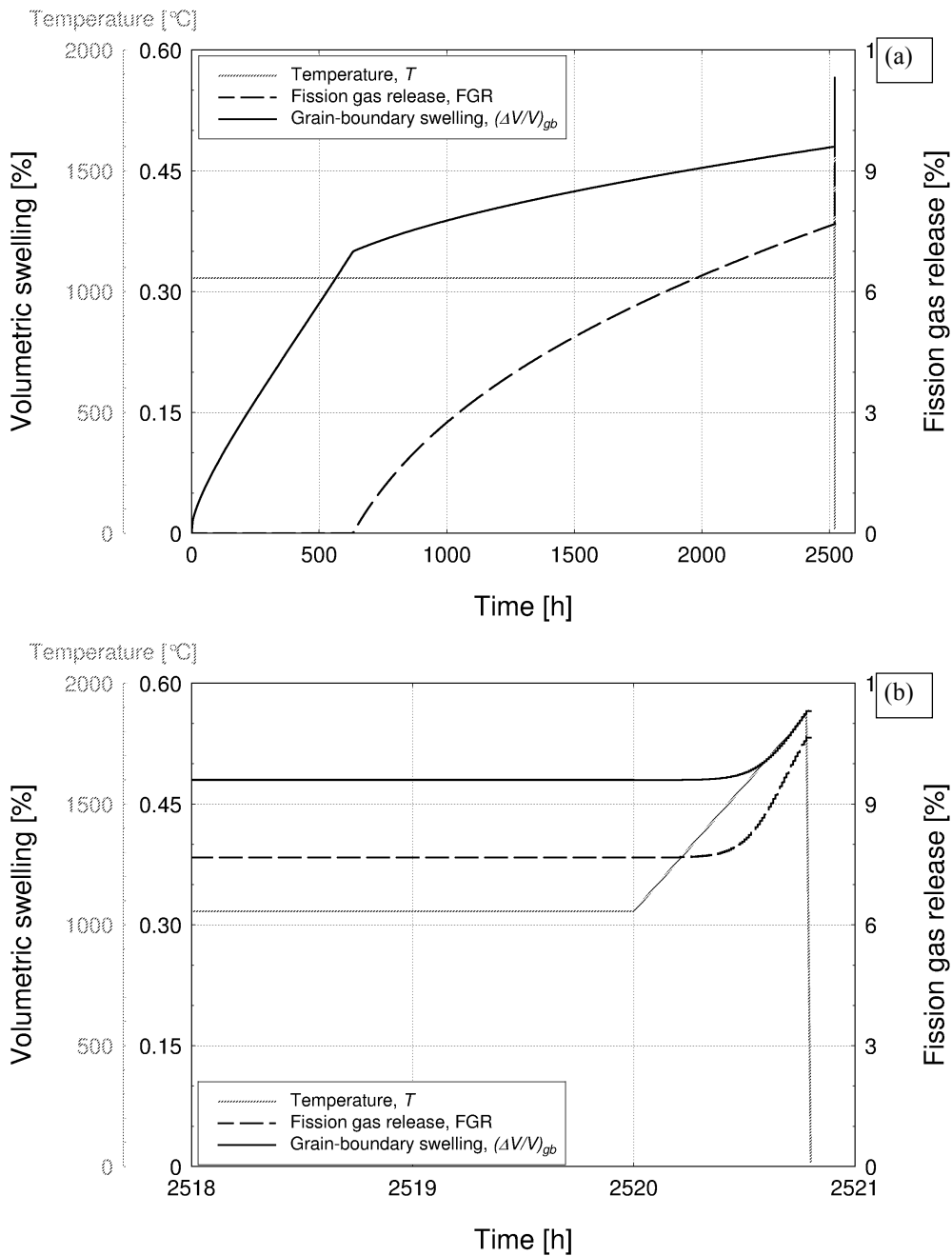
Fig. 3.15. Calculated grain-boundary swelling and fission gas release (defined as the ratio of the released to the generated gas) as a function of the time for the SEM zone 4064-A. (a) Entire ramp test, (b) zoom on the ramp.

As an example of power cycle case, the calculation results are presented for the SEM zone 4159-A. The fuel specimen was characterized by a burn-up of 20.2 GWd·(tM)$^{-1}$, and was subject to 114 power cycles of 4 h duration (Tables 3.1 and 3.3). The time-dependent input quantities (specific

power, temperature and hydrostatic stress) are presented in Fig. 3.16. The specific power was about 14 W·g^{-1} at the start of each cycle, and about 21 W·g^{-1} at the top of each cycle. The temperature ranged from 980°C (start) to 1360°C (top), and the compressive hydrostatic stress from 0.3-0.5 MPa (start) to 0.5-35 MPa (top), approximately.
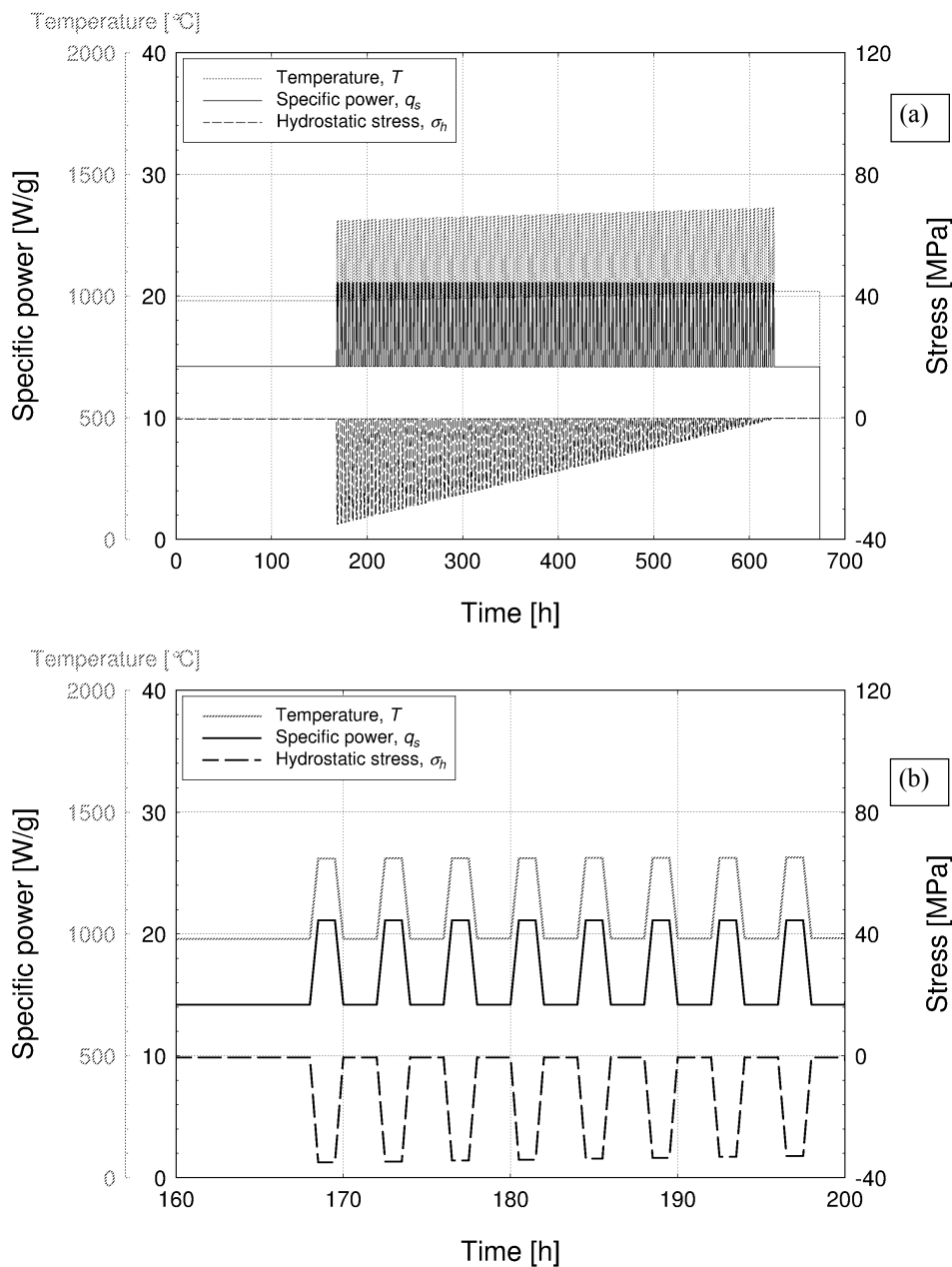

Fig. 3.16. Temperature, specific power, and hydrostatic stress as a function of the time for the SEM zone 4159-A. The temperature is also shown. (a) Entire cycling test, (b) zoom on the first cycles.

Figure 3.17 displays the radius of curvature of the grain-boundary bubbles and the bubble pressure to equilibrium pressure ratio as a function the time. The temperature-dependence of the bubble radius and over-pressure on the terms discussed above is confirmed.

Figure 3.18 shows the calculated grain-boundary swelling and FGR, pointing out the temperature-dependence of and coupling between these quantities, as well as the incubation behaviour of the FGR. Therefore, the analysis of this case qualitatively confirms the model calculations as a physically sound representation of the relevant processes.
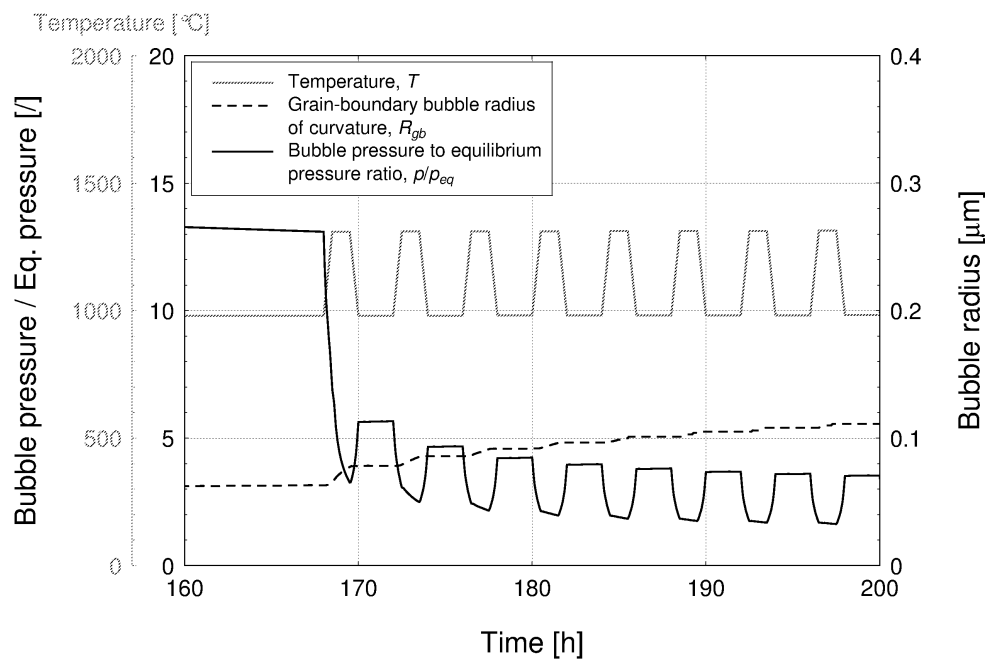

Fig. 3.17. Calculated grain-boundary bubble radius of curvature and ratio of the gas pressure in the bubble to the mechanical equilibrium pressure as a function of the time for the SEM zone 4159-A. The temperature is also shown. Zoom on the first cycles is displayed.
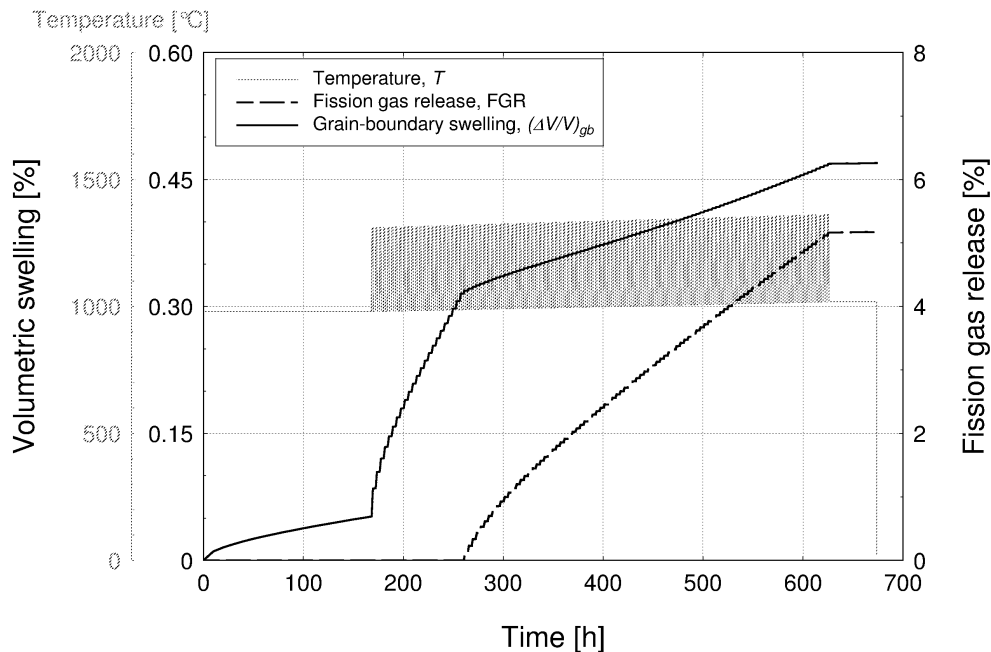
Fig. 3.18. Calculated grain-boundary swelling and fission gas release (defined as the ratio of the released to the generated gas) as a function of the time for the SEM zone 4159-A. The temperature is also shown. The entire cycling test is displayed.

3.4.2   Assessment of the results against experimental data of grain-boundary swelling

As a first step of verification of the model, the comparison of the calculations with all the 46 post-irradiation experimental data of grain-boundary swelling considered in the present work (Table 3.4) is shown in Fig. 3.19. Even if a moderate but systematic under-estimation is observed, this first quantitative assessment points out a reasonable overall agreement, without any tuning of the model parameters. Given the different characteristics of the simulated experiments, the model appears to be applicable to various irradiation conditions. This flexibility is a fundamental advantage pertaining to physics-based models. The discrepancies are expected to be to some degree associated with errors in the specific power, temperature, and hydrostatic stress values used as input data for the present calculations. Moreover, the uncertainties pertaining to the model parameters unavoidably limit the predictive accuracy of any model of fission gas swelling and release (Section 2.1). For example, the model results in terms of both grain-boundary swelling and FGR depend on the calculated arrival rate of gas at the grain-boundaries, that is, on the intra-granular diffusion calculations (Chapter 2). In turn, the accuracy of the intra-granular diffusion calculations is affected

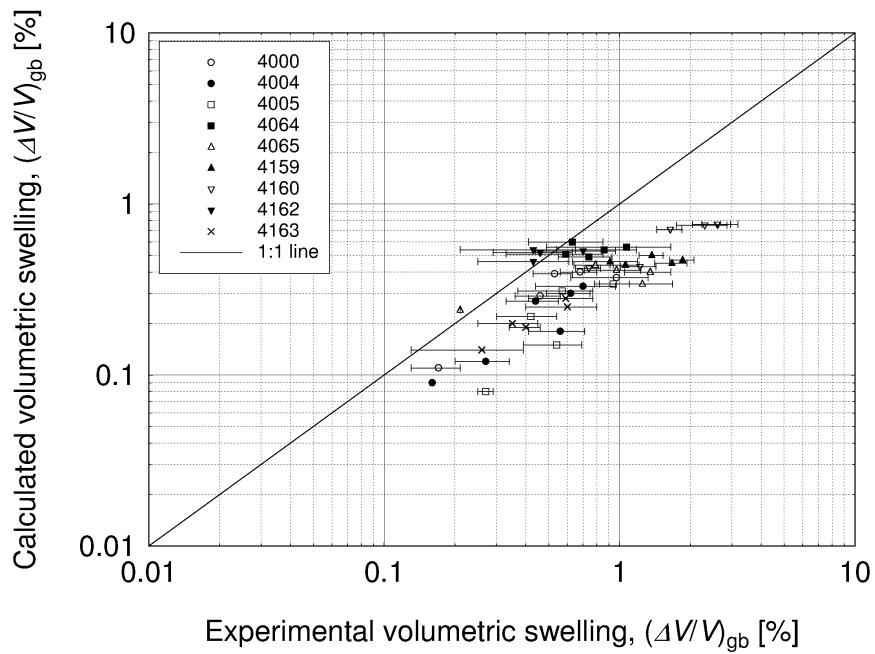Fig. 3.19. Comparison between the calculated values of grain-boundary swelling and the experimental data. All the 46 cases analysed in the present work are considered.
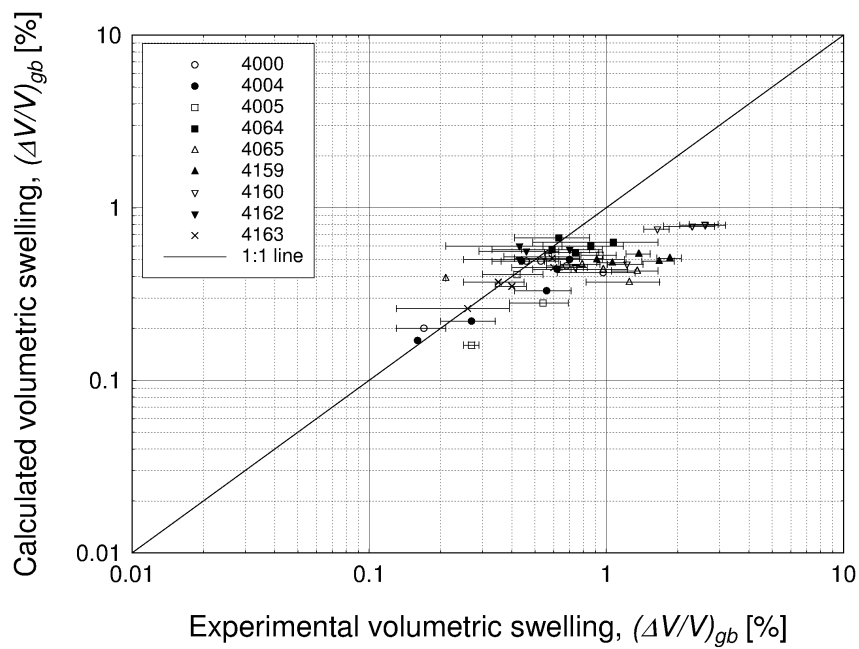

Fig. 3.20. Comparison between the calculated values of grain-boundary swelling, obtained by applying a gas atom diffusion coefficient multiplied by a factor of 5, and the experimental data. All the 46 cases analysed in the present work are considered.

by the uncertainties associated to the model parameters, above all the gas atom diffusion coefficient, which is characterized by an uncertainty of at least a factor of 10 (Section 2.1). In order to preliminarily evaluate the predictive capability of the new model in the light of this intrinsic limitation, a sensitivity analysis was carried out taking into consideration the uncertainties pertaining to the gas atom diffusion coefficient by means of a multiplication by a factor of 5. The results in terms of grain-boundary swelling are reported in Fig. 3.20. A remarkable difference is noticed in comparison with the results presented in Sub-section 3.4.2, pointing out that the systematic under-estimation observed in Fig. 3.19 may be largely ascribed to the uncertainties pertaining to the diffusion coefficient. It is concluded that the level of detail of the physical description adopted in the model is consistent with the intrinsic uncertainties.

3.5   Concluding remarks

As a preliminary step towards the implementation in a fuel rod analysis code, the developed model of fission gas swelling and release was coded as stand-alone version and applied to the analysis of either power ramped or power cycled fuel specimens. A qualitative study of the calculation results pointed out that the model consistently reproduces the main peculiarities of the fission gas behaviour, on a physical basis and in accordance with the observations reported in the literature. In particular, the model was proven to consistently describe:

- The development of the grain-boundary gas bubbles in terms of growth kinetics and progressive number density decrease.
- The over-pressurization of the grain-boundary bubbles.
- The coupling between the fission gas swelling and release.
- The dependence of both the fission gas swelling and release on the irradiation time (burn-up).
- The dependence of both the fission gas swelling and release on the temperature.
- The reduction of the fission gas swelling by the compressive hydrostatic stress.
- The reduction and delay of the fission gas release by the compressive hydrostatic stress.
- The incubation behaviour of the fission gas release.

A first quantitative assessment was carried out of the predictive capability of the model against a dataset of grain-boundary swelling measurements from the IFPE database. The systematic

comparison of the calculation results with the experimental data, along with a sensitivity analysis on the gas atom diffusion coefficient, pointed out that:

- The average predictive accuracy is reasonable, without any fitting of the model parameters.
- The model is applicable to various irradiation conditions.
- A moderate but systematic under-estimation is observed, which may be largely ascribed to the uncertainties pertaining to the diffusion coefficient.
- The level of detail of the physical description adopted in the model is consistent with the intrinsic uncertainties.

Despite its simplicity, the model therefore appears to provide both a physically acceptable representation of the relevant processes and an effective predictive character. Moreover, due to its physical basis, the model exhibits advantages in comparison with empirical correlations, both in terms of understanding of the relevant physical details and flexibility of application. However, the implementation in a fuel rod analysis code is needed in order to demonstrate the applicability of the model to integral fuel rod analyses, and therefore to the nuclear fuel design and licensing. This is dealt with in the next chapter.

Chapter 4

Model testing in the TRANSURANUS code

Abstract. *In this chapter, the implementation of the new integrated model of fission gas swelling and release in the TRANSURANUS fuel rod analysis code and the results obtained through integral fuel rod analyses are discussed. After incorporation in the mathematical-numerical framework of the code, the model was evaluated for the simulation of power ramped LWR fuel rods. The application of the model to the TRANSURANUS code was proven to bring about a sound description of the fuel rod behaviour in terms of fission gas swelling and release, with reasonable computational times. The main innovative aspects with respect to the treatments previously adopted in the code include the physical foundation of the model and the coupling between the fission gas swelling and release. Moreover, the experimentally observed dependence of both the fission gas swelling and release on the local hydrostatic stress in the fuel is reproduced. The appropriate modelling of this peculiarity is of high importance in view of the current tendency to extend the flexibility of use (load-following) and the discharge burn-up of the nuclear fuel, which can involve the occurrence of strong PCMI and consequently of high compressive hydrostatic stress in the fuel due to cladding restraint. The comparison of the results with experimental data from the IFPE database in terms of integral fuel rod FGR is presented, pointing out a reasonable overall agreement without any tuning of the physical model parameters, along with some improvements compared to the predictions obtained using the standard models of the TRANSURANUS code. The chapter is organized as follows. In Section 4.1, the main issues and methods concerning the implementation of the model in the TRANSURANUS code are briefly overviewed. In Section 4.2, the experimental databases considered for the verification of the model are described. In Section 4.3, the results of the analyses are presented, showing the capabilities of the new model to reproduce the peculiarities of the fission gas swelling and release, as well as the obtained predictive accuracy in terms of integral fuel rod FGR. Conclusions are drawn in Section 4.4.*

4.1   Implementation of the model in the TRANSURANUS code

After being developed coherently with the goals of the work (Chapters 1 and 2) and subsequently applied as stand-alone version with encouraging results (Chapter 3), the new integrated model of fission gas swelling and release was successfully implemented in the TRANSURANUS fuel rod analysis code. The new model was incorporated in the mathematical-numerical framework of the code as an implicit model, which provides calculation of both the fission gas swelling and release. The model was coupled with the pre-existing TRANSURANUS subprograms for the calculation of the fission gas generation rate and the solution of the intra-granular gas diffusion equation (Section 1.2). Also, the TRANSURANUS models (Lassmann et al., 2011) were adopted for taking into account the athermal release mechanisms and the grain boundary sweeping effect (Section 1.1). Moreover, the new model was integrated with the MATPRO (1979) model for the swelling due to solid fission products (solid swelling), in order to provide a comprehensive and consistent calculation of the fuel swelling.

As a contribution to the non-elastic strains, the calculated swelling affects the calculated stresses through the mechanical analysis. Since the gas bubbles contribute to the fuel porosity (gaseous porosity), the fission gas swelling also influences the fuel thermal conductivity and temperature. On the other hand, the FGR acts to degrade the thermal conductance of the fuel-cladding gap and to increase the fuel rod internal pressure (Lassmann et al., 2011). In turn, the whole thermo-mechanical analysis provides the input parameters for the model in terms of stresses, temperatures and source term of fission products. The local hydrostatic stress is considered in the model calculations, while in the fission gas swelling and FGR models currently adopted in the fuel rod analysis codes, the hydrostatic stress is often neglected, or approximated as constant and uniform, or represented by the external pressure of the fuel pellet (e.g., Koo et al., 2000; Suzuki, 2000; Van Uffelen et al., 2004; Lassmann et al., 2011). The new model was therefore implemented as an interactive part of the mathematical-numerical structure of the TRANSURANUS code, providing a consistent matching between the non-linear, stress-dependent fission gas swelling and release calculations and the thermo-mechanical fuel rod analysis. Also, given that the differential equations involved in the model and governing the grain-boundary gas behaviour are solved incrementally (Section 2.3), a simple accuracy-controlling time step criterion was developed and implemented. In a preliminary approach, the following limitation was proven to assure suitable accuracy of the fission gas swelling and release calculations for all the cases analysed in the present work:

$$\Delta t \leq 3.6 \left[N_{gb} \left(\frac{\partial A_{gb}}{\partial t} \right)_g \right]^{-1} \tag{4.1}$$

where Δt [s] is the time step length, N_{gb} [(bub.)·m^{-2}] the number density of grain-boundary gas bubbles, and $(\partial A_{gb}/\partial t)_g$ [m^2·s^{-1}] the variation of the bubble area owing to bubble growth (Section 2.3). The performed calculations pointed out the obtainment of stable numerical solutions in all the considered conditions, with reasonable computational times (see also Sub-section 4.3.3), thus proving the meeting of the numerical convergence and computational cost requirements.

Adopting the new integrated model, the TRANSURANUS code was employed for the analysis of the irradiation experiments of the Super-Ramp and Inter-Ramp Projects (Djurle 1979, 1984). The results in terms of fission gas swelling and release were critically evaluated and compared with the predictions obtained using the standard models of the code. Moreover, the model was evaluated against experimental data of integral fuel rod FGR[6], as discussed in the next sections.

4.2 Experimental databases

The databases of the Super-Ramp and Inter-Ramp Projects refer to PWR-UO$_2$ and BWR-UO$_2$ fuel rods, respectively, power ramp-tested in the Studsvik reactor R2 after base-irradiation. During the Super-Ramp and Inter-Ramp Projects, 46 fuel rods (26 and 20, respectively) were tested, that means a total irradiation time of approximately 180 equivalent years in reactor.

The Super-Ramp rods were base-irradiated in a burn-up range of 28 to 45 GWd·(tM)$^{-1}$, while those of Inter-Ramp experienced burn-ups of 8-20 GWd·(tM)$^{-1}$. In addition to PWR and BWR standard type fuel rods, several rods with different design parameters (i.e., gap width, fuel density and grain size, ^{235}U enrichment, annular and solid pellets, gadolinium content) were tested through these two Projects. The main pre-irradiation characterization data for the different groups of rods are summarized in Tables 4.1 and 4.2. An example of base-irradiation and power ramp is shown in Fig. 4.1, and the power ramp test features for all the fuel rods considered in the present work are

---

[6] Integral quantities are those referred to the entire fuel rod – e.g., total amounts of fission gas generated and released in the fuel rod, inner rod pressure.

reported in Tables 4.3 and 4.4. The ramp test consists of a conditioning time and a subsequent power ramp, followed by a holding time at the ramp terminal level (RTL), and reactor shut-down.

Table 4.1 - Pre-irradiation data for the different groups of PWR fuel rods from the Super-Ramp Project.

Group	Pellet type	Average burn-up [GWd/tU]	Diametral gap width [μm]	UO$_2$ density [%TD]	Average grain size [μm]	Enrichment [wt% ^{235}U]
PK1	Standard	33–36	191–200	95*	6.0	3.20
PK2	Standard	41–45	145	94[*]	5.5	3.21
PK4	Gd$_2$O$_3$ (4.1 wt%)	33–34	167–169	94[*]	5.5	3.19
PK6	Large grain	34–37	145–146	95[*]	22.0	2.99
PW3	Standard	28–31	170	94**	10.5	8.26
PW5	Annular	32–33	162–165	95**	16.9	5.74

[*]Calculated from pellet density measurements. [**]Calculated from measurements of pellet weights and dimensions.

Table 4.2 - Pre-irradiation data for the different groups of BWR fuel rods from the Inter-Ramp Project.

Group	Pellet type	Average burn-up [GWd/tU]	Diametral gap width [μm]	UO$_2$ density [%TD] [*]	Average grain size [μm]	Enrichment [wt% ^{235}U]
LR	Standard	8.5–10.3	150	95	8.3	2.82
LS	Standard	8.2–10.4	150	95	8.3	2.82
TR	Standard	10	80	95	8.3	2.82
TS	Standard	9.8	80	95	8.3	2.82
DR	Standard	7.9	150	93	10.9	2.82
HR	Standard	16.6–19.8	150	95	8.4	3.50
HS	Standard	16.6–19.3	150	95	8.4	3.50
BR	Standard	19.9	250	95	8.4	3.50

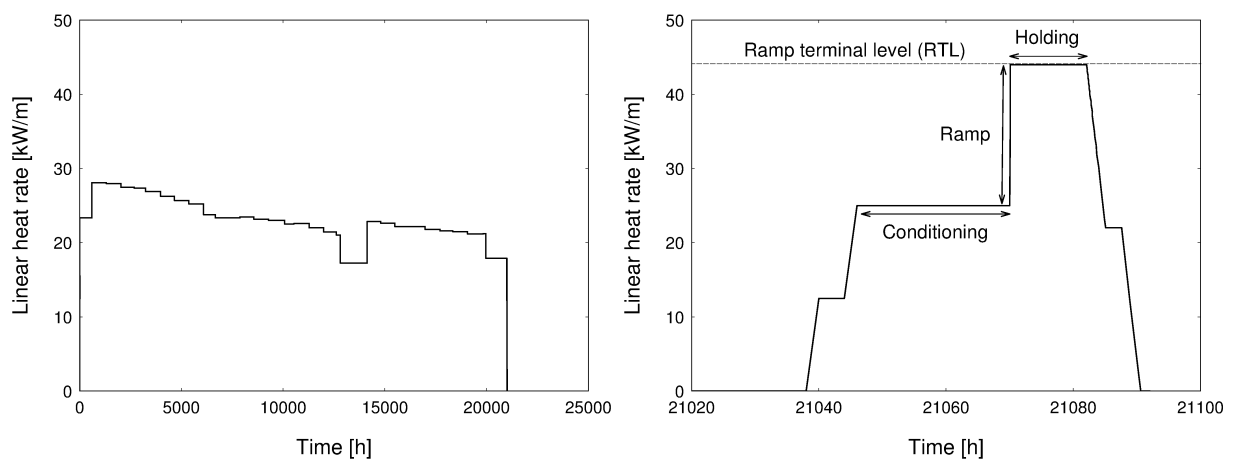[*] Design specifications.

Fig. 4.1. Linear heat rate history in axial peak position for the Super-Ramp PK1-2 rod, during the base-irradiation (left-hand side) and the ramp test (right-hand side).

Table 4.3 - Features of the ramp tests in axial peak position for the Super-Ramp PWR fuel rods considered in the present work.

Rod	Conditioning power level [kW·m^{-1}]	Conditioning time [min]	Power ramp rate [kW·m^{-1}· min^{-1}]	Ramp terminal level [kW·m^{-1}]	Holding time at RTL [min]
PK1-1	25.0	1440	9.0	41.5	720
PK1-2	25.0	1440	8.0	44.0	720
PK1-3	25.0	1440	8.5	47.5	720
PK1-4	25.0	1440	9.5	47.5	720
PK2-1	25.0	1440	8.5	41.0	720
PK2-2	25.0	1440	9.5	46.0	720
PK2-3	25.0	1440	8.5	49.0	720
PK2-4	25.0	1440	8.5	44.0	1°
PK2-S	25.0	1440	8.5	44.0	720
PK4-1	25.0	1440	8.0	39.0	720
PK4-2	25.0	1440	8.5	44.5	720
PK4-3	25.5	1440	11.0	50.5	720
PK6-2	25.5	1440	9.0	40.0	720
PK6-3	25.0	1440	9.0	43.0	720
PK6-S	24.0	1440	10.0	41.0	720
PW3-2	25.5	1440	10.0	35.3	720
PW3-3	25.0	1440	10.0	37.2	720

° Intentionally interrupted.

Table 4.4 - Features of the ramp tests in axial peak position for the Inter-Ramp BWR fuel rods considered in the present work.

Rod	Conditioning power level [kW·m^{-1}]	Conditioning time [min]	Power ramp rate [kW·m^{-1}· min^{-1}]	Ramp terminal level [kW·m^{-1}]	Holding time at RTL [min]
LR1	29.8	1440	4.8	43.8	1440
LS2	31.8	1440	3.9	43.8	1440
LS3	25.0	1440	3.9	41.8	1440
TR1	30.7	1440	4.2	42.2	1440
DR1	22.9	1440	4.5	43.2	1440
HR2	23.0	1440	4.5	38.0	1440
HR4	29.0	1440	4.2	46.1	1440
HR5	29.0	1440	4.2	47.9	1440
HS1	30.3	1440	3.9	47.8	26°
HS2	24.8	1440	3.9	41.0	1440
BR1	31.1	1440	3.9	51.0	1440

° Intentionally interrupted.

With reference to an extensive experimental analysis program and to detailed records of fuel rods power histories (Djurle, 1979, 1984), wide experimental databases were constructed during the Super-Ramp and Inter-Ramp Projects, which were made available through the IFPE database

(Sartori et al., 2010) and constitute a useful basis for the verification of the fuel rod analysis codes. Most of the rods (namely, the PK6 and PW3 rod groups of the Super-Ramp Project and all the rods of the Inter-Ramp Project) were selected within the FUMEX-III co-ordinated research project of the IAEA (Killeen et al., 2009) as cases of priority interest for comparison and validation of different fuel rod analysis codes.

All the fuel rod irradiation experiments from the Super-Ramp and Inter-Ramp Projects were simulated in the present work by means of the TRANSURANUS code, using the new, implemented model for the calculation of the fission gas swelling and release. The available information on the fuel rod fabrication data and irradiation conditions was critically analysed and consistent input files were set up for the TRANSURANUS code. The analyses were carried out coherently with the power histories and coolant conditions from the beginning-of-life (BOL) to the end of the ramp test (end-of-life – EOL), using the design specifications and pre-irradiation characterization data of the analysed rods provided in (Djurle, 1979, 1984). With reference to the various options available to the TRANSURANUS code for the treatment of the other relevant phenomena and material properties, a suitable setup for the test conditions of interest was established on the basis of previous assessments of the code (Luzzi, 2002; Van Uffelen et al., 2007; Di Marcello and Luzzi, 2008; Luzzi et al., 2008; Pastore et al., 2009a, 2009b), taking into account the different specificity of PWR and BWR type fuel rods.

4.3   Results and discussion

4.3.1   Model capabilities

As a first exemplifying case[7], the results of the analysis of the PK1-1 fuel rod from the Super-Ramp Project are presented. The linear heat rate (input quantity) and the calculated fuel central temperature as a function of the burn-up are shown in Fig. 4.2. The considered axial position is the fuel rod mid-plane (peak linear heat rate and temperature position). The PK1-1 rod was characterized by a peak linear heat rate of 17.5-27.1 kW·m^{-1} during the base-irradiation, approximately, and it was raised from a conditioning power level (CPL) of 25.0 kW·m^{-1} to a RTL of

---

[7] Analyses were systematically performed of all the 46 fuel rods of the Super-Ramp and Inter-Ramp Projects. The exemplifying cases discussed here are representative of the general model capabilities observed for the whole set of simulations.
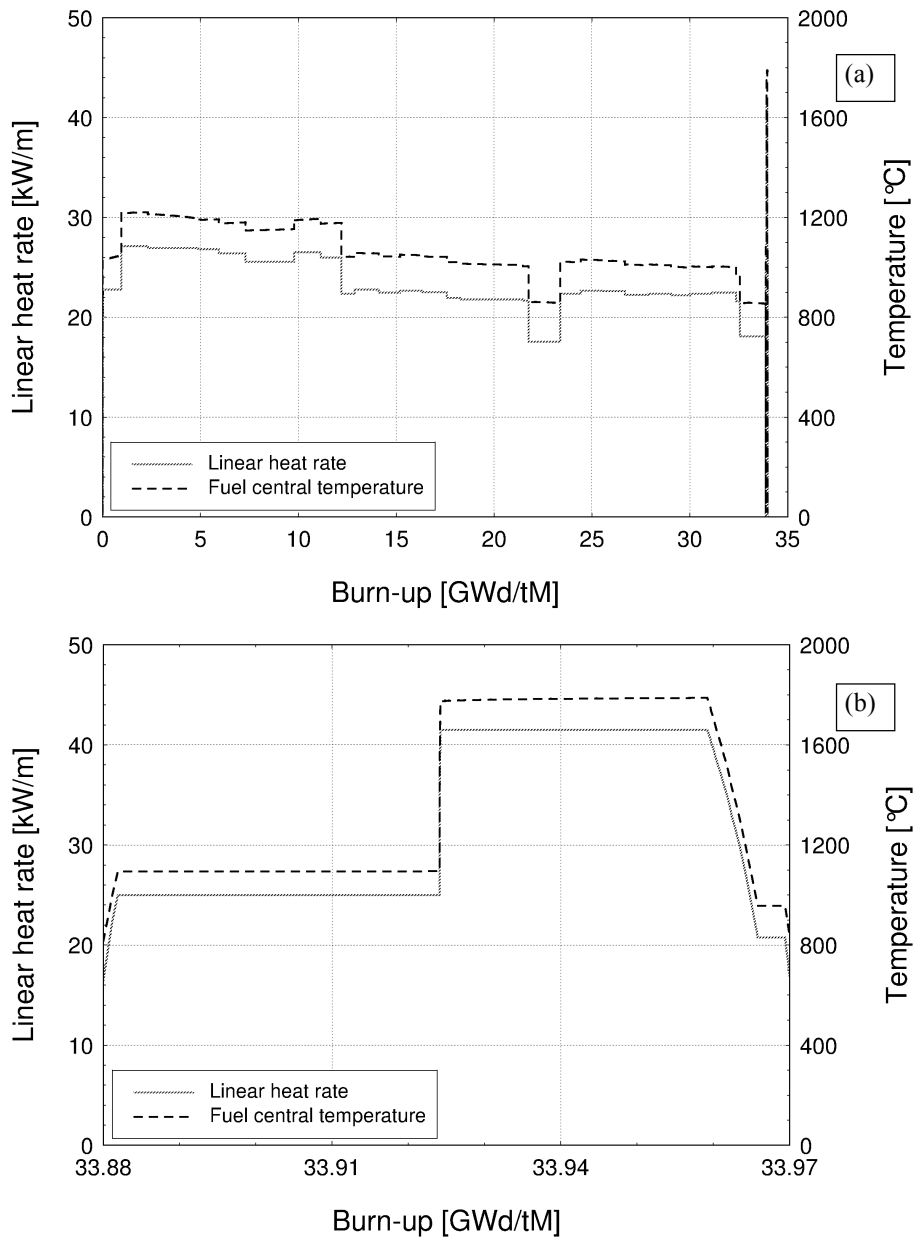
Fig. 4.2. Linear heat rate and fuel central temperature as a function of the burn-up at the mid-plane of the PK1-1 fuel rod. (a) Entire irradiation time, (b) zoom on the ramp test.

41.5 kW·m^{-1} during the ramp test (Table 4.3). At the top of the power ramp (beginning of the holding time), the calculated fuel temperature reached a value of about 1770°C at the pellet centre, and about 410°C at the pellet surface. Figure 4.3 displays the radial width of the fuel-cladding gap at the fuel rod mid-plane as a function of the burn-up.
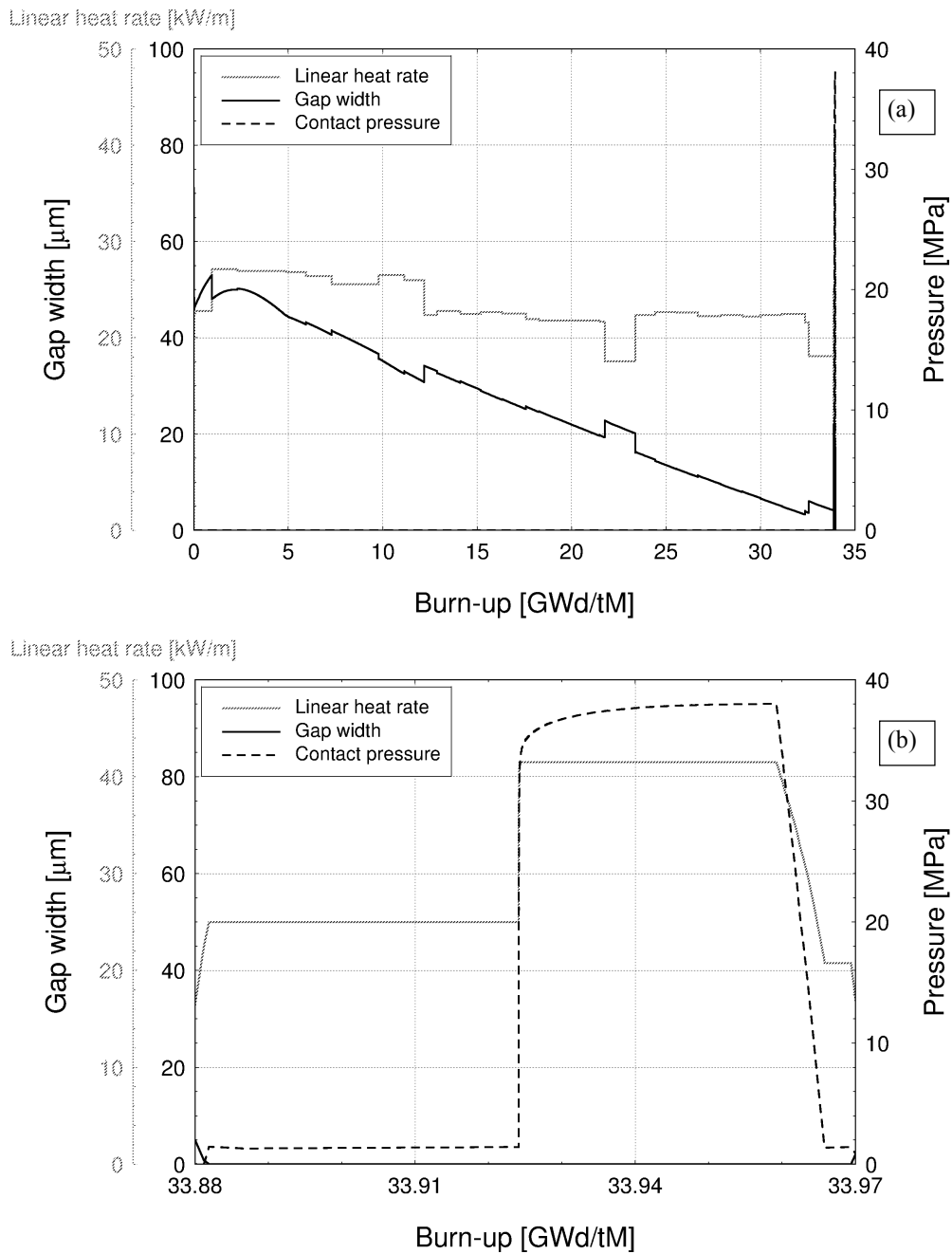
Fig. 4.3. Linear heat rate, radial gap width and fuel-cladding contact pressure as a function of the burn-up at the mid-plane of the PK1-1 fuel rod. (a) Entire irradiation time, (b) zoom on the ramp test.

Starting from the initial value of 100 μm, the gap width abruptly decreases at BOL due to pellet-fragment relocation. During the early stages of the base-irradiation (burn-up < 2.3 GWd·(tM)$^{-1}$, approximately), the gap width tends to increase due to fuel densification. Subsequently, the gap

width progressively reduces as a consequence of the fuel swelling and of the cladding creep-down due to the external coolant pressure. At the beginning of the conditioning time, the gap closes and pellet-cladding mechanical interaction (PCMI) occurs, leading to the onset of fuel-cladding contact pressure (Fig. 4.3). The contact pressure strongly increases during the power ramp as a consequence of the fuel swelling and the differential thermal expansion of the fuel and the cladding, and may determine high compressive hydrostatic stress in the fuel.

The calculated volumetric fission gas swelling, FGR and temperature for the PK1-1 rod at a burn-up of about 10 GWd·(tM)$^{-1}$ are displayed in Fig. 4.4 as a function of the pellet radius. The considered axial position is the fuel rod mid-plane. The summation of the contributions due to intra-granular and grain-boundary gas bubbles is considered as the fission gas swelling (Section 2.3). The grain-boundary swelling, however, was proven to be the dominant contribution to the calculated fission gas swelling for all the cases analysed in the present work. The FGR is defined as the ratio of the released to the generated gas. It is worth underlining that the gas locally released/generated (hence,
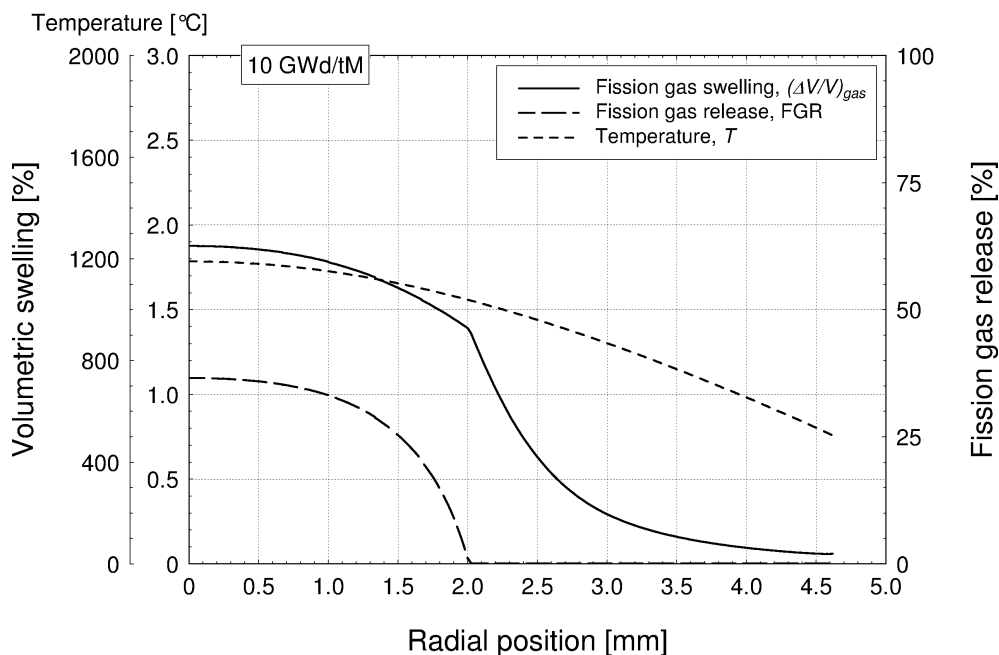

Fig. 4.4. Fission gas swelling, fission gas release and temperature as a function of the pellet radius at the mid-plane of the PK1-1 fuel rod. The figure refers to a burn-up of 10 GWd·(tM)$^{-1}$.

the local FGR) is represented in the profile shown in Fig. 4.4, which differs from the integral FGR considered further in this chapter. Figure 4.4 shows that both the calculated swelling and FGR decrease with increasing distance from the pellet centre, reflecting the spatial dependence of the temperature in the fuel. In fact, the temperature drives both the inflow of gas atoms and the vacancy absorption at the grain-boundary bubbles, thus determining the bubble growth and coalescence rate, and in turn the fission gas swelling and release (Sections 2.3 and 3.4). As predicted by the model, the FGR does not occur beyond a certain distance from the pellet centre (apart from the small contribution due to the athermal release that is not perceptible in the figures). The fuel zone, which is not affected by significant FGR, lies towards the decreasing temperatures, where the condition of grain boundary saturation (Section 2.3) is not attained. It is also noticed that the swelling gradient abruptly changes at the radial position delimiting the zone where FGR takes place. In fact, the new model physically considers the swelling as dependent on the amount of gas retained on the grain boundaries, which is in turn affected by the FGR. The curves presented in Fig. 4.4 therefore reflect the physical basis of the model and demonstrate the consistent coupling between the fission gas swelling and release. This peculiarity was previously not considered in the TRANSURANUS code (see Sub-section 4.3.3) and represents an innovative contribution of the present work.

Figure 4.5 shows the fission gas swelling, FGR and temperature radial profiles for the PK1-1 rod at burn-ups of about 20 GWd·$(tM)^{-1}$ and about 30 GWd·$(tM)^{-1}$. The dependence of the swelling and the FGR on the temperature is evident. Also, the comparison between Fig. 4.4 and Fig. 4.5 points out that the model catches the dependence of both phenomena on the burn-up. In particular, the swelling increases with burn-up due to the progressive inflow of gas atoms and vacancy absorption at the grain-boundary bubbles (see also Section 3.4). Bubble growth with burn-up is also reflected in progressive broadening of the fuel portion affected by the FGR. The physical complementarity between the fission gas swelling and release can be appreciated.

When also considering the calculated solid swelling (not shown here), the predicted rate of (radially averaged) total volumetric fuel swelling for the PK1-1 rod during the base-irradiation is of about 0.09% per GWd·$(tM)^{-1}$. This value falls within the experimental range of 0.08-0.1% per GWd·$(tM)^{-1}$ for burn-ups $\leq$ 40 GWd·$(tM)^{-1}$ (Assmann and Manzel, 1977; Zimmermann, 1978; Franklin et al., 1984; Spino et al., 2005), thus proving the physical acceptability and reasonable predictive accuracy of the new model in terms of swelling.
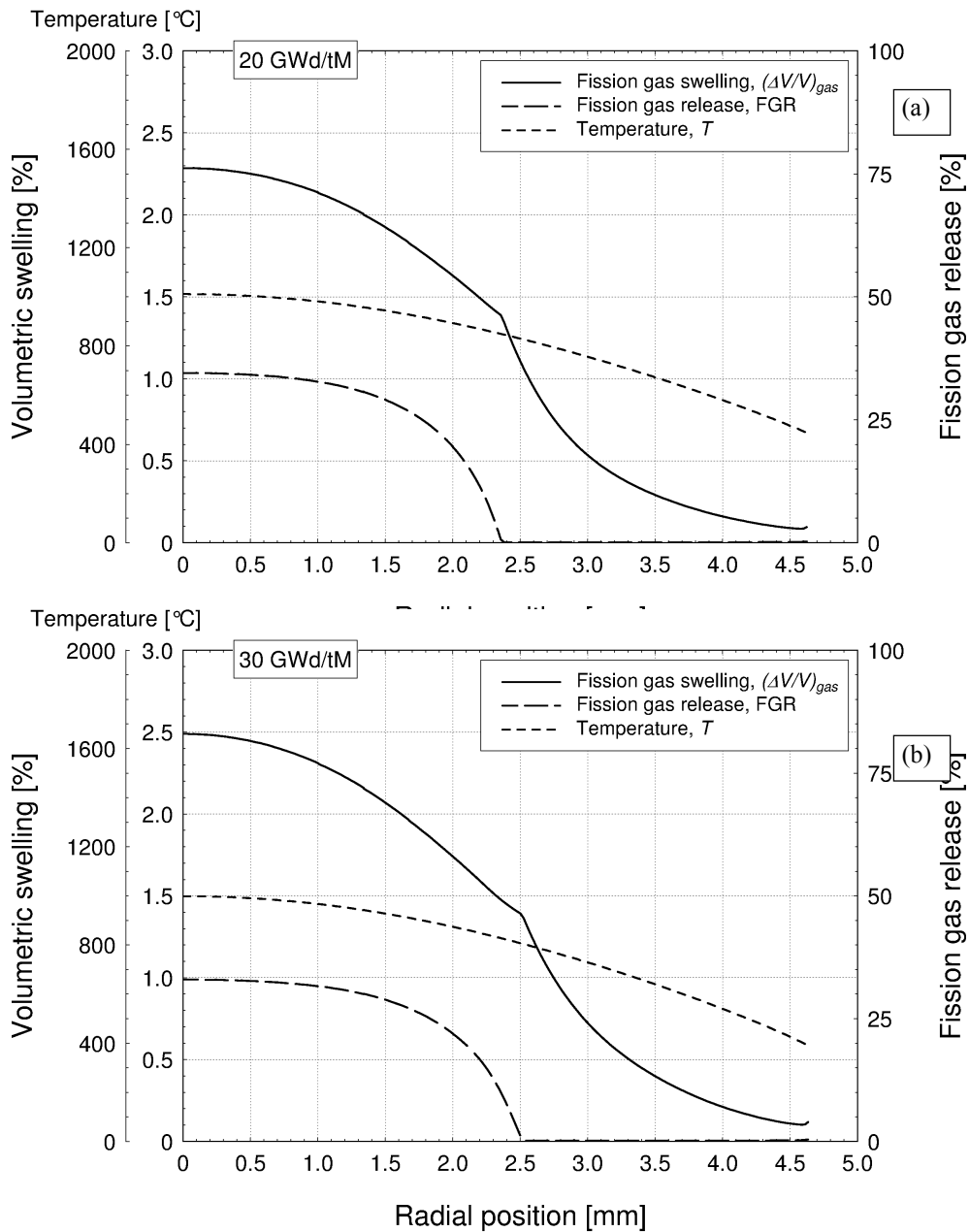
Fig. 4.5. Fission gas swelling, fission gas release and temperature as a function of the pellet radius at the mid-plane of the PK1-1 fuel rod. The graphs refer to burn-ups of (a) 20 GWd·(tM)$^{-1}$ and (b) 30 GWd·(tM)$^{-1}$.

The radial profiles of fission gas swelling, hydrostatic stress and temperature for the PK1-1 rod at the top of the power ramp (beginning of the holding time, see Fig. 4.1) are shown in Fig. 4.6. It is
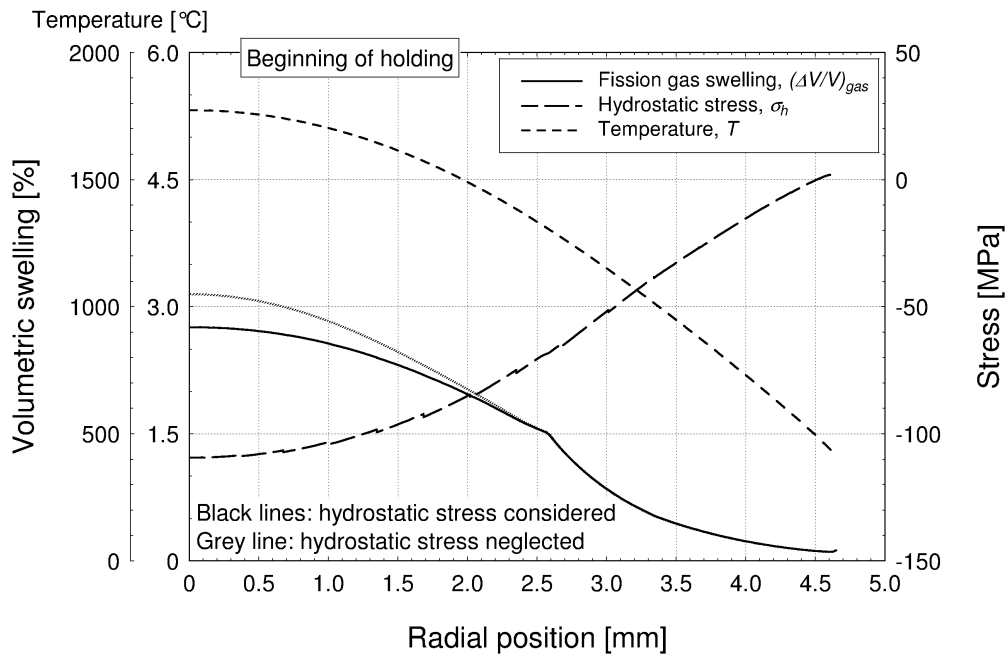
Fig. 4.6. Fission gas swelling, hydrostatic stress (considered to be negative if compressive) and temperature as a function of the pellet radius at the mid-plane of the PK1-1 fuel rod. The fission gas swelling calculated by neglecting the stress-dependence is also shown. The figure refers to the beginning of the holding time.

worth pointing out that the discontinuities observed in the stress profile represent a characteristic of the TRANSURANUS code analyses and are related to the different elastic constants calculated at the different zones of spatial discretization. Due to strong PCMI, high compressive hydrostatic stress takes place in the central zone of the fuel pellet (about 110 MPa at the pellet centre) following the power ramp. High compressive hydrostatic stress due to cladding restraint under PCMI conditions was experimentally observed to significantly affect both the fission gas swelling and release (Zimmermann, 1978; Kogai et al., 1988; Walker et al., 1988, Mogensen et al., 1993; Kashibe and Une, 1997). In particular, the compressive stress reduces the growth rate of the grain-boundary bubbles and consequently suppresses the fission gas swelling, also delaying and reducing the FGR. An improved understanding of the fuel behaviour under PCMI conditions is of high importance in view of the current tendency to extend the discharge burn-up and the flexibility of use (load-following) of the nuclear fuel. From this viewpoint, it is essential to develop models that properly take into consideration the dependence of the fission gas swelling and release on the hydrostatic stress

(OECD/NEA, 2004). The grey line in Fig. 4.6 represents the swelling profile calculated by neglecting the stress-dependence in the model. The effect of the stress in suppressing the swelling, as reproduced by the new model, is noticeable.

The calculated integral fission gas release[8] and fuel central temperature as a function of the burn-up for the PK1-1 rod are presented in Fig. 4.7. The experimentally observed incubation behaviour of the FGR (Vitanza et al., 1978), and its dependence on the temperature, can be appreciated. Figure 4.8 compares the integral FGR during the ramp test as a function of the burn-up with that obtained by neglecting the stress-dependence in the model. The radially averaged hydrostatic stress in the fuel as a function of the burn-up is also displayed. It is worth emphasizing that the new model consistently takes into account the local hydrostatic stress. The radially averaged value is presented in Fig. 4.8 only as indicative of the development of a high compressive hydrostatic stress during the power ramp test, which results from PCMI and the associated fuel-cladding contact pressure (Fig. 4.3). As for the complementary phenomenon of fission gas swelling, the FGR is remarkably affected by the hydrostatic stress during the power ramp test. As the FGR proceeds by growth of the grain-boundary bubbles, inhibition of the bubble growth by the compressive stress significantly reduced the FGR (see also Section 3.4). It is also noticed that, during the stages of irradiation before the ramp, the FGR in absence of stress is slightly lower than that calculated by considering the stress. This was proven to be ascribed to the higher swelling in absence of stress, that means lower fuel temperature during the base-irradiation in this case since the fuel-cladding gap is narrower, and its thermal conductance is consequently higher. Since the temperature affects the FGR by driving the inflow of gas atoms and the vacancy absorption at the bubbles (Section 2.3), the above indirect effect of the swelling on the FGR turns out to dominate in this case during the stages before the ramp.

As a further exemplifying case, the results of the analysis of the LR1 fuel rod from the Inter-Ramp Project are presented. The linear heat rate and the calculated fuel central temperature as a function of the burn-up at the fuel rod mid-plane are shown in Fig. 4.9. The LR1 rod was characterized by a peak linear heat rate of 25.0-39.7 kW·m^{-1} during the base-irradiation, approximately, and it was raised from a CPL of 29.8 kW·m^{-1} to a RTL of 43.8 kW·m^{-1} during the ramp test (Table 4.4). At the beginning of the holding time, the calculated fuel temperature reached a value of about 1675°C at the pellet centre, and about 455°C at the pellet surface.

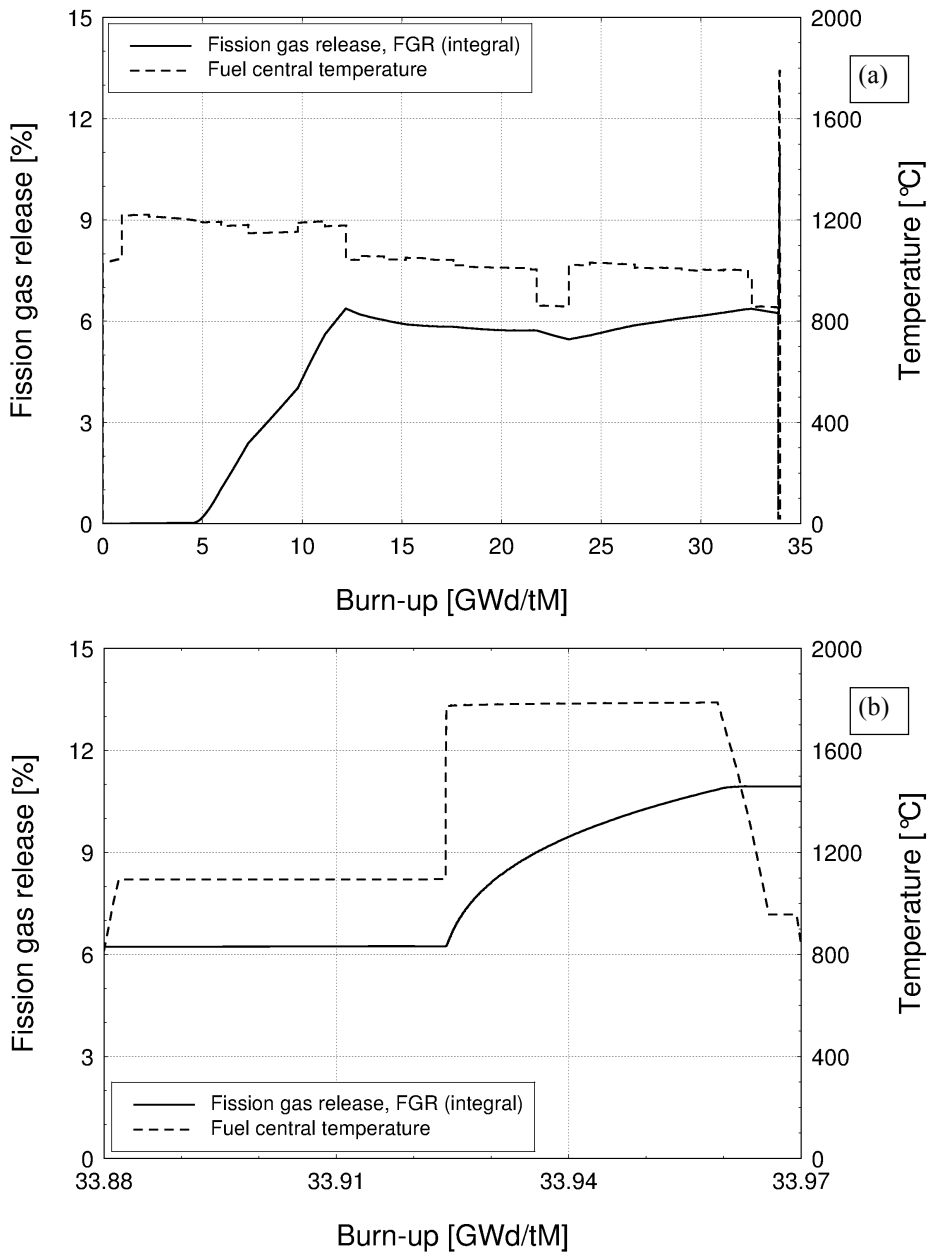[8] Ratio of the total fission gas released to the total fission gas generated in the fuel rod.

Fig. 4.7. Integral fission gas release and fuel central temperature as a function of the burn-up at the mid-plane of the PK1-1 fuel rod. (a) Entire irradiation time, (b) zoom on the ramp test.
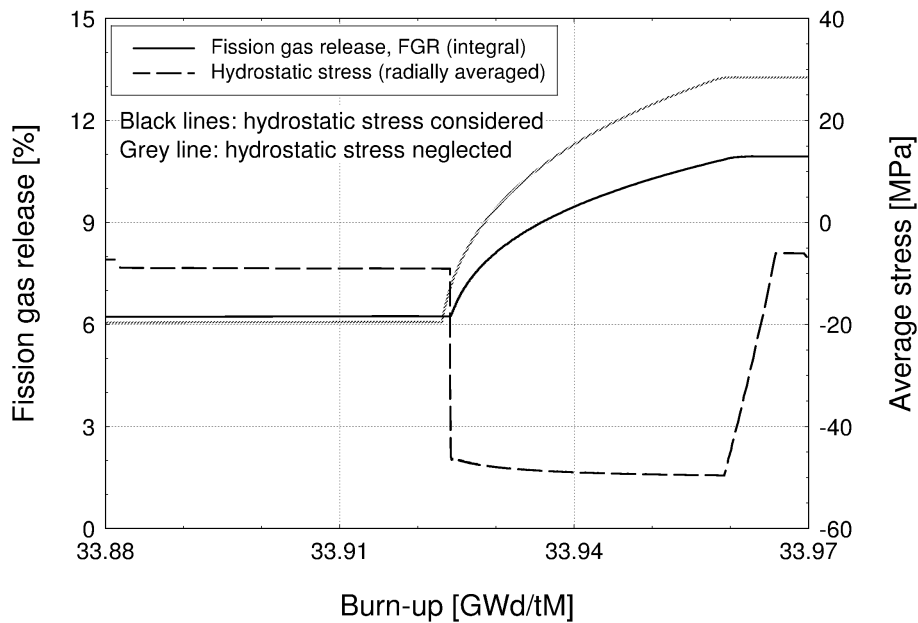
Fig. 4.8. Integral fission gas release and radially averaged hydrostatic stress (considered to be negative if compressive) in the fuel as a function of the burn-up at the mid-plane of the PK1-1 fuel rod. Both curves obtained by considering and by neglecting the hydrostatic stress are shown. Zoom on the ramp test is displayed.

Figure 4.10 shows the fission gas swelling, FGR and temperature radial profiles at the mid-plane of the LR1 rod, for burn-ups of about 5 GWd·(tM)$^{-1}$ and about 10 GWd·(tM)$^{-1}$. As for the previously discussed case of the PK1-1 rod, the burn-up and temperature-dependence of both swelling and FGR, as well as the consistent coupling between these phenomena, is evident.

Considering the calculated solid swelling, the predicted rate of radially averaged total fuel swelling is of about 0.11% per GWd·(tM)$^{-1}$ for the LR1 fuel rod during the base-irradiation, which is close to the experimental range of 0.08-0.1% per GWd·(tM)$^{-1}$. The reasonable predictive accuracy of the new model in terms of swelling is therefore confirmed.

The radial profiles of fission gas swelling, hydrostatic stress and temperature for the LR1 rod at the top of the power ramp (beginning of the holding time) are shown in Fig. 4.11. Also in this case, the compressive hydrostatic stress in the central zone of the pellet is high (about 60 MPa at the pellet centre), as a consequence of strong PCMI. The calculated swelling is remarkably affected by the stress, as highlighted by the comparison with the curve obtained by neglecting the stress-dependence in the model (grey line). These results confirm the capability of the model to take into account the role of the hydrostatic stress on the fission gas swelling. Since the stresses are computed
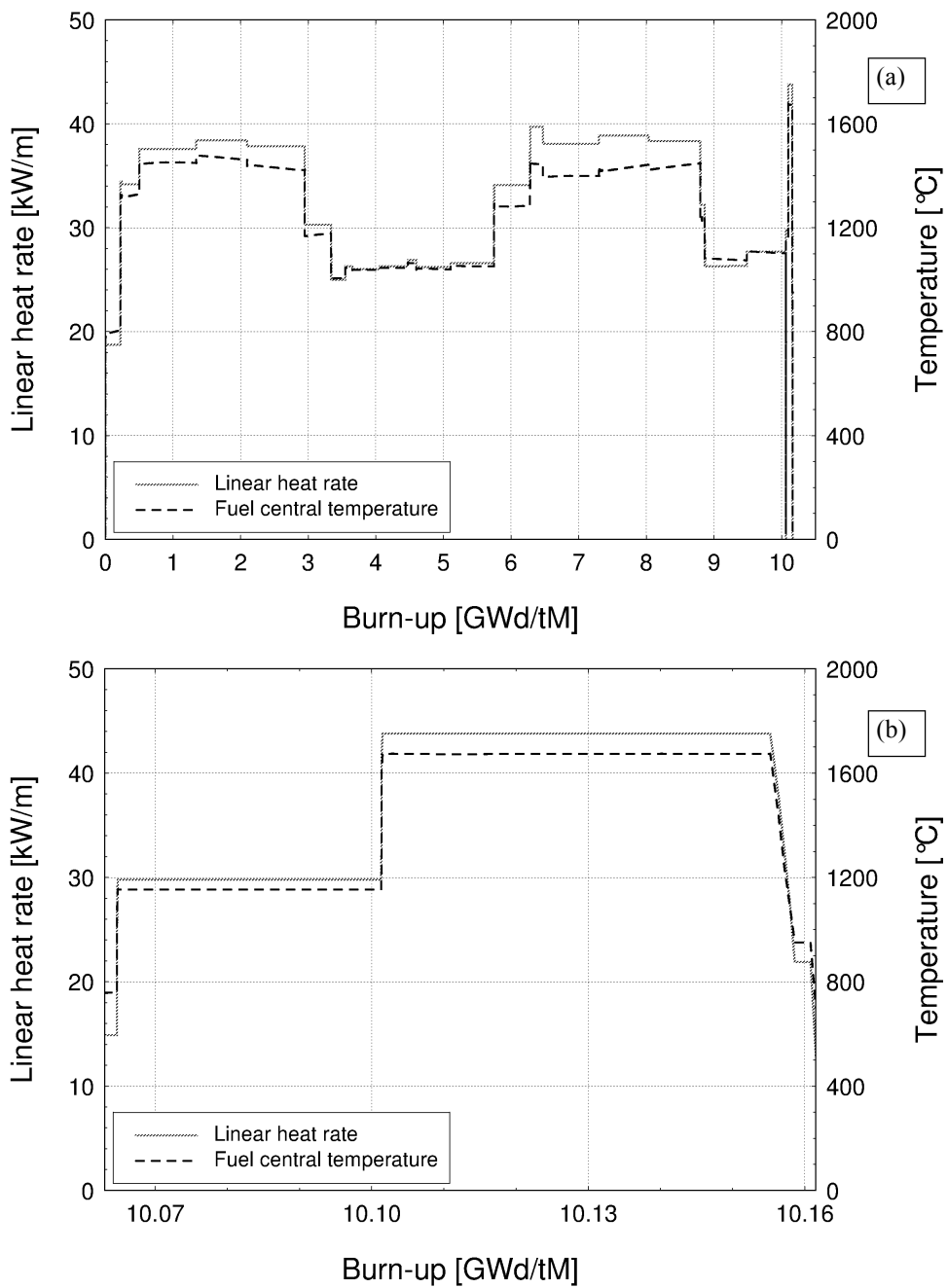
Fig. 4.9. Linear heat rate and fuel central temperature as a function of the burn-up at the mid-plane of the LR1 fuel rod. (a) Entire irradiation time, (b) zoom on the ramp test.
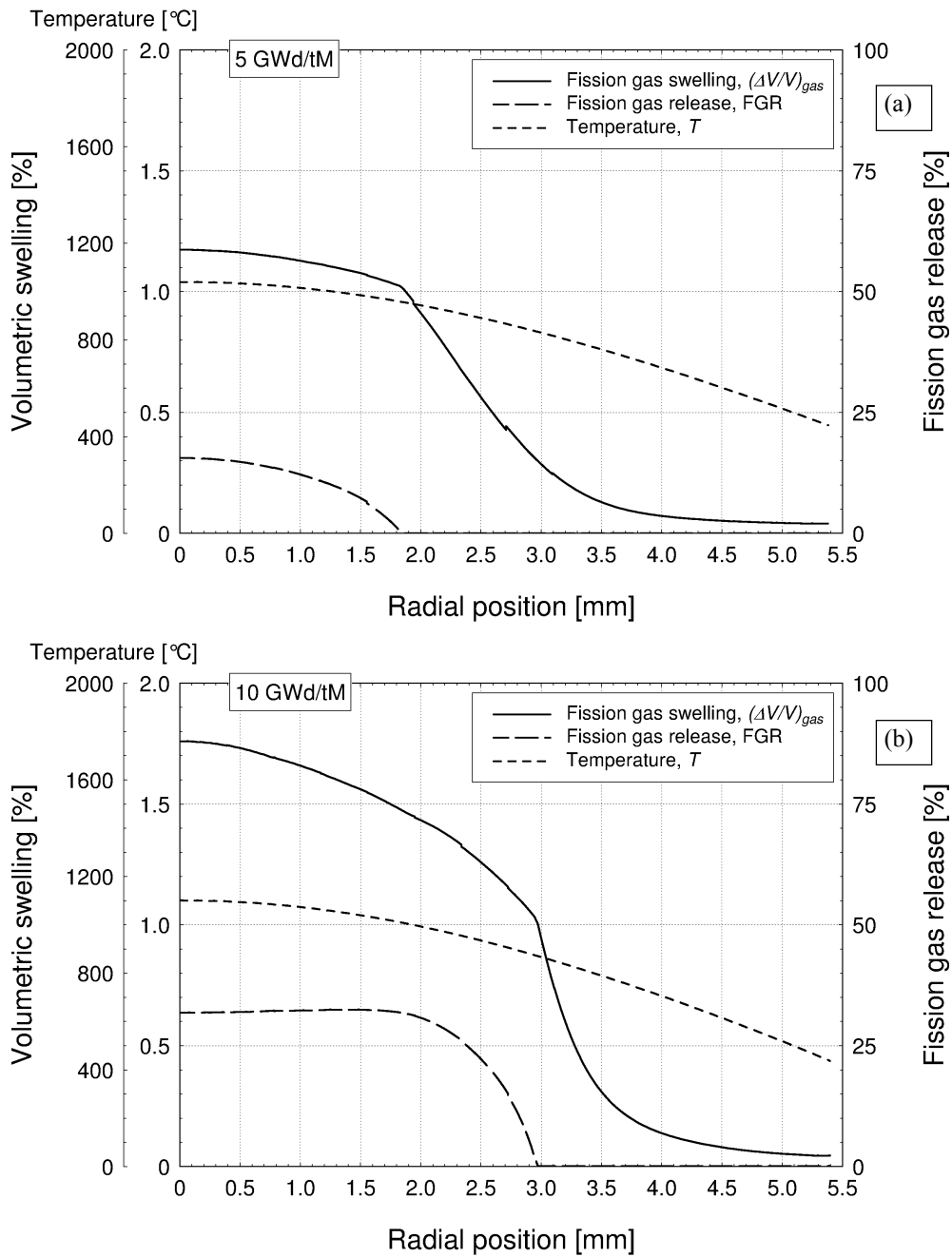
Fig. 4.10. Fission gas swelling, fission gas release and temperature as a function of the pellet radius at the mid-plane of the LR1 fuel rod. The graphs refer to burn-ups of (a) 5 GWd·(tM)⁻¹ and (b) 10 GWd·(tM)⁻¹.

starting from the calculated strains in the TRANSURANUS code, the stress is in turn affected by the swelling (for instance, note the rapid change of the both the swelling and the stress gradients in correspondence of a pellet radius of about 3 mm in Fig. 4.11).
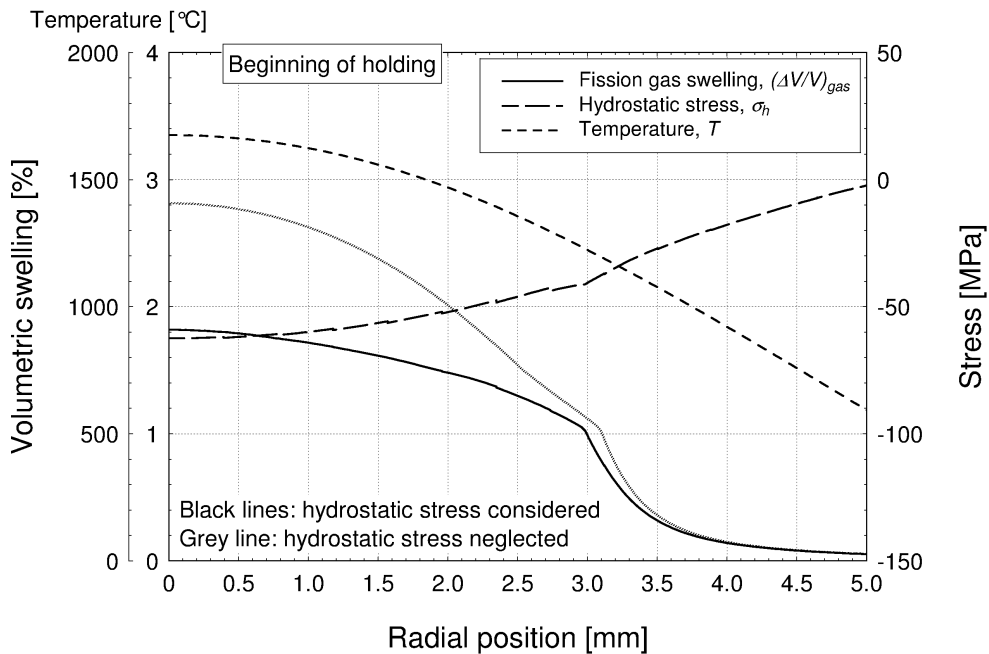
Fig. 4.11. Fission gas swelling, hydrostatic stress (considered to be negative if compressive) and temperature as a function of the pellet radius at the mid-plane of the LR1 fuel rod. The fission gas swelling calculated by neglecting the hydrostatic stress is also shown. The figure refers to the beginning of the holding time.

Fig. 4.12. Integral fission gas release and fuel central temperature as a function of the burn-up at the mid-plane of the LR1 fuel rod. The fission gas release calculated by neglecting the hydrostatic stress is also shown. The entire irradiation time is displayed.

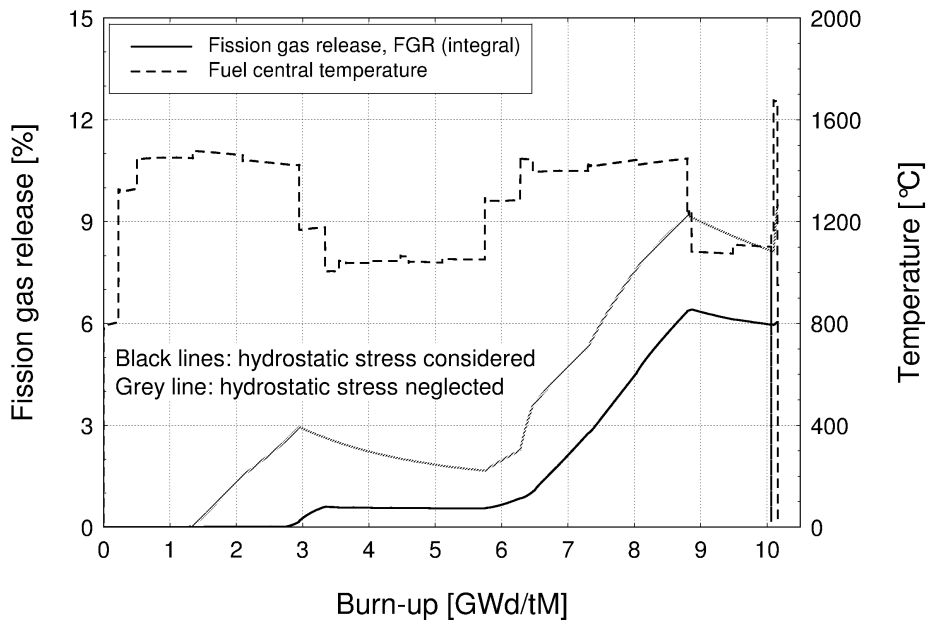The calculated integral fuel rod fission gas release and fuel central temperature as a function of the burn-up at the mid-plane of the LR1 rod are presented in Fig. 4.12. The incubation behaviour and temperature-dependence of the FGR can be appreciated. The FGR obtained by neglecting the stress-dependence in the model (grey line) is also reported. The comparison points out the effect of the compressive hydrostatic stress in delaying and reducing the FGR by inhibiting the growth of the grain-boundary bubbles. It is noticed that the stress markedly affects the FGR during the whole irradiation, also in absence of PCMI. These results point out the importance of the role played by the hydrostatic stress, and the significance of developing stress-dependent models of fission gas swelling and release.

4.3.2   Assessment of the results against experimental data of integral FGR

In order to verify the new integrated model of fission gas swelling and release implemented in the TRANSURANUS code, the results of the performed analyses were systematically compared with experimental data of integral FGR, which is a quantity of direct interest for fuel design, licensing, and for safety assessments. Since measurements of fission gas swelling are not available, a direct evaluation of the model in terms of swelling predictions is not viable through the analysis of the Super-Ramp and Inter-Ramp cases. In this work, the model was evaluated in terms of swelling predictions only as stand-alone version (Section 3.4), and a verification in these terms through integral fuel rod analyses would be useful in perspective. However, given the interrelation between the integral FGR and the other multiple aspects of the fuel rod thermo-mechanical behaviour, the results presented in this sub-section are indicative of the overall performance of the new model integrated in the TRANSURANUS code.

Experimental data of integral FGR at the EOL are available for 18 rods of the Super-Ramp Project and 11 rods of the Inter-Ramp Project. All these cases are considered here, except for the Super-Ramp rod PK4-S, because the corresponding experimental FGR is stated as unreliable (Djurle, 1984). Being a highly non-linear process, strongly influenced by the temperature and feedback effects, accurate modelling of the FGR by means of the fuel rod analysis codes is recognised to be difficult (IAEA, 1998). Moreover, the calculated integral FGR is influenced by the uncertainties pertaining to the whole fuel rod analysis. For instance, Bernard et al. (2002) found that a 5% uncertainty on the calculated temperature could lead to a 30% uncertainty on the calculated FGR. Finally, the accuracy of the predictions is unavoidably limited by the uncertainties pertaining to the model parameters

like the fission gas diffusion coefficient (Section 2.2 and Section 3.4). In view of these uncertainties, a deviation within a factor of 2 between the predicted and the experimental values of FGR is commonly regarded as satisfactory.

The comparison between the FGR results obtained by using the new model and the experimental values at the EOL for the Super-Ramp cases is presented in Fig. 4.13. The overall agreement is good. The average deviation between the predicted and the experimental values is a factor of about 1.5.

The comparison between the calculated and the experimental FGR at the EOL for the Inter-Ramp cases is presented in Fig. 4.14. On average, the predicted values deviate from the experimental ones by a factor of about 1.8. However, a significant over-prediction is observed of the FGR values lower than 10%. Indeed, it is known that the region of FGR of the order of 1% is extremely difficult to predict accurately by means of the fuel rod analysis codes (IAEA, 1998).
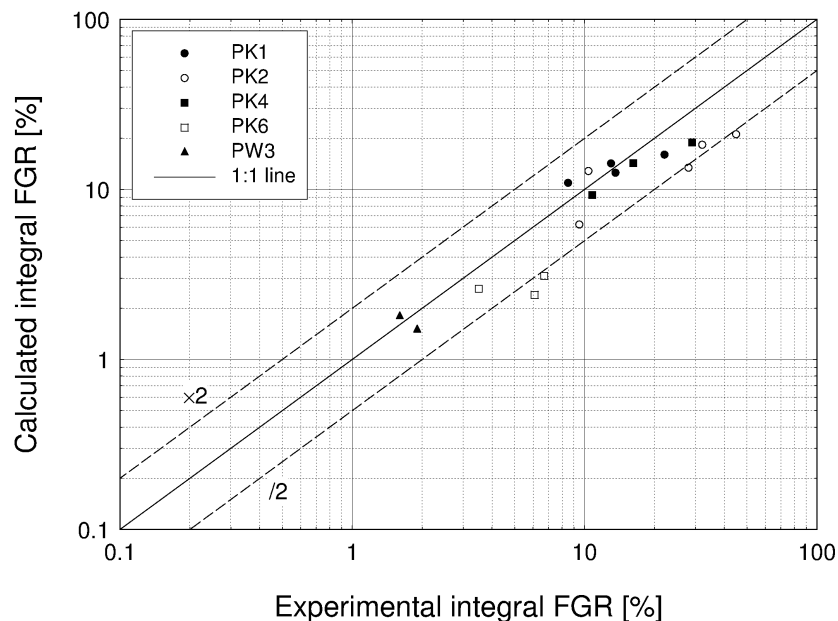
Fig. 4.13. Comparison between the calculated values of integral fission gas release at the EOL and the experimental data for the Super-Ramp cases.
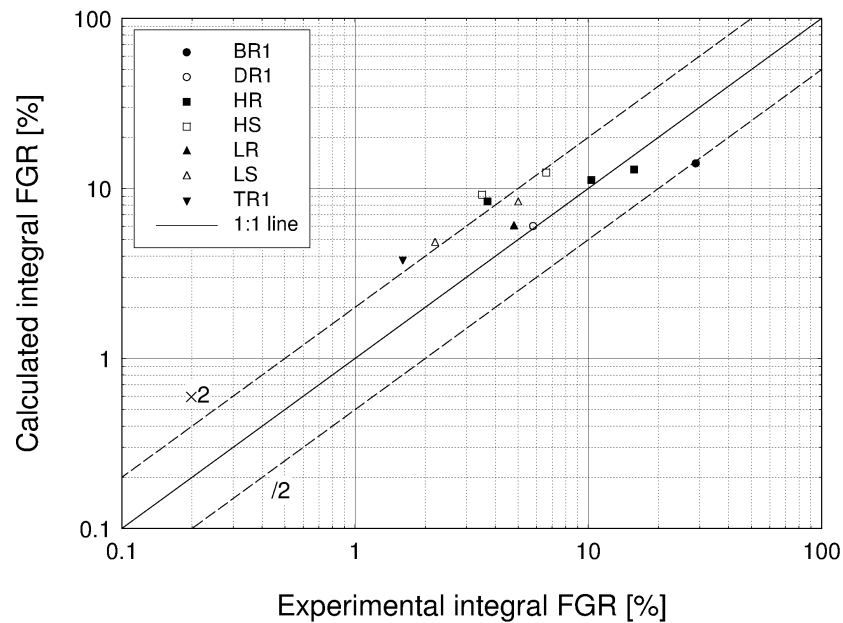
Fig. 4.14. Comparison between the calculated values of integral fission gas release at the EOL and the experimental data for the Inter-Ramp cases.

It is concluded that the new integrated model of fission gas swelling and release applied to the TRANSURANUS code allows a reasonable predictive accuracy in terms of FGR, without applying any fitting to the model parameters. Also, the overall agreement appears to be consistent with the intrinsic uncertainties.

4.3.3   Comparison with the standard models of the TRANSURANUS code

In order to compare the new model with the standard models of the TRANSURANUS code in terms of capability to represent the peculiarities of the fission gas swelling and release, the representative case of the PK1-1 fuel rod is considered. Figure 4.15 shows the linear heat rate as a function of the burn-up at the rod mid-plane during the ramp test. Figure 4.16 adds the contact pressure between the fuel and the cladding, and the radially averaged hydrostatic stress in the fuel. As mentioned in Sub-section 4.3.1, the fuel-cladding gap is closed during the whole ramp test of the PK1-1 rod, and contact pressure consequently takes place. As a result of the fuel swelling and the differential
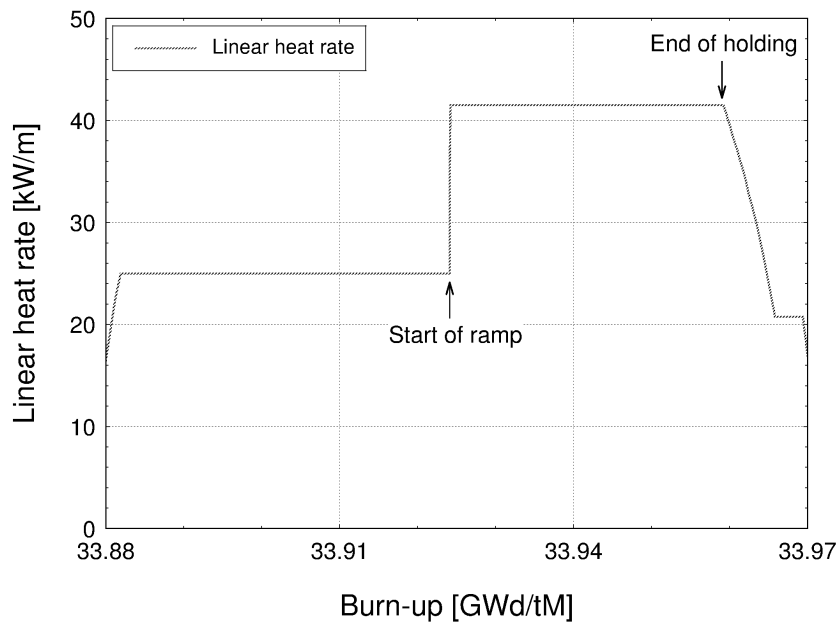
Fig. 4.15. Linear heat rate as a function of the burn-up at the mid-plane of the PK1-1 fuel rod. Zoom on the ramp test is displayed. The two significant instants considered further in this sub-section are highlighted.
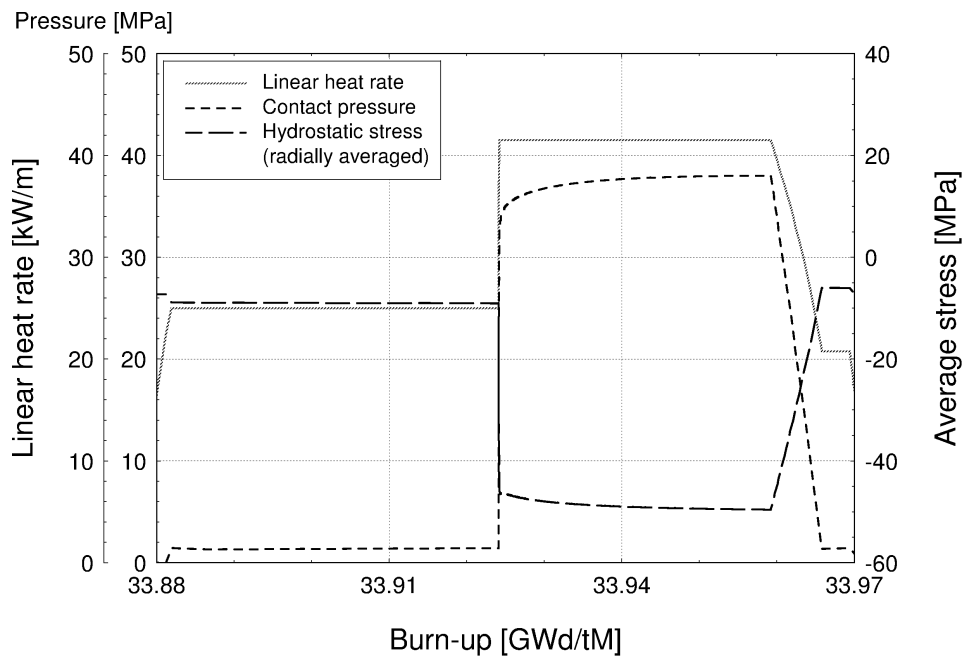
Fig. 4.16. Linear heat rate, fuel-cladding contact pressure and radially averaged hydrostatic stress (considered to be negative if compressive) in the fuel as a function of the burn-up at the mid-plane of the PK1-1 fuel rod. The figure refers to the adoption of the new model. Zoom on the ramp test is displayed.

thermal expansion of the fuel and the cladding, the contact pressure strongly increases during the power ramp and the subsequent holding time, causing the development of high compressive hydrostatic stress in the fuel (Fig. 4.16).

Figure 4.17 shows the radial profiles of fission gas swelling calculated by using the new model, at the significant instants highlighted in Fig. 4.15 (start of the ramp and end of the holding time). The partial inhibition of the fission gas swelling by the compressive hydrostatic stress, as taken into account by the new model, is pointed out by the comparison between the curves obtained by considering (black lines) and neglecting (grey lines) the hydrostatic stress. In particular, the swelling at the end of the holding time would be remarkably higher in absence of compressive hydrostatic stress, as evidenced by the difference between the dashed lines in Fig. 4.17. The predicted swelling is therefore considerably suppressed during the power ramp and the subsequent holding time by the high compressive hydrostatic stress that develops in the fuel as a consequence of strong PCMI. The difference between the full black line (start of the ramp) and the dashed black line (end of the holding time) in Fig. 4.17 represents the increment of fission gas swelling during the ramp and the subsequent holding time.
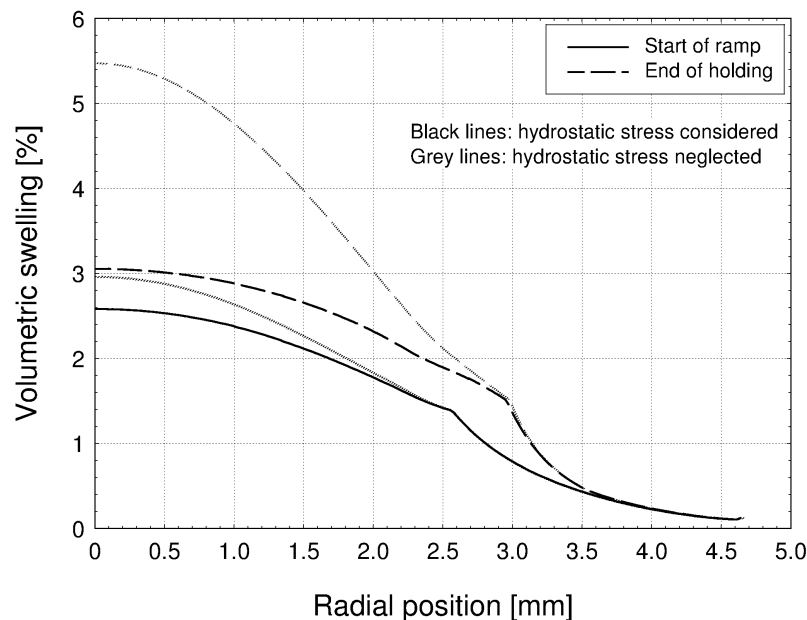

Fig. 4.17. Fission gas swelling as a function of the pellet radius at the mid-plane of the PK1-1 fuel rod. The considered instants are the start of the ramp and the end of the holding time. The figure refers to the adoption of the new model. The fission gas swelling calculated by neglecting the hydrostatic stress is also shown.

Although partially inhibited by the compressive hydrostatic stress, the calculated fission gas swelling significantly increases during this period, as a consequence of the high power and temperature. The significance of the fission gas swelling during power ramps is confirmed by indications from the literature and has safety-relevant consequences in terms of cladding strain and possible cladding failure (Arimescu, 2004; Cheon et al., 2004).

Figure 4.18 compares the results obtained by adopting the new model with those obtained by using the standard models of TRANSURANUS, in terms of fission gas swelling and FGR as a function of the pellet radius at the mid-plane of the PK1-1 rod. Again, the significant instants highlighted in Fig. 4.15 (start of the ramp and end of the holding time) are considered. The quantitative differences between the results of the different models are ascribed to the different features and parameters of the standard TRANSURANUS models (Section 1.2) and the new model (Chapter 2). However, qualitative differences are also observed, which point out the innovative aspects pertaining to the modelling approach developed in the present work.

As mentioned in Section 1.2, the standard swelling model of the TRANSURANUS code does not take into account the fission gas swelling in presence of contact pressure between the fuel and the cladding (PCMI conditions). Since contact pressure is present during the whole ramp test of the PK1-1 rod (Fig. 4.16), no swelling increment is considered by the standard TRANSURANUS model between the start of ramp and the end of holding time. In fact, the swelling profiles of Fig. 4.18-a are superimposed. However, this simplified approach does not allow for the significant swelling that (although partially inhibited by the compressive hydrostatic stress) can occur during a power ramp as a result of the high power and temperature, and the related issues. As an innovative aspect of the present work, the new model introduces the dependence of the fission gas swelling on the hydrostatic stress, and consistently calculates the increment of swelling during the power ramp and the subsequent holding time (Fig. 4.17 and Fig. 4.18-b). In consideration of this capability, the new model may allow to improve the TRANSURANUS code for the analysis of the fuel behaviour under PCMI conditions, which is of high importance in view of the current tendency to extend the operating margins of the nuclear fuel rods.

As shown in Fig. 4.18, both the new model and the standard TRANSURANUS model predict a remarkable increment of FGR from the start of the ramp to the end of the holding time, brought about by the high power and temperature. However, the physical coupling between the fission gas
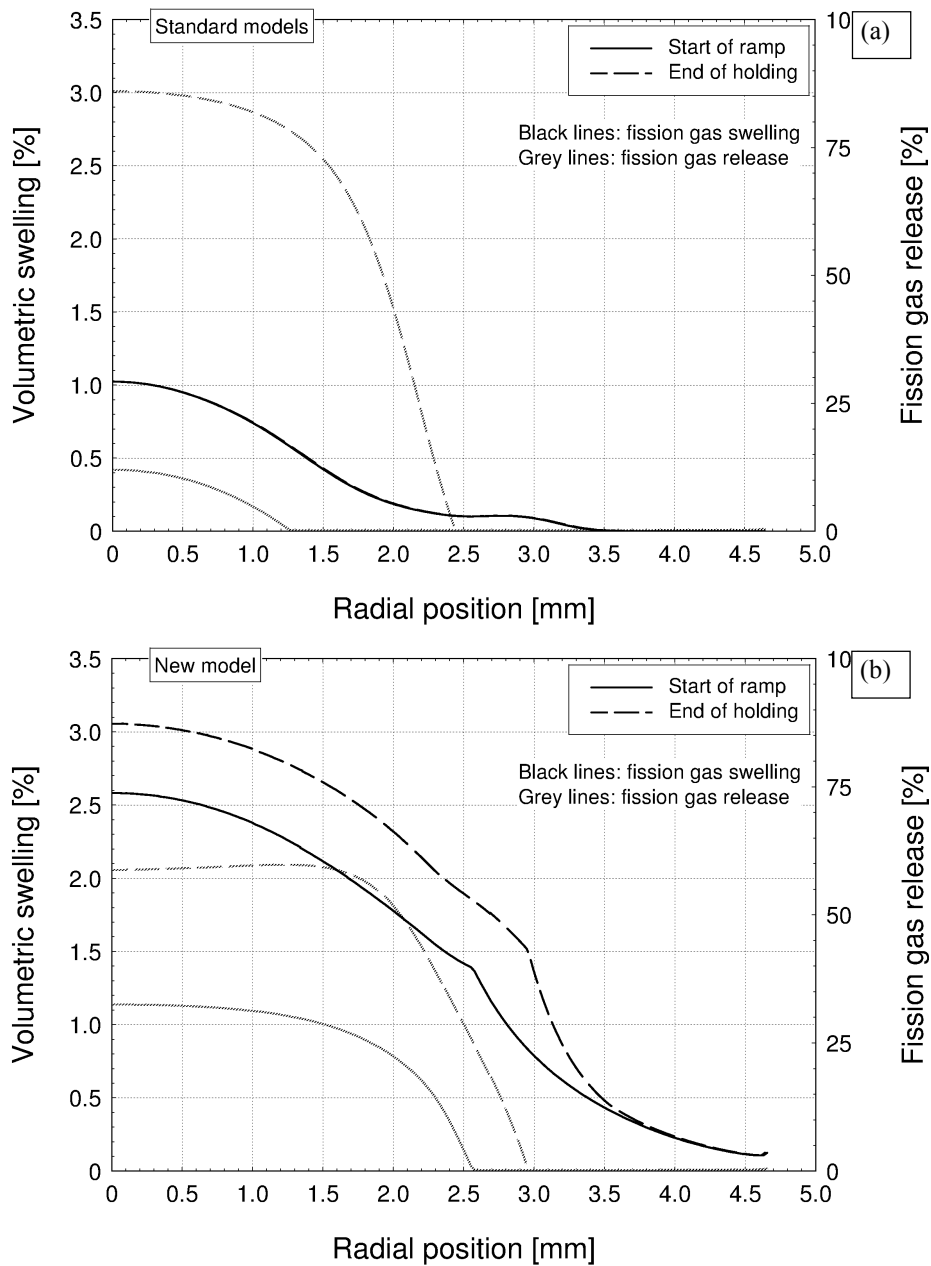
Fig. 4.18. Fission gas swelling and fission gas release as a function of the pellet radius at the mid-plane of the PK1-1 fuel rod. The considered instants are the start of the ramp and the end of the holding time. (a) Standard models of TRANSURANUS, (b) new model. In Fig. 4.18-a, the swelling curves are superimposed.

swelling and release, as well as the dependence of the FGR on the hydrostatic stress, are not considered by the standard TRANSURANUS models, while the new model introduces these peculiarities (see also Sub-section 4.3.1).

In general, the new integrated model of fission gas swelling and release allows a deeper insight into the relevant physical details compared to the standard TRANSURANUS models.
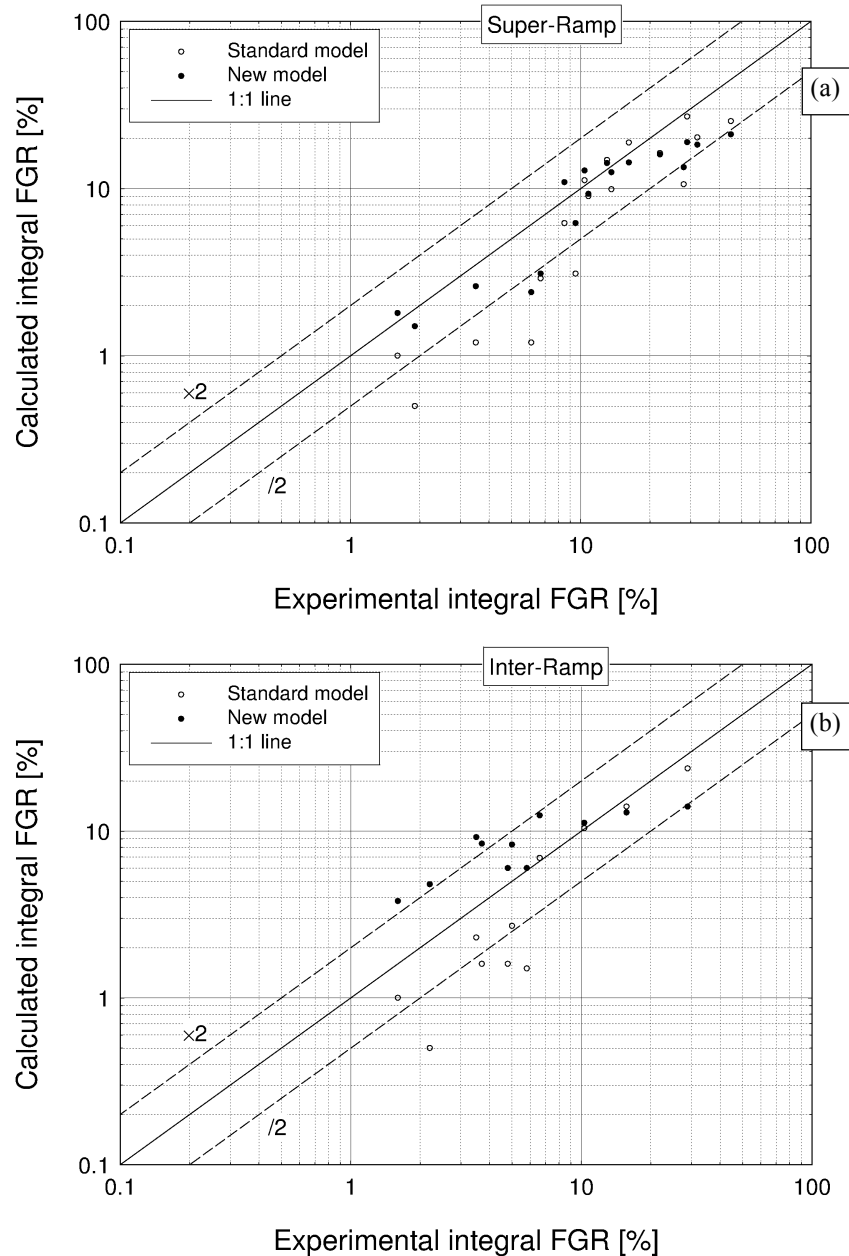
Fig. 4.19. Comparison between the calculated values of integral fission gas release at the EOL and the experimental data for (a) the Super-Ramp cases and (b) the Inter-Ramp cases. Both the results obtained by adopting the new model and the standard model of TRANSURANUS are reported.

Figure 4.19 shows the predictions in terms of integral FGR at the EOL for the Super-Ramp and Inter-Ramp cases. The comparison is proposed between the results obtained by adopting the standard FGR model of the TRANSURANUS code and the new model of fission gas swelling and release. By using the standard model, a systematic under-estimation of the experimental data is observed, and the predicted values deviate on average from the experimental ones by a factor of about 2.1 for both the Super-Ramp and the Inter-Ramp databases. By adopting the new model, the average deviation is of a factor of about 1.5 for the Super-Ramp cases, and about 1.8 for the Inter-Ramp cases (Sub-section 4.3.2). Also, the systematic under-estimation that occurs when the standard model is used appears to be overcome. Hence, the results indicate that the new model may allow to improve the predictive accuracy of the TRANSURANUS code in terms of FGR.

For the analyses performed in the present work, when adopting the new model the computational time increased by a factor of about 3-7 (depending on the considered case) compared to that obtained when using the standard models of the TRANSURANUS code. Anyhow, when the new model is adopted, the computational times are reasonable and of the order of few minutes in all the considered cases (see footnote 3).

4.4 Concluding remarks

The applicability of the developed model of fission gas swelling and release to the fuel rod analysis codes was demonstrated by successful implementation in the TRANSURANUS code. During the implementation, consistent matching was provided between the non-linear, stress-dependent model calculations and the thermo-mechanical fuel rod analysis. Numerical stability and reasonable computational times were obtained. This new model, applied to the TRANSURANUS code, was evaluated through the simulation of power ramped LWR fuel rods from the Super-Ramp and Inter-Ramp Projects of the IFPE database. With reference to the study of the calculation results, the following main conclusions are drawn:

- The model catches the dependence of both the fission gas swelling and release on the burn-up and the temperature.
- The physical coupling between the fission gas swelling and release is consistently described.
- The role of the compressive hydrostatic stress in suppressing the fission gas swelling and in delaying and reducing the FGR is reproduced, in accordance with the observations reported in

the literature. This aspect represented a major challenge of the present work from the viewpoint of the numerical stability of the fuel rod calculations.

• The predictions in terms of integral fuel rod FGR are in reasonable agreement with the experimental data, without any tuning of the model parameters.

The comparison with the results obtained by using the standard models of the TRANSURANUS code indicated that the implementation of the new model represents a significant innovation. The character of the present work as a progress in the development of the TRANSURANUS code is threefold:

• The physical foundation of the code was enhanced by replacing a semi-empirical description with a physics-based and integrated treatment of the fission gas swelling and release.

• A stress-dependent description of the fission gas swelling and release was introduced in the code. This feature is of particular importance for the proper simulation of the fuel behaviour under PCMI conditions.

• The predictive capability of the code in terms of integral FGR turns out to be improved for the considered irradiation experiments, as emerges from the assessment of the results against the experimental data.

In view of future developments, the new model provides a framework to integrate further physical details. Specifically, for the purpose of the improved simulation of power ramps, the burst release effect due to pellet micro-cracking during rapid power changes (for which a model is presently available in the TRANSURANUS code, see Sub-ection 1.2.2) may be considered. The incorporation of such effect in the new model would lead to a complete transient fission gas behaviour model in the TRANSURANUS code that could deal with design basis accident conditions such as LOCA and RIA. In view of the stochastic nature of pellet micro-cracking, however, only semi-empirical approaches to the modelling of the burst release effect were proposed (e.g., Koo et al., 2000), and this aspect is beyond the scope of the present work. Finally, for the improved analysis of high burn-up fuel, taking into account the peculiarities of the fission gas behaviour in the high burn-up structure (HBS) is advisable (Blair et al., 2006).

In perspective, integrating in the new model suitable treatments of the burst release effect and of the fission gas behaviour in the HBS, as well as a physics-based description of the athermal release mechanisms, represents an interesting development of the present work.

Conclusions

In the context of fuel rod modelling, the analysis of the coupled phenomena of fission gas swelling and release represents a challenging issue in view of the complexity of the underlying physical processes. In this work, an integrated model of fission gas swelling and release in oxide fuel during irradiation was developed and applied to the TRANSURANUS code, presently used in the European Union by nuclear safety authorities, industry, research centres and universities. The main outcomes of the work may be summarized as follows:

- The new model practically combines a physics-based description and the level of simplicity that is a prerequisite for the effective implementation in the fuel rod analysis codes.

- By application as stand-alone version, the model was firstly proven to reproduce the main peculiarities of the fission gas behaviour, on a physical basis and in accordance with the observations reported in the literature. Despite its simplicity, the model consistently describes the intrinsic coupling between the fission gas swelling and release, the incubation behaviour of the FGR, and the dependence of both the fission gas swelling and release on the compressive hydrostatic stress in the fuel.

- As resulting from the analysis of either power ramped or power cycled fuel specimens using the stand-alone version of the model, and from a first assessment of the predictions against experimental data, the predictive accuracy in terms of grain-boundary swelling is reasonable, without tuning of the model parameters.

- The new model of fission gas swelling and release was consistently implemented in the TRANSURANUS code. Matching was provided between the non-linear, stress-dependent model calculations and the thermo-mechanical fuel rod analysis. Stability of the numerical solutions and reasonable computational times were obtained.

- Adopting the new model, the TRANSURANUS code was employed for an extensive set of simulations of LWR fuel rods irradiation experiments involving power ramps. The main peculiarities of the phenomena are confirmed to be reproduced consistently with the experimental observations.

- The assessment of the results of the fuel rod analyses against experimental data of integral fuel rod FGR pointed out a reasonable overall agreement, without any fitting of the model parameters.

- The successful application to the TRANSURANUS code indicated that (i) the model can be employed in integral fuel rod analyses (hence, in the nuclear fuel design and licensing), and (ii) the model may be of interest for implementation in other fuel rod analysis codes.

- The comparison with the capabilities of the standard models of the TRANSURANUS code indicated that the implementation of the new model represents a significant progress in the code development. The innovative aspects are mainly related to (i) the advantages of a physics-based and integrated treatment in terms of flexibility of application and understanding of the underlying mechanisms, compared to the previously adopted empirical and semi-empirical models, and (ii) the consistent evaluation of the dependence of both the fission gas swelling and release on the hydrostatic stress. Being of high importance in order to properly analyse the fuel rod behaviour under PCMI conditions and the related, safety-relevant issues, the latter aspect is topical in view of the tendency to extend the burn-up of the nuclear fuel rods.

- The current results are promising in view of future applications of the model, implemented in the TRANSURANUS code, in both research and industrial frameworks.

To summarize, the general features of the model developed in the present work, in terms of physical foundation and computational efficiency, constitute a framework that allows the application to fuel rod modelling of the physics-based, integrated and stress-dependent treatment of the fission gas swelling and release. These fundamental characteristics were developed in order to obtain applicability of the model to different types of oxide fuel (both MOX and UO_2) and up to high burn-up. The underlying approach is generally applicable and can be reproduced in order to develop increasingly complex and advanced models (e.g., see the Appendix) with the above fundamental capabilities to be implemented in the fuel rod analysis codes.

In perspective, a more extensive verification of the model, both in terms of comparison with experimental data and numerical stability of the fuel rod calculations, is envisaged. Moreover, integrating further physical details (e.g., burst release, HBS effects, athermal release mechanisms) represents an interesting development in view of improving the predictive capability and extending the range of applicability of the new model.

References

Ainscough J.B., Oldfield B.W., Ware J.O. (1973). Isothermal grain growth kinetics in sintered UO_2 pellets, Journal of Nuclear Materials, vol. 49, pp. 117-128.

Arimescu, V.I. (2004). Fuel Swelling Importance in PCI Mechanistic Modelling, Proceedings of the International Seminar on Pellet-Clad Interaction in Water Reactor Fuels, Aix-en-Provence, France, March 9-11, 2004.

Assmann H., Manzel R. (1977). The matrix swelling rate of UO_2, Journal of Nuclear Materials, vol. 68, pp. 360-364.

Aybar H.S., Ortego P. (2005). A review of nuclear fuel performance codes, Progress in Nuclear Energy, vol. 46, no. 2, pp. 127-141.

Baker C. (1977a). The fission gas bubble distribution in uranium dioxide from high temperature irradiated SGHWR fuel pins, Journal of Nuclear Materials, vol. 66, pp. 283-291.

Baker C. (1977b). The migration of intragranular fission gas bubbles in irradiated uranium dioxide, Journal of Nuclear Materials, vol. 71, pp. 117-123

Bernard L.C., Jacoud J.L., Vesco P. (2002). An efficient model for the analysis of fission gas release, Journal of Nuclear Materials, vol. 302, pp. 125-134.

Blair P., Romano A., Hellwig Ch., Chawla R. (2006). Calculations on fission gas behaviour in the high burnup structure, Journal of Nuclear Materials, vol. 350, pp. 232-239.

Booth A.H. (1957). A Method of Calculating Gas Diffusion from UO_2 Fuel and its Application to the X-2-f Loop Test, AECL-496, Atomic Energy of Canada Ltd.

Calvin C., Nowak D. (2010). High performance computing in nuclear engineering, in: Cacuci D.G. (Ed.), Handbook of Nuclear Engineering, Springer, pp. 1449-1517.

Cheon J-S., Koo Y.-H., Lee B-H., Oh J-Y., Sohn D.-S. (2004). Modeling of a Pellet-Clad Mechanical Interaction in LWR Fuel by Considering Gaseous Swelling, Proceedings of the International Seminar on Pellet-Clad Interaction in Water Reactor Fuels, Aix-en-Provence, France, March 9-11, 2004.

Cornell R.M. (1971). An electron microscope examination of matrix fission-gas bubbles in irradiated uranium dioxide, Journal of Nuclear Materials, vol. 38, pp. 319-328.

Cornell R.M., Speight M.V., Masters B.C. (1969). The role of bubbles in fission gas release from uranium dioxide, Journal of Nuclear Materials, vol. 30, pp. 170-178.

Di Marcello V., Luzzi L. (2008). Modelling of Pellet Cladding Interaction during Power Ramps in PWR Rods by means of Transuranus Fuel Rod Analysis Code, Proceedings of the OECD/NEA-IAEA Workshop on Structural Materials for Innovative Nuclear Systems (SMINS), NEA No. 6260, pp. 417-428.

Djurle S. (1979). The Studsvik Inter-Ramp Project, Final Report STUDSVIK-STIR-53, Studsvik AB Atomenergi, Sweden.

Djurle S. (1984). The Super-Ramp Project, Final Report STUDSVIK-STSR-32, Studsvik Energiteknik AB, Nykoping, Sweden.

Elton P.T., Lassmann K. (1987). Calculational methods for diffusional gas release, Nuclear Engineering and Design, vol. 101, pp. 259-265.

Franklin D.G., Roberts J.T.A., C.-Y. Li (1984). Low temperature swelling and densification properties of LWR fuels, Journal of Nuclear Materials, vol. 125, pp. 96-103.

Govers K., Lemehov S., Verwerft M. (2008). In-pile Xe diffusion coefficient in UO_2 determined from the modeling of intragranular bubble growth and destruction under irradiation, Journal of Nuclear Materials, vol. 374, pp. 461-472.

Grimes R.W., Catlow C.R.A (1991). The stability of fission products in uranium dioxide, Philosophical Transactions of the Royal Society A, vol. 335, pp. 609-634.

Gulden M.E. (1967). Migration of gas bubbles in irradiated uranium dioxide, Journal of Nuclear Materials, vol. 23, pp. 30-36.

Ham F.S. (1958). Theory of diffusion-limited precipitation, Journal of Physics and Chemistry of Solids, vol. 6, pp. 335-351.

IAEA (1998). Fuel modelling at extended burnup, Technical Report IAEA TECDOC 998.

Kashibe S., Une K. (1997). Effect of external restraint on bubble swelling in UO_2 fuels, Journal of Nuclear Materials, vol. 247, pp. 138-146.

Kashibe S., Une K., Nogita K. (1993). Formation and growth of intragranular fission gas bubbles in UO_2 fuels with burnup of 6-83 GWd/t, Journal of Nuclear Materials, vol. 206, pp. 22-34.

Killeen J., Sartori E., McGrath M. (2009). FUMEX-III: A new IAEA coordinated research project on fuel modelling at extended burnup, Proceedings of the International Conference on Water Reactor Fuel Performance, Paris, France, September 6-10, 2009, pp. 336-343.

Kim Y.-s. (2004). Theoretical analysis of two-stage fission gas release processes: grain lattice and grain boundary diffusion, Journal of Nuclear Materials, vol. 326, pp. 97-105.

Kogai T. (1997). Modelling of fission gas release and gaseous swelling of light water reactor fuels, Journal of Nuclear Materials, vol. 244, pp. 131-140.

Kogai T., Ito K., Iwano Y. (1988). The effect of cladding restraint on fission gas release behavior, Journal of Nuclear Materials, vol. 158, pp. 64-70.

Koo Y.-H., Lee B.-H., Sohn D.-S. (2000). Analysis of fission gas release and gaseous swelling in UO_2 fuel under the effect of external restraint, Journal of Nuclear Materials, vol. 280, pp. 86-98.

Lassmann K. (1980). The structure of fuel element codes, Nuclear Engineering and Design, vol. 57, pp. 17-39.

Lassmann K (1992). TRANSURANUS: a fuel rod analysis code ready for use, Journal of Nuclear Materials, vol. 188, pp. 295-302.

Lassmann K (2001). The TRANSURANUS Code – Past, present and future (Review Article), ITU Activity Report 2001 - EUR 20252, ISBN 92-894-3639-5, pp. 16-22.

Lassmann K., Benk H. (2000). Numerical algorithms for intragranular fission gas release, Journal of Nuclear Materials, vol. 280, pp. 127-135.

Lassmann K., Schubert A., Van Uffelen P., Győri C., van de Laar J. (2011). TRANSURANUS Handbook, Copyright ©1975-2011, Institute for Transuranium Elements, Karlsruhe, Germany.

Lewis B.J. (1987). Fission product release from nuclear fuel by recoil and knockout, Journal of Nuclear Materials, vol. 148, pp. 28-42.

Lösönen P. (2000). On the behaviour of intragranular fission gas in UO_2 fuel, Journal of Nuclear Materials, vol. 280, pp. 56-72.

Lösönen P. (2002). Modelling intragranular fission gas release in irradiation of sintered LWR UO_2 fuel, Journal of Nuclear Materials, vol. 304, pp. 29-49.

Luzzi L. (2002). Validation of TRANSURANUS Code on the Basis of the Studsvik Super-Ramp PWR Database Files, Technical Report JRC-ITU-TN-2002/08, Institute for Transuranium Elements, Karlsruhe, Germany.

Luzzi L, Di Marcello V., Botazzoli P., Győri C., Schubert A., Spino J., van de Laar J., Van Uffelen P. (2008). Analysing Operational Transients by means of the TRANSURANUS Code, Proceedings of the Enlarged Halden Programme Group Meeting, Loen, Norway, May 18-23, 2008.

Manley A.J. (1968). Transmission electron microscopy of irradiated UO_2 fuel pellets, Journal of Nuclear Materials, vol. 27, pp. 216-224.

Massih A.R., Forsberg K. (2008). Calculation of grain boundary gaseous swelling in UO_2, Journal of Nuclear Materials, vol. 377, pp. 406-408.

MATPRO (1979). Version 11 – A Handbook of Material Properties for Use in the Analysis of LWR Fuel Rod Behaviour, NUREG/CR-0497, TREE-1280.

Matthews J.R. (1978), Fast reactor fuel pin performance, Review of SMiRT 4, Nuclear Energy, vol. 17, pp. 211-216.

Matthews J.R., Wood M.H. (1979). Modelling the transient behaviour of fission gas, Journal of Nuclear Materials, vol. 84, pp. 125-136.

Matzke H. (1980). Gas release mechanisms in UO_2 – a critical review, Radiation Effects, vol. 53, p. 219-242.

Metcalf M., Reid J., Cohen M. (2004). Fortran 95/2003 explained, Oxford University Press.

Mogensen M., Bagger C., Walker C.T. (1993). An experimental study of the distribution of retained xenon in transient-tested UO_2 fuel, Journal of Nuclear Materials, vol. 199, pp. 85-101.

Mogensen M., Walker C.T., Ray I.L.F., Coquerelle M. (1985). Local fission gas release and swelling in water reactor fuel during slow power transients, Journal of Nuclear Materials, vol. 131, pp. 162-171.

OECD/NEA (2004). Pellet-Clad Interaction in Water Reactor Fuels, Seminar Proceedings, Aix-en-Provence, France, March 9-11, 2004.

Olander D.R. (1976). Fundamental aspects of nuclear reactor fuel elements, Technical Information Center - Energy Research and Development Administration, University of California, Berkeley.

Olander D.R., Van Uffelen P. (2001). On the role of grain boundary diffusion in fission gas release, Journal of Nuclear Materials, vol. 288, pp. 137-147.

Olander D.R., Wongsawaeng D. (2006). Re-solution of fission gas – A review: Part I. Intragranular bubbles. Journal of Nuclear Materials, vol. 354, pp. 94-109.

Pastore G., Botazzoli P., Di Marcello V., Luzzi L. (2009a). Simulation of Power Ramp Tested LWR Fuel Rods by means of the TRANSURANUS Code, Proceedings of the International Conference on Water Reactor Fuel Performance, Paris, France, September 6-10, 2009, pp. 223-232.

Pastore G., Botazzoli P., Di Marcello V., Luzzi L. (2009b). Assessment of the Prediction Capability of the TRANSURANUS Fuel Performance Code on the Basis of Power Ramp Tested LWR Fuel Rods, Proceedings of the 8th International Conference on WWER Fuel Performance, Modelling and Experimental Support, Bourgas, Bulgaria, September 26-October 4, 2009, pp. 300-308.

Rest J. (2003). The effect of irradiation-induced gas-atom re-solution on grain-boundary bubble growth, Journal of Nuclear Materials, vol. 321, pp. 305-312.

Reynolds G.L., Burton B. (1979). Grain-boundary diffusion in uranium dioxide: the correlation between sintering and creep and a reinterpretation of creep mechanism, Journal of Nuclear Materials, vol. 82, p. 22.

Sartori E., Killeen J., Turnbull J.A. (2010). International Fuel Performance Experiments (IFPE) Database, OECD-NEA, http://www.oecd-nea.org/science/fuel/ifpelst.html.

Schubert A., Botazzoli P., Boneva S., Di Marcello V., Pastore G., van de Laar J., Van Uffelen P. (2011). Application of the extended TRANSURANUS code in the FUMEX-III Project, Proceedings of the 9th International Conference on WWER Fuel Performance, Modelling and Experimental Support, Bourgas, Bulgaria, September 17 – 24, 2011.

Speight M.V. (1969). A Calculation on the Migration of Fission Gas in Material Exhibiting Precipitation and Re-solution of Gas Atoms Under Irradiation, Nuclear Science and Engineering, vol. 37, pp. 180-185.

Speight M.V., Beere W. (1975). Vacancy Potential and Void Growth on Grain Boundaries, Metal Science, vol. 9, pp. 190-191.

Spino J., Rest J., Goll W., Walker C.T. (2005). Matrix swelling rate and cavity volume balance of UO_2 fuels at high burn-up, Journal of Nuclear Materials, vol. 346, pp. 131-144.

Suzuki M. (2000). Light Water Reactor Fuel Analysis Code FEMAXI-V (Ver. 1), JAERI-Data/Code 2000-030.

Tucker M.O., White R.J. (1979). The release of unstable fission products from UO_2 during irradiation, Journal of Nuclear Materials, vol. 87, pp. 1-10.

Turnbull J.A. (1971). The distribution of intragranular fission gas bubbles in UO_2 during irradiation, Journal of Nuclear Materials, vol. 38, pp. 203-212.

Turnbull J.A. (1974), The effect of grain size on the swelling and gas release properties of UO_2 during irradiation, Journal of Nuclear Materials, vol. 50, pp. 62-68.

Turnbull J.A., Friskney C.A., Findlay J.R., Johnson F.A., Walter A.J. (1982). The diffusion coefficients of gaseous and volatile species during the irradiation of uranium oxide, Journal of Nuclear Materials, vol. 107, pp. 168-184.

Turnbull J.A., Tucker M.O. (1974). Swelling in UO_2 under conditions of gas release, Philosophical Magazine, vol. 30, no. 1, pp. 47-63.

Turnbull J.A., White R.J., Wise C.A. (1988). The diffusion coefficient for fission gas atoms in uranium dioxide, Proceedings of Technical Committee Meeting on Water Reactor Fuel Element Computer Modelling in Steady State, Transient and Accidental Conditions, Preston, England, September 18-22, 1988.

Van Uffelen P. (2002). Contribution to the Modelling of Fission Gas Release in Light Water Reactor Fuel, Ph.D. thesis, University of Liege.

Van Uffelen P., Konings R.J.M., Vitanza C., Tulenko J. (2010). Analysis of reactor fuel rod behavior, in: Cacuci D.G. (Ed.), Handbook of Nuclear Engineering, Springer, pp. 1519-1627.

Van Uffelen P., Pastore G., Di Marcello V., Luzzi L. (2011). Multiscale modelling for the fission gas behaviour in the TRANSURANUS code, Nuclear Engineering and Technology, vol. 43, no. 6, pp. 477-488.

Van Uffelen P, Schubert A., van de Laar J., Győri C., Elenkov D., Boneva S., Georgieva M., Georgiev S., Hózer Z., Märtens D., Spykman G., Hellwig C., Nordstrøm Å., Luzzi L., Di Marcello V., Ott L. (2007). The Verification of the TRANSURANUS Fuel Performance Code - an Overview, Proceedings of the 7th International Conference on WWER Fuel Performance, Modelling and Experimental Support, Albena, Bulgaria, September 17-21, 2007, pp. 305-320.

Van Uffelen P., Sheindlin M., Rondinella V., Ronchi C. (2004). On the relations between the fission gas behaviour and the pellet-cladding mechanical interaction in LWR fuel rods, Proceedings of the International Seminar on Pellet-Clad Interaction in Water Reactor Fuels, Aix-en-Provence, France, March 9-11, 2004.

Veshchunov M.S. (2008). Modelling of grain face bubbles coalescence in irradiated UO_2 fuel, Journal of Nuclear Materials, vol. 374, pp. 44-53.

Vitanza C., Graziani U., Fordestrommen N.T., Vilpponen K.O. (1978). Fission gas release from in-pile measurements, Technical Report HPR-221.10, OECD Halden Reactor Project.

Walker C.T., Knappik P., Mogensen M. (1988). Concerning the development of grain face bubbles and fission gas release in UO$_2$ fuel, Journal of Nuclear Materials, vol. 160, pp. 10-23.

White R.J. (1994). A new mechanistic model for the calculation of fission gas release, Proceedings of the International Topical Meeting on Light Water Reactor Fuel Performance, West Palm Beach, Florida, USA, April 17-21, 1994.

White R.J. (2004). The development of grain-face porosity in irradiated oxide fuel, Journal of Nuclear Materials, vol. 325, pp. 61-77.

White R.J., Corcoran R.C., Barnes J.P. (2006). A Summary of Swelling Data Obtained from the AGR/Halden Ramp Test Programme, Report R&T/NG/EXT/REP/0206/02, 2006.

White R.J., Tucker M.O. (1983). A new fission-gas release model, Journal of Nuclear Materials, vol. 118, pp. 1-38.

Wise C. (1985). Recoil release of fission products from nuclear fuel, Journal of Nuclear Materials, vol. 136, pp. 30-47.

Wood M.H., Matthews J.R. (1980). A simple operational gas release and swelling model. I: intragranular gas, Journal of Nuclear Materials, vol. 91, pp. 35-40.

Zimmermann H. (1978). Investigations on swelling and fission gas behaviour in uranium dioxide, Journal of Nuclear Materials, vol. 75, pp. 154-161.

Appendix

Fission gas release models for MOX fuels

Abstract. *In this Appendix, an overview of the current models of fission gas and helium release in (U,Pu) Mixed Oxide fuels is presented. On the basis of the studied approaches, models have been developed and are proposed for the implementation in the TRANSURANUS fuel performance code. A specific model for the helium release has been implemented in TRANSURANUS and preliminarily tested on the basis of the ATR (Advanced Test Reactor) irradiation test.*

A-1 Introduction

Depending on the manufacturing method, heterogeneity can exist in the microstructure of MOX fuel pellets due to incomplete mixing of PuO_2 powder with UO_2 powder. There is some controversy whether or not fission gas release is enhanced in MOX fuel compared with UO_2 fuel under similar operating conditions as a result of a heterogeneous microstructure. High gas release observed in MOX fuel is mainly being attributed to lower thermal conductivity and higher operating powers in MOX fuel later in its life because the reactivity of MOX fuel falls more slowly with burn-up than UO_2 fuel.

The analysis of the ATR irradiation test by means of the TRANSURANUS code (Botazzoli, 2008) showed that fission gas release is underestimated at high burn-up by using the fission gas release model of (homogeneous) UO_2. In order to assess the contribution of the microstructure on the fission gas release in MOX fuel, it is necessary to have the ability to model its effect. When describing the gas behaviour in MOX fuel at high burn-up, it is also important to properly model the behaviour of helium. In fact, the production of helium increases exponentially as a function of the burn-up and this behaviour is more pronounced in the case of MOX fuels, due to the presence of plutonium. Due to the high diffusion coefficient, the created helium can be easily released in the gap between the fuel and the cladding, enhancing the fuel rod inner pressure (Botazzoli et al., 2009).

This Appendix is structured as follows. The current approaches for modelling the fission gas and helium release in MOX fuels are discussed in the next section. In Section A-3, models for fission

gas release in MOX fuels and helium release are proposed. In Section A-4, a specific model for helium release, implemented in the TRANSURANUS code, is tested on the basis of the ATR irradiation test.

A-2   Current approaches for modelling fission gas and helium release

A-2.1   *Available models for fission gas release in MOX fuels*

In this section, an overview of the approaches currently adopted and published in the open literature is reported. Some of them are simple empirical modifications of the model for the UO_2, some of them are more elaborate models taking into account the heterogeneity effect in a physical manner.

The model of the FGR for MOX fuels of the FEMAXI-V code (fuel performance code of the Japan Atomic Energy Research Institute, e.g., see (Suzuki, 2000)) is the same as used for UO_2 fuels. However, as an option, the fraction of gas release obtained with this model can be multiplied by a factor 1.3.

The model of FRAPCON-3 (fuel performance code of the Pacific Northwest National Laboratories) is the same as used for UO_2 fuels but with a different diffusion coefficient. In particular, the diffusion coefficient is multiplied by a factor 1.75. In fact, the final results are very similar to those obtained by applying a factor to the final FGR (as in FEMAXI).

Some models taking into account the presence of plutonium-rich agglomerates have been proposed by Belgonucleaire (Billaux and van Vliet, 1986), NFD (Nippon Nuclear Fuel Development) (Ishida and Korei, 1994), and KAERI (Korea Atomic Energy Research Institute) (Koo et al., 2001). The basic ideas of these models are presented hereinafter.

NFD model

In contrast with the PuO_2 spherical particle (Belgonucleaire and KAERI models), the proposed model uses the statistical frequency distribution of the local Pu-content (measured by electron probe microanalysis) in as-fabricated MOX fuels in combination with the usual fission gas release model based on the diffusion theory for homogeneous UO_2 fuel.

This model is based on the following assumptions:

- each radial node of a fuel pellet consists of a large number of fuel grains, the change in their size being given by a grain growth kinetic equation;

- the FGR model by White and Tucker (White and Tucker, 1983) is employed, where the plutonium concentration in a single fuel grain is uniformly distributed;

- the probability that a fuel grain has a specific Pu concentration in the as-fabricated fuel pellet is initially given by a binomial (discrete) distribution (fitted to the experimental data);

- the Pu concentration of each discrete group changes as the fuel burn-up proceeds due to fission and capture reactions of Pu and U;

- mitigation of the Pu heterogeneity through interdiffusion of Pu and U is not taken into account, except that the binomial distribution model already assumes homogenisation within the fission fragment range.

Belgonucleaire model

This model computes the fraction of fission gas released on the basis of the classical FGR model for UO$_2$. In particular, a PuO$_2$ spherical particle surrounded by a depleted UO$_2$ matrix is considered. As the irradiation proceeds, plutonium can be produced in the matrix (by U-238 transmutation), consumed in the agglomerate (by fission) and it can diffuse from the agglomerate to the matrix. Thus, the solution of the following non-linear diffusion equation gives the evolution of plutonium concentration in the average agglomerate surrounded by a UO$_2$ region:

$$\frac{1}{\Phi}\frac{\partial c}{\partial t} = k\frac{1}{r^2}\frac{\partial}{\partial r}\left[r^2\left(\alpha \cdot c + \beta\right)\frac{\partial c}{\partial t}\right] + \gamma \cdot c + \delta$$

where:

k = constant [cm^5]

Φ = neutron flux [n/cm^{2}s]

$\alpha = 100\,(\sigma_{f239}\,x_{239} - \sigma_{f235}\,e_{235})$

$\beta = \sigma_{f235}\,e_{235}$

$\gamma = -(\sigma_{c238} - \sigma_{a239})$

$\delta = \sigma_{c238}$

where, the plutonium diffusion coefficient $D_{Pu} \approx k\dot{F}$, with $\dot{F}$ [1/cm^{3}s] = local fission rate = $(\alpha \cdot c + \beta) \cdot \Phi$

In the above notation, 238 refers to U-238, 239 refers to Pu-239, 235 refers to U 235; σ_c, σ_a and σ_f correspond to the capture, the absorption and the fission cross-sections, respectively; x_{239} represents the fraction of Pu-239 atoms in the plutonium, and e_{235} is the U-235 enrichment.

Furthermore, the production of gaseous fission fragments is calculated taking into account the fact that the xenon and krypton appear at approximately 7 to 9 µm, from the end location of the mother fissile atom. This gives the source term of the diffusion equation of the gas atoms within the grains, where different grains have a different Pu content.

The approximation of the method consists in neglecting the amount of gas released from the plutonium-poor grains and in considering only an "average grain" of the plutonium-rich agglomerate.

Summarizing, this model is based on the following assumptions:
- FGR is computed on the basis of the FGR model for UO$_2$ fuel;
- all the plutonium is considered to be in the plutonium-rich agglomerates;
- no fissile material is present in the UO$_2$ matrix (all the gas is created inside the agglomerates);
- an average agglomerate size is considered;
- an average grain size (both for the Pu agglomerates and the U matrix) is considered;
- the Pu concentration changes as the fuel burn-up proceeds, due to fission and capture reactions of Pu and U;
- mitigation of the Pu heterogeneity through interdiffusion of Pu and U is taken into account by means of a diffusion equation.

KAERI model

This model is based on the assumption that the gas release mechanism in Pu-rich particles is the same as that in UO$_2$ fuel. The different release behaviour in Pu-rich particles and in UO$_2$ matrix would originate from different fission densities in the two regions due to different fissile Pu contents. The equivalent cell can be schematized by an inner part that considers the Pu-rich agglomerate plus a layer of 6-7 µm considering the recoil length of fission products (equivalent

spherical particle) and an outer shell considering the UO_2 matrix (equivalent spherical cell). Local fission density (F_{loc}) in a MOX fuel pellet is derived from local power density using the fact that each fission generates 200 MeV. The fission rate in the agglomerate would be proportional to the fissile Pu content, and can be expressed as: $(e_a/e_p)F_{loc}$, where e_p and e_a are the average plutonium contents in the fuel pellet and in the Pu-rich agglomerate, respectively.

The amount of gas released in an equivalent spherical cell is:

$$REL_{cell} = REL_{eq,gr} \frac{V_{eq}}{V_{eq,gr}} + REL_{m,gr} \frac{V_m}{V_{m,gr}}$$

where:

$REL_{eq,gr}$ = gas release in a grain located in an equivalent particle

$V_{eq} = \frac{4}{3}\pi \left(D_{eq}/2 \right)^3$ = volume of an equivalent particle

$V_{eq,gr} = \frac{4}{3}\pi \left(D_{eq,gr}/2 \right)^3$ = volume of a grain located in the equivalent particle

$D_{eq,gr}$ = diameter of a grain in the equivalent particle

$REL_{m,gr}$ = release from a grain in the matrix

$V_m = \frac{4}{3}\pi \left\{ \left(D_{cell}/2 \right)^3 - \left(D_{eq}/2 \right)^3 \right\}$ = volume of the matrix in an equivalent cell

$V_{m,gr} = \frac{4}{3}\pi \left(D_{m,gr}/2 \right)^3$ = volume of a grain in the matrix

$D_{m,gr}$ = diameter of a grain located in the matrix of an equivalent cell

Summarizing, the main assumptions of this model are:

- FGR is computed on the basis of the FGR model for UO_2 fuel;
- fission of U-235 is neglected;
- not all the plutonium is considered to be in the plutonium-rich agglomerates;
- an average agglomerate size is considered;
- the Pu concentration does not change as the fuel burn-up proceeds;
- mitigation of the Pu heterogeneity through interdiffusion of Pu and U is not taken into account.

A-2.2   *Available models for helium release in LWR oxide fuels*

Helium is produced in oxide fuels (UO$_2$ and MOX) by means of: (i) α decay of the actinides, (ii) ternary fission, and (iii) (n,α) reactions. In LWRs, the relevant actinides decaying α with a relatively short decay constant are ^{238}Pu, ^{242}Cm and ^{244}Cm, while the main (n,α) reaction is ^{16}O(n,α)^{13}C, because of the high abundance of ^{16}O. On the basis of these assumptions, a model has been developed and included as an extension of the burn-up module (TUBRNP) of the TRANSURANUS code (Botazzoli, 2008; Botazzoli et al., 2011).

Due to the high diffusion coefficient (Ronchi and Hiernaut, 2004; Yakub et al., 2010), the created helium can be easily released in the gap between the fuel and the cladding, enhancing the fuel rod inner pressure. However, if the helium initially loaded in the gap is at a sufficient high pressure, the release of the amount created in the fuel is inhibited and part of the helium in the gap can be absorbed by the fuel (Barker et al., 2006). In this section, an overview of the approaches adopted for treating the helium release in oxide fuels is reported.

The simplest approach is the previous approach of TRANSURANUS, where the release is assumed as a constant fraction (user defined) of the total produced helium (Lassmann et al., 2011).

Since the production of helium is low compared to the amount of fission gases (xenon and krypton) generated, some authors suggest that helium can be released only once the fission gas bubbles interconnect. For this reason, they suppose that in case of unpressurized rods (i.e., absorption can be neglected) it should be linked to the fission gas release. In Fig. A-1, released helium measured in unpressurized MOX fuel rods (BWR (Kamimura et al., 1999), FBR (Katsuyama et al., 2010), ATR (Hodge et al., 2005)) are reported as a function of the fission gas release, and compared with the curves proposed by Federici and co-authors (Federici et al., 2007).

Since the solubility of helium is low (Maugeri et al., 2009), Federici and co-authors assumed that the grain boundary would work as a perfect sink, as in the case of fission gases. Hence, by solving the diffusion equation in a sphere with homogeneous Dirichelet boundary conditions under constant conditions (i.e., constant temperature and domain volume), the amount of fission gases leaving the domain divided by the amount of gas generated can be expressed by (Booth, 1957):

$$f(\tau) = 1 - \frac{1}{15\tau}\left(1 - 90\sum_{n=1}^{\infty}\frac{\exp\left(-n^2\pi^2\tau\right)}{n^4\pi^4}\right)$$

where τ is an equivalent time defined as:

$$\tau = \frac{D_{eff}}{a^2} \cdot t$$

where D_{eff} is an effective diffusion coefficient taking into account trapping and resolution (Speight, 1969), a is the radius of the equivalent sphere and t the real time.

The short time approximation can be expressed as:

$$f(\tau) = 4\sqrt{\frac{\tau}{\pi}}$$

Federici and co-authors assumed that the ratio between the helium effective diffusion coefficient and that of fission gas is between 10 and 100. The curves reported in Fig. A-1 represent $f(\tau \cdot 10)$ as a function of $f(\tau)$, and $f(\tau \cdot 100)$ as a function of $f(\tau)$. However, the assumption of a factor of 10 to 100 between the diffusion coefficients seems an adaptation in order to find a factor between 3 and 10 in terms of fractional releases, in accordance with the experimental evidences. In fact, by using the short time approximation, the fractional releases are proportional to the square root of the diffusion coefficient.
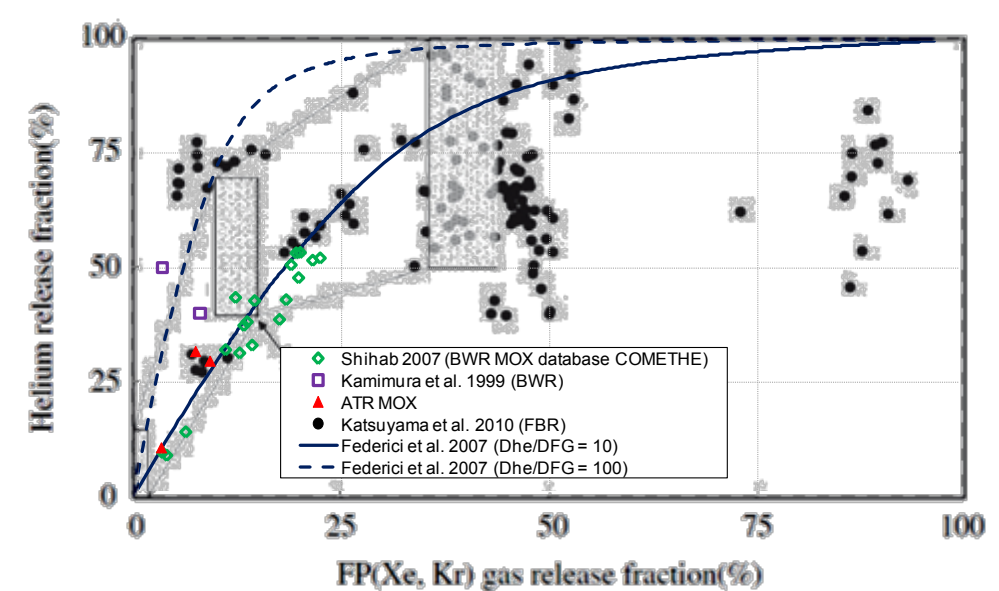

Fig. A-1. Fractional helium releases as a function of the fractional fission gas release for unpressurized fuel rods. The graph is taken from (Katsuyama et al., 2010).

The thermal diffusion coefficients of helium reported by Federici and co-authors, which refer to both ion implantation and infusion experiments by different authors (Bostrom, 1958; Rufeh et al., 1965; Sung, 1967; Guilbert et al., 2004; Roudill et al., 2004; Blanpain et al., 2006), are quite dispersed, meaning that they do not reflect a simple volume diffusion. They are rather representative of an effective behaviour depending on the experimental conditions and the way the results are interpreted. However, they are confined between the following equations which are valid in the range (800°C, 1500°C):

$$D_{He,\min} = 8.887 \cdot 10^{-14} \cdot \exp(-17505.9/T)$$
$$D_{He,\max} = 2.222 \cdot 10^{-11} \cdot \exp(-17505.9/T)$$

By dividing these equations by the thermal diffusion coefficient of Xe provided by Matzke (Lassmann et al., 2011) , we found a ratio quite different with respect to the factor 10-100 suggested by the authors (Fig. A-2). However, they do not indicate which fission gas diffusion coefficient they used. It is worth noting that the migration energy of Xe and He are quite different, meaning that the ratio of the diffusion coefficients of He and Xe strongly depends on the temperature, and a simple factor cannot be representative of the whole temperature range inside a fuel pellet.

On the other hand, Kamimura and co-authors (Kamimura et al., 1999) assumed a ratio between the diffusion coefficient of helium and fission gases of 1000. Considering the short-time approximation, this means that the helium release should be 30 times larger than fission gas release. Since in contradiction with the experimental evidences (where helium fractional releases are 3 to 10 the fission gas releases), they argued that at the boundary area grain boundary bubbles are small, and frequent exchange of gas atoms between matrix and bubbles caused by trapping by fission gas bubbles and re-solution by fission fragments makes the proportion of helium to fission gases in the bubbles the same as that in the matrix. This means that helium and fission gas volumes on the grain boundary (and/or in the matrix) are proportional to each generation, and the proportion of helium to fission gas in each area coincides to that of its yield.
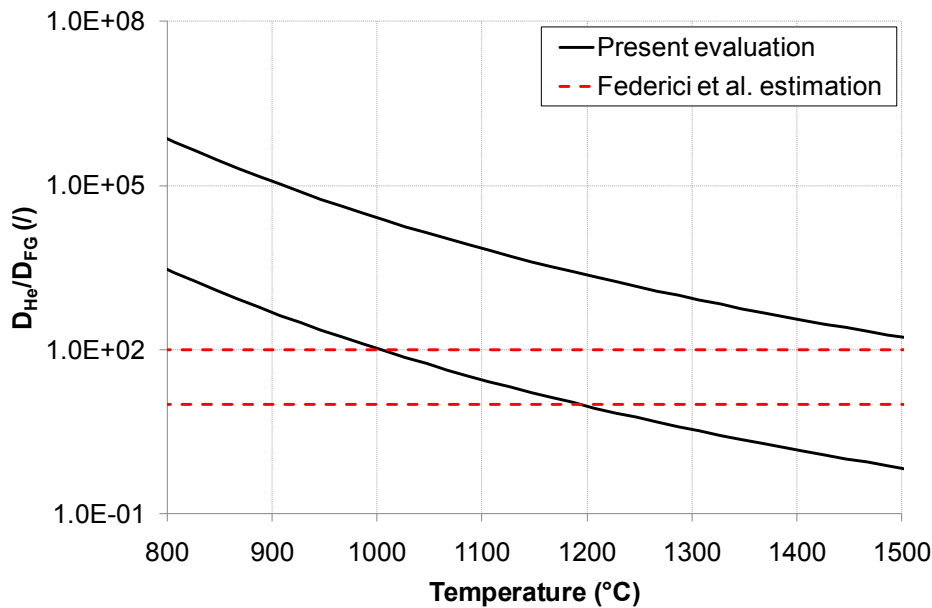
Fig. A-2. Ratio between the thermal diffusion coefficient of helium and fission gases.

Kurita and co-authors (Kurita et al., 1999), showed their results in terms of volume of helium released as a function of volume of fission gas (FG) released. These data refer to MOX fuels irradiated in the Advanced Test Reactor FUGEN in Japan. A clear correlation can be seen in Fig. A-3-a. However, when including the data of the ATR irradiation test and of Kamimura and co-authors the dispersion increases. In Fig. A-3-b, a rough estimation of the data of Katsuyama and co-authors (which refer to FBR conditions) is reported and compared with the other data. It is important to mention that the data of Katsuyama and co-authors are actually quite dispersed, especially in the region around 500 cm^3/ kg_{fuel} of released FPs.

In the open literature, it is also possible to find a model developed by Ronchi and Hiernaut (Ronchi and Hiernaut, 2004) used for interpreting helium release curves of experiments conducted in Knudsen cells. They modelled the helium behaviour by means of three reaction rate equations:

$$\frac{dc}{dt} = -Kc - (H+S)c$$

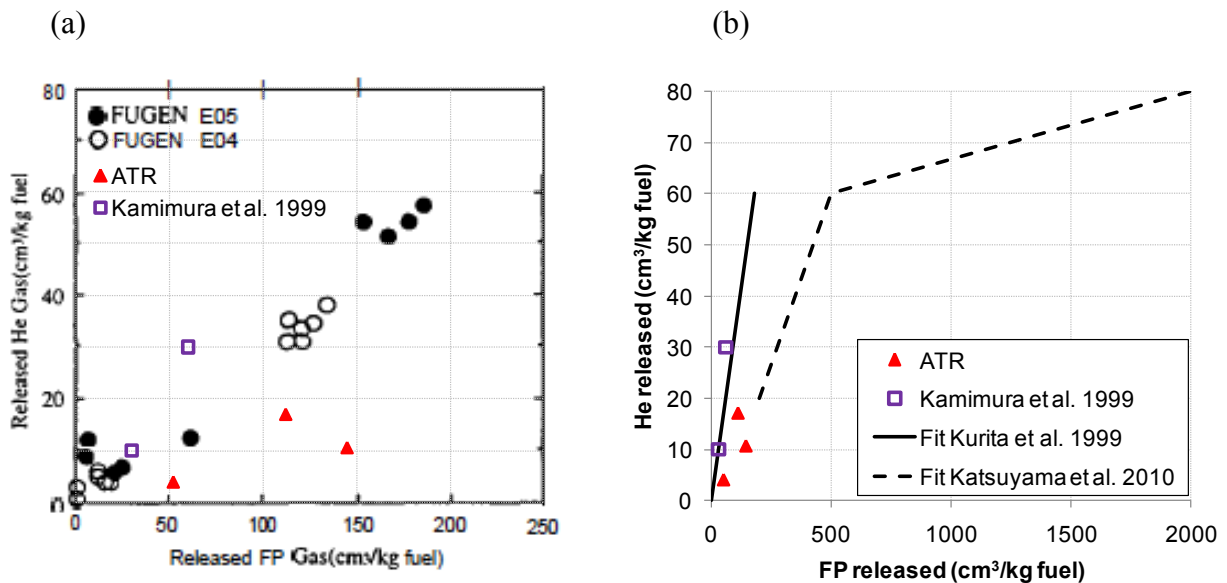$$\frac{db}{dt} = Kc - Ub$$

$$\frac{dg}{dt} = (H+S)c + Ub$$

Fig. A-3. Amount of helium released as a function of amount of FG released, (a) LWR conditions,(b) comparison between LWR and FBR conditions.

where c is the amount of gas in solution, b the amount trapped, and g the amount released, K is the trapping rate, H the de-trapping rate, S the de-sorption rate, U the release rate of the amount trapped. However, the coefficients K, H, S and U are not known *a priori*, and the values fitted on the basis of the release curves were quite different for the different samples. For this reason, this model has been disregarded.

As far as the absorption mechanism is concerned, the only work describing a possible approach is the one of Federici and co-authors. They assume that the thermodynamical equilibrium induced by the thermal resolution is reached when the He partial pressures in the intergranular cavities and in the free volume are equal. The molar concentration of He can then be calculated according to the ideal gas low considering the free volume He partial pressure (hot conditions) and the volume fraction of intergranular cavities. In order to calculate the kinetics associated with this mechanism, they suggest that one can replace the grain boundary "lattice", along which He is diffusing and being trapped, by a homogeneous volume of the equivalent sphere representing the fuel fragment. Introducing the grain boundary (GB) equivalent time, τ_{GB}, defined by using a GB effective diffusion coefficient, the analytical expression for the calculation of the kinetics can be written as:

$$C_{He}\left(\tau_{GB}\right) = C_{He,eq}\left(1 - \frac{6}{\pi^2}\sum_{n=1}^{\infty}\frac{\exp\left(-n^2\pi^2\tau_{GB}\right)}{n^2}\right)$$

τ_{GB} being an equivalent time defined as:

$$\tau_{GB} = \frac{D_{eff,GB}}{a^2}\cdot t$$

where $D_{eff,GB}$ is an equivalent grain boundary diffusion coefficient, a the equivalent sphere diameter and t the real time. However, they do not discuss the values to be adopted in the model, but they write that empirical evidences seem to indicate that the equilibrium in the intergranular cavities is reached after one reactor irradiation cycle.

In Fig. A-4, experimental data of released helium measured in PWR reactors reported by Barker and co-authors (Barker et al., 2006) are shown. They refer to SBR MOX fuels irradiated in the reactor Beznau-1 in Switzerland. An infusion of helium can be seen for low burn-up, but a release is in any case achieved for higher burn-ups. Although not reported, the uncertainty of these data should be not negligible. In fact, this is the sum of the uncertainty of the moles measured after the irradiation plus the uncertainty of the moles initially loaded. By considering the geometry and initial pressure of these rods, it is possible to estimate about $1.5\cdot10^{-2}$ moles initially loaded, meaning 335 cm^3 STP at 273 K. This means that even an uncertainty of ±1% on both the measurements leads to an uncertainty of ±7cm^3, which is not negligible compared with the net difference.
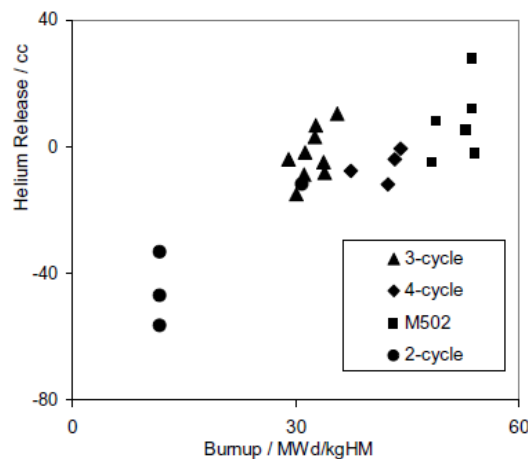

Fig. A-4. Helium release from SBR MOX fuel irradiated in the PWR reactor Beznau-1. Graph is taken from Barker et al. (2006).

A-3   Model development

A-3.1   Fission gas release

The basic difference between the microstructure of MIMAS MOX fuel and UO_2 fuel is the possible presence of Pu-rich agglomerates: in these agglomerates, the fission rate is higher than in the surrounding matrix. These heterogeneities influence the diffusion of the fission gases and the rate of grain boundary concentration.

The influence of the higher fission rate inside the agglomerates is essentially due to the fact that where the fission rate is higher the gas production is higher. This means that the saturation concentration at grain boundary is reached earlier and then the fraction released is higher. Neglecting the temperature difference ΔT between the agglomerate and the matrix (it has been demonstrated that this ΔT is no more then 10-15°C (Ishida and Korei, 1994), lower than the uncertainties of the fuel temperatures, ≈10% (Van Uffelen, 2006)) and considering a diffusion coefficient only dependent on temperature, it is possible to see that the release due to diffusion from a heterogeneous fuel is the same as the release from a homogeneous fuel with the same average plutonium content. A second effect of the higher fission rate is the higher diffusion coefficient (irradiation induced component). When allowing for the increased mobility of gas atoms in the agglomerates, the release will be enhanced.

Taking into account the matrix around the Pu-rich agglomerates can provide an explanation for the observed error in predicted FGR as a function of burn-up in the simulation of ATR MOX (Botazzoli, 2008). At low burn-up, the matrix can operate as a buffer, whereas at high burn-up, when the buffer or matrix is saturated, the FGR from the very high burn-up region could explain the increased FGR observation.

The elementary cell schematized in Fig. A-5 can be considered. The diameter of the uranium matrix cell is chosen in order to preserve the average content of plutonium. The average plutonium agglomerate size is taken into account:

$$D_{cell} = D_{agg} \cdot \sqrt[3]{\left(\frac{e_{agg} - e_m}{e_{av} - e_m} \right)}$$

where:

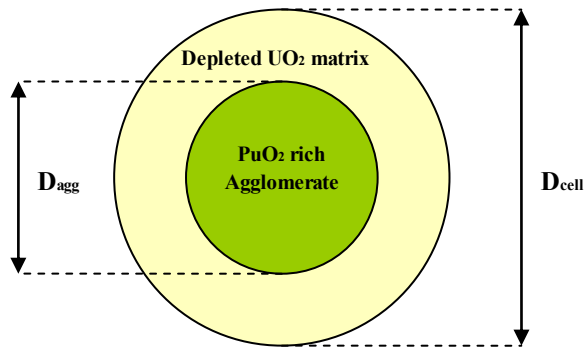e_{agg} = fissile Pu concentration in the agglomerate;

Fig. A-5. Scheme of the cell used for the model.

e_m = fissile Pu concentration in the matrix;

e_{av} = average fissile Pu concentration in the fuel.

The intragranular diffusion equation is solved for the matrix grains and for the agglomerates grains taking into account the different parameters: production rate, diffusion coefficient and grain size surface energy (or grain boundary saturation value). Concerning the intergranular behaviour, a grain boundary saturation concentration can be assumed until the gas bubble will interconnect and the gas will be released, as commonly adopted for homogeneous UO_2 fuel. Because of the higher fission rate the gas bubble interconnection will occur earlier in the plutonium-rich agglomerate. Thus, the following assumption can be made: when the bubble interconnection occurs in the grains of the plutonium-rich agglomerate, the gas will be released to the agglomerate boundary. This gas will be stored in the agglomerate boundary until also the gas in the matrix grain boundaries will reach the saturation concentration. In order to consider the possibility of release before the interconnection of the grain boundary bubbles of the matrix, it should be possible to use the percolation theory to represent the degree of opening in the surrounding UO_2 matrix (cracks, saturation, open pores).

A-3.2   Helium release

An approach of intermediate complexity has been considered for the treatment of the helium release. In fact, as discussed in Sub-section A-2.2, simple correlations coupling the helium release to the fission gas release are applicable only in un-pressurized rods, and can fail since over-simplified. On the other hand, detailed reaction rate equations can be hardly developed because of the uncertainty of all the parameters and the scarcity of experimental data in the open literature.

A simple model has been developed that takes separately into account the intra- and inter-granular behaviour and that is consistent with the current model for fission gas release in the TRANSURANUS code.

The intra-granular behaviour is considered by solving the diffusion equation inside a spherical grain by means of an effective diffusion coefficient. Three different diffusion coefficients have been implemented in the TRANSURANUS code based on thermal diffusion coefficients available in literature:

$$D_{He,\min} = 8.887 \cdot 10^{-14} \cdot \exp(-17505.9/T)$$

$$D_{He,average} = 1.405 \cdot 10^{-12} \cdot \exp(-17505.9/T)$$

$$D_{He,Max} = 8.000 \cdot 10^{-7} \cdot \exp(-23163.5/T)$$

The first two are the lower limit and the average value of the diffusion coefficients of (Bostrom, 1958; Rufeh et al., 1965; Sung, 1967; Guilbert et al., 2004; Roudill et al., 2004; Blanpain et al., 2006), while the third one is the coefficient proposed by Ronchi and Hiernaut. However, the last one is an atomic diffusion coefficient derived from the interpretation of the experimental data by means of a more complex model, which takes into account trapping and resolution separately. Furthermore, it is representative of a [238]Pu MOX doped fuel. For these reasons, it should be used only as a conservative case.

The treatment of the inter-granular behaviour is based on the experimental evidence that the diffusivity of helium at the grain boundary is accelerated if temperatures are above 800°C (Martin et al., 2010). The grain boundary behaviour is then taken into account in the following way: (i) when the threshold for the fission gas release is not yet reached[9], helium is trapped in gas bubbles (mainly composed by fission gases) if temperatures are lower than 800°C, and is instantaneously released in the free volume, if temperatures are higher; (ii) if the threshold for the fission gas release is exceeded, all the helium reaching the grain boundary is instantaneously released.

---

[9] Once the fission gases reach the grain boundary, they are not immediately released to the free volume, but they are trapped in bubbles that grow continuously. Once the bubbles are large enough, they start to interconnect, forming tunnels, from which the gas atoms are vented out. It is then clear that fission gas release occurs only after a certain threshold, due to the bubble interconnection.

As far as the absorption is concerned, a model is currently under development for the implementation in TRANSURANUS. It could be treated by considering that helium present in the gap is absorbed instantaneously reaching the solubility limit (which depends on the pressure and temperature, obeying the Henry's law). However, solubility limits are not well characterized and the available data are quite dispersed (Federici et al., 2007; Maugeri et al., 2009). Another approach could be considering that helium can infuse in the fuel towards open porosities and assuming that the thermo-dynamical equilibrium induced by the thermal resolution is reached when the He partial pressures in the intergranular cavities and in the free volume are equal, as proposed by Federici and co-authors. As a first approximation, it can be considered that the concentration of helium in the intergranular cavities reach instantaneously the equilibrium and can be calculated by means of the ideal gas law.

A-4 Model verification

In order to verify models describing the gas behaviour in fuels, the temperatures must be known. For this reason, a complete thermo-mechanical analysis has to be performed. However, for most of the data present in Sub-section A-2.2, fuel pin geometries and irradiation histories are not known. The only data that can be used are those of the ATR irradiation test, since it has been already analysed (Botazzoli, 2008). This irradiation test consists of nine weapon-grade MOX fuels fabricated at Los Alamos National Laboratories, irradiated in the Advanced Test Reactor at Idaho National Laboratory and analysed at Oak Ridge National Laboratories, in the context of the Fissile Material Disposition Program. The fuel rods reached a burn-up ranging from 20 to 50 MWd/kgHM. For all the rods, helium production has been estimated by means of the depletion code ORIGEN, which has been modified including ternary fission yield and effective cross sections of the ATR reactor. For the fuel rods reaching 50 MWd/kgHM (CAP5FP8, CAP6FP9, CAP12FP15), helium released in the gap has been measured. These three fuel rods have been simulated. For the details of the input setting, see (Botazzoli, 2008).

It is worth noting that the helium production model of TRANSURANUS does not include effective cross sections of the ATR, hence standard LWR MOX cross sections have been used. However, a good agreement has been found, with differences smaller than 10%.
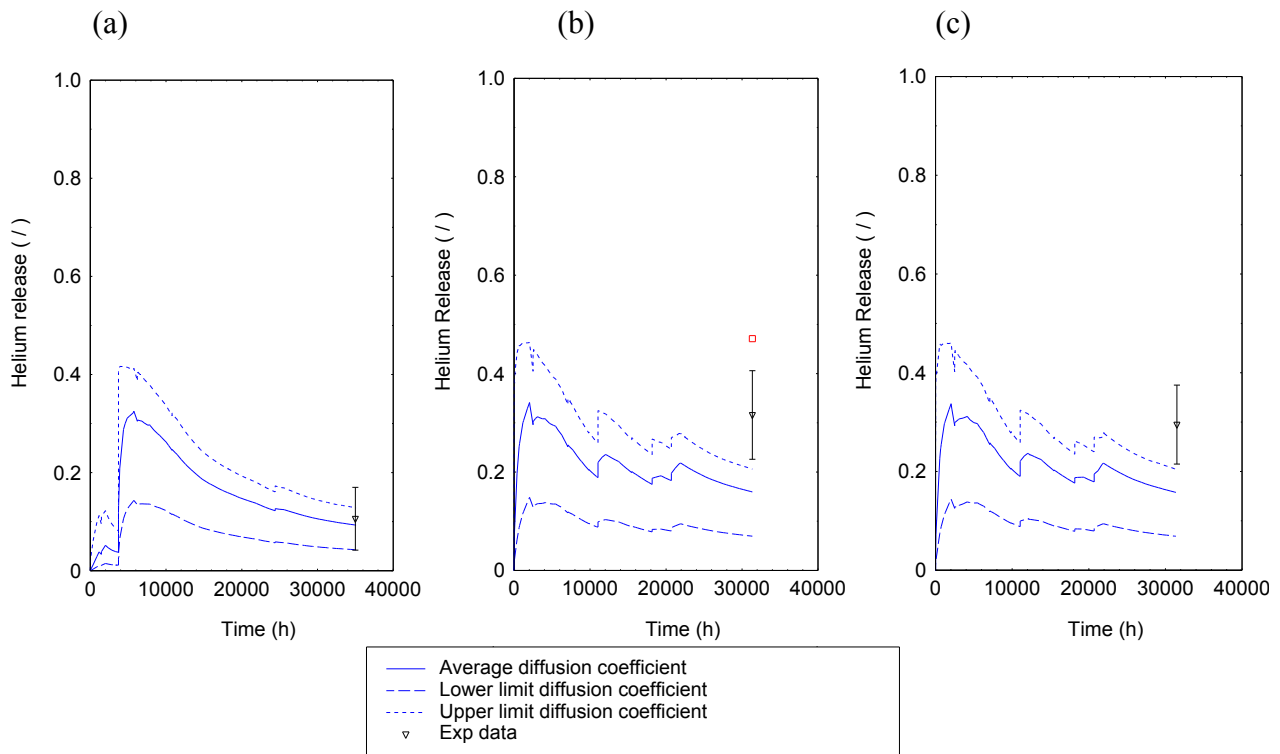
Fig. A-6. Comparison between measured and computed Helium release in (a) CAP5FP8, (b) CAP6FP9 and (c) CAP12FP15. Red square in b) is the value calculated by considering the measured inner pressure, rod free volume, fraction of helium moles in the gap and produced helium.

The computed fractional releases are shown in Fig. A-6 by using the different diffusion coefficients, and compared with the experimental data.

Before commenting the results, it is worth mentioning that the declared helium fractional release of the fuel pin CAP6FP9 is not consistent with other measured quantities. In fact, the declared fractional release is 31.6±9%, while a value of 47.1% can be calculated by considering the measured inner pressure, rod free volume, fraction of helium moles in the gap and produced helium. Helium release is well predicted with all the diffusion coefficients for the fuel rod CAP5FP8, while it is underestimated for the fuel pins CAP6FP9 and CAP12FP15.

However, the fission gas release is strongly underestimated. Measured fission gas release fractions are 3.37, 7.49 and 9.23%, while the present simulations lead to 0.97, 1.12 and 1.21% for CAP5FP8, CAP6FP9 and CAP12FP15, respectively. It is possible to see that for the CAP5FP8, where the fission gas release underestimation is less important, the helium release is well predicted, while for

the other two fuel rods the under-prediction of helium release is important. The underestimation of fission gas release can be due to the Pu heterogeneity effect (Billaux and van Vliet, 1986; Ishida and Korei; 1994; Koo et al., 2001), which is not considered in the present simulations, or to an underestimation of the fuel temperature, which can be due to several reasons (e.g., underestimation of fuel thermal conductivity, overestimation of gap size). However, fuel temperature and fission gas release are strongly coupled, since (i) the release of fission gases decreases the thermal conductance of the gap, increasing the fuel temperature, and (ii) the increase of the fuel temperature affects the diffusion coefficient of fission gases, enhancing the release. This means that, if fission gas release is underestimated because of the Pu heterogeneity, lower temperatures are also computed, increasing the underestimation of fission gas release. As far as the helium is concerned, if lower temperatures are evaluated, less helium is predicted at the grain boundary, being available for the release. Furthermore, if the amount of fission gases at the grain boundary (in the areas of the pellet with a temperature lower than 800°C) is incorrectly predicted to be below the release threshold, also the amount of helium release from the grain boundaries of those areas is incorrectly under-predicted.

A-5   Concluding remarks

In the present Appendix, models for the fission gas and helium release in (U,Pu) Mixed Oxide nuclear fuels have been discussed. Models have been developed and have been proposed for the implementation in the TRANSURANUS fuel performance code. A specific model for the helium release has been implemented in the TRANSURANUS code, coupled with the helium production and grain growth models and preliminarily validated on the basis of the ATR irradiation test. The agreement is satisfactory, although some discrepancies have been noticed (the underestimation in the helium release for two of the simulated rods can be caused by the underestimation of the fission gas release, which in turn can be caused by errors in the temperature calculation). More experimental data are needed for a better assessment of the model parameters (diffusion coefficients, solubilities) and for a complete validation of the model for LWR MOX fuels. Although related to LWR conditions, the present work could be extended to fast reactors. This could be achieved by including specific one-group cross sections in the helium production model, by considering the columnar grain growth and the relative release process from columnar grains.

A-6 Bibliography

Barker M.A., Matthews E.C., Stephenson K., Brémier S., Papaioannou D., Walker C.T., Parmar Y. (2006). Post-irradiation examination of high burnup SBR MOX fuel, Transactions of Topfuel 2006, pp. 5–9, Salamanca, Spain, October 22-26, 2006.

Billaux M., van Vliet J. (1986). Impact of Fuel Heterogeneities on Fission Gas Release for LWR U-Pu mixed oxide fuels, Res Mechanica 17.

Blanpain P., Lippens M., Schut H., Federov A.V., Bakker K. (2006). The HARLEM Project, Workshop MMSNF-5, Nice, France, June 1-2, 2006.

Booth A.H. (1957). A suggested method for calculating the diffusion of radioactive rare gas fission products from UO_2 elements and a discussion of proposed in-reactor experiments that may be used to test its validity, Report DCI-27, AECL, Chalk River, Ontario, Canada.

Bostrom W. A. (1958). In J. Belle's Paper, Properties of Uranium Dioxide, Proc. of the Second United Nations International Conference on Peaceful Uses of Atomic Energy, Geneva, 6, 569–589.

Botazzoli P. (2008). Verification of the Fission Gas Release Predictions of the TRANSURANUS Code for LWR MOX Fuel, Technical Note, JRC-ITU-TN-2008/20, © European Communities.

Botazzoli P. (2009). A model describing the helium production in PWR oxide fuels, Technical Report, Deliverable 1 – Service Contract Nr. 211551-2008-11 F1ED KAR IT, 2009.

Botazzoli P., Luzzi L., Schubert A., Van Uffelen P., Haeck W. (2009). Applying Advanced Neutron Transport Calculations for Improving Fuel Performance Codes, Proceedings of Top Fuel 2009, Paper 2173, Paris, September 6-10, 2009.

Botazzoli P., Luzzi L., Brémier S., Schubert A., Van Uffelen P., Walker C.T., Haeck W., Goll W. (2011). Extension and Validation of the TRANSURANUS Burn-up Model for Helium Production in High Burn-up LWR Fuels, Journal of Nuclear Materials, vol. 419, Nos. 1-3, pp. 329–338.

Federici E., Courcelle A., Blanpain P., Cognon H. (2007). Helium production and behavior in nuclear oxide fuels during irradiation in LWR, Proceedings of the 2007 International LWR Fuel Performance Meeting, Paper 1057, San Francisco, California, September 30 - October 3, 2007.

Guilbert S., Sauvage T., Garcia P., et al. (2004). Helium Migration in Implanted UO2 Sintered Disks, Journal of Nuclear Materials, 327, pp. 88–96.

Hodge S.A., Morris R.N., Ott L.J. (2005). Weapons-derived Mixed Oxide fuel test irradiation summary, Report ORNL/TM-2005/255, Oak Ridge National Laboratory, Oak Ridge, Tennessee.

Ishida M., Korei Y. (1994). Modelling and parametric studies of the effect of Pu-mixing heterogeneity on fission gas release from mixed oxide fuels of LWRs and FBRs, Journal of Nuclear Materials, 210.

Kamimura K., Kobayashi Y., Nomata T. (1999). Helium generation and release in MOX Fuels, Proceedings of the symposium on MOX Fuel Cycle Technologies for Medium and Long Term Deployment, IAEA-SM-358/19, Vienna, Austria, May 17-21, 1999.

Katsuyama K., Ishimi A., Maeda K., Nagamine T., Asaga T. (2010). Helium release from the uranium–plutonium mixed oxide (MOX) fuel irradiated to high burn-up in a fast breeder reactor (FBR), Journal of Nuclear Materials 401, Issues1-3, pp. 86–90.

Koo Y., Lee B., Cheon J., Sohn D. (2001). Modeling and parametric studies of the effect of inhomogeneity on fission gas release in LWR MOX fuel, Annals of Nuclear Energy, 13.

Kurita I., Kikuchi K., Abe T. (1999). MOX Fuel Irradiation Behaviour in a Thermal Reactor, Proceedings of the symposium on MOX Fuel Cycle Technologies for Medium and Long Term Deployment, IAEA-SM-358/17, Vienna, Austria, May 17–21, 1999.

Lassmann K., Schubert A., Van Uffelen P., Győri C., van de Laar J. (2011). TRANSURANUS Handbook, Copyright ©1975-2011, Institute for Transuranium Elements, Karlsruhe, Germany.

Martin G., Garcia P., Sabathier C., Carlot G., Sauvage T., Desgardin P., Raepsaet C., Khodja H. (2010). Helium release in uranium dioxide in relation to grain boundaries and free surfaces, Nuclear Instruments and Methods in Physics Research B, vol. 268, pp. 2133–2137.

Maugeri E., Wiss T., Hiernaut J.P., Desai K., Thiriet C., Rondinella V.V., Colle J.Y., Konings R.J.M. (2009). Helium solubility and behaviour in uranium dioxide, Journal of Nuclear Materials 385, pp. 461–466.

Ronchi C., Hiernaut J.P. (2004). Helium diffusion in uranium and plutonium oxides, Journal of Nuclear Materials, vol. 325, pp. 1–12.

Roudil D., Deschanels X., Trocellier P., Jegou C., Peuget S., Bart J.M. (2004). Helium Thermal Diffusion in a Uranium Dioxide Matrix, Journal of Nuclear Materials, 325, pp. 148–158.

Rufeh F., Olander D.R., Pigford T.H. (1965). The Solubility Of Helium In Uranium Dioxide, Nuclear Science and Engineering, 23, pp. 335–338.

Shihab S. (2007). Model Development for Helium Release and Swelling Behaviour in Pu and MA HTR Fuels, Technical Note 0701484, Belgonucleaire.

Speight M.V. (1969). A calculation on the migration of fission gas in material exhibiting precipitation and resolution of gas atoms under irradiation, Nuclear Science and Engineering, 37.

Sung P. (1967). Equilibrium Solubility and Diffusivity of Helium in Single-Crystal Uranium Oxide, Ph.D. Thesis, Univ. Washington.

Suzuki M. (2000). Light Water Reactor Fuel Analysis Code FEMAXI-V (Ver. 1), JAERI-Data/Code 2000-030.

Van Uffelen P. (2006). Modelling of nuclear fuel behaviour, EUR 2231 EN, Institute for Transuranium Elements, Karlsruhe, Germany.

White J.R., Tucker M.O. (1983). Journal of Nuclear Materials 118.

Yakub E., Ronchi C., Staicu D. (2010). Diffusion of helium in non-stoichiometric uranium dioxide, Journal of Nuclear Materials, vol. 400, pp.189–195.

Short scientific curriculum of the working team

Lelio Luzzi graduated from the Politecnico di Milano (POLIMI, Italy) in Nuclear Engineering. He obtained his Ph.D. in Science and Technology in Nuclear Plants at POLIMI (1999). From 1999 to 2001, he worked as POLIMI post-doctoral researcher. During that period, he was detached for 2 years at the Materials Research Unit of JRC-ITU, within the TRANSURANUS Developers Team. Since 2001, he is a permanent researcher and assistant professor of Nuclear Design and Technology at POLIMI. He belongs to the POLIMI Department of Energy, Nuclear Engineering Division - CeSNEF (Nuclear Reactors Group, http://www.nuclearenergy.polimi.it) and to the Faculty of the Doctorate School in Energy and Nuclear Science and Technology. He is Italian representative of the IAEA-CRP-FUMEX-III and of the OECD/NEA International Fuel Performance Experiments database. His research activities in Italy and abroad include nuclear fuel rod modelling and thermo-mechanics, as well as the development of multi-physics simulation tools. In the framework of a lasting collaboration with JRC-ITU, he was involved in MSc. and Ph.D. projects, aimed at the development of TRANSURANUS fuel performance code and mainly focusing on analysis of fuel rod irradiation experiments and fission product behaviour modelling. Author of more than 90 peer-reviewed scientific publications.

See also: http://www.energia.polimi.it/english/department/scheda_persona.php?id=89

Pietro Botazzoli and *Giovanni Pastore* graduated in Nuclear Engineering (2007; 2008, respectively) at POLIMI, where they obtained also the Ph.D. (2011; 2012) in Radiation Science and Technology, under the supervision of prof. Luzzi. During both the MSc. and the Ph.D., their field of research concerned the modelling and the analysis of fuel rod performance. They worked on the topics of the present report in the frame of a contract collaboration with the Nuclear Reactors Group (Department of Energy, Nuclear Engineering Division, POLIMI).

(This page has been intentionally left blank)